Non-Trivial θ-Vacuum Effects in the 2-d $O(3)$ Model

and

Quantum Simulation of Non-Abelian Lattice Gauge Theories

Inauguraldissertation
der Philosophisch-naturwissenschaftlichen Fakultät
der Universität Bern

vorgelegt von

Michael Bögli

von Münsingen BE

2014

Leiter der Arbeit:

Prof. Dr. U.-J. Wiese

Albert Einstein Center for Fundamental Physics
Institut für theoretische Physik, Universität Bern

Abstract

This thesis consists of two parts:

In the first part, we study the 2-d $O(3)$ model and investigate the relevance of the θ-vacuum angle. In addition to the standard lattice action, we use a so-called topological action, which is invariant under small field deformations and does not have the correct classical continuum limit. Despite several deficiencies, this action still leads to the correct quantum continuum limit. Furthermore we construct an optimized constraint action, whose cut-off effects are extremely small. We will extend Hasenbusch's concept of an improved estimator to address the sign problem that arises for non-vanishing θ-vacuum angles. By calculating the continuum value of the step scaling function we show that dislocations do not spoil the continuum limit of this theory and that we obtain a different continuum theory for each value of θ. In addition we are able to confirm the analytic predictions of the S-matrix theory by unprecedented precision. This indirectly confirms the WZNW model as the low-energy effective theory of the 2-d $O(3)$ model at $\theta = \pi$.

In the second part of the thesis, we discuss quantum link models in the context of quantum simulating lattice gauge theories. We work out the Hamiltonian formulation of Wilson's approach to lattice gauge theories and show its connection to quantum link models, which are lattice implementations of gauge theories with a finite-dimensional Hilbert space per link. We show how to couple the quantum links to staggered fermions. Quantum link models are discussed in detail, especially for the cases of $U(2)$ and $SO(3)$ gauge groups. We present a so-called rishon representation, which allows the representation of the gauge links in terms of fermion bi-linears. This allows us to suggest an implementation in ultra-cold atoms in an optical lattice setup to quantum simulate this system. We present exact diagonalization results to show the physical relevance of these models. In this context we study the spontaneous breaking of the chiral symmetry, its restoration at a finite baryon density, and dynamical phenomena such as the expansion of a chirally restored hot-spot in a chiral broken vacuum.

Contents

Part I.

Non-Trivial θ-Vacuum Effects in the 2-d $O(3)$ Model

Chapter 1.

Introduction

In the first part of this thesis, we investigate θ-vacuum effects in the $O(3)$ model in two space-time dimensions. This models serves as a toy model for QCD – the theory of the strong interaction. The 2-d $O(3)$ model shares important features with QCD: both theories are asymptotically free (see section 6.2). They both have a massgap, which is generated non-perturbatively. This implies that the massgap can not be studied using perturbation theory but can only be computed, for example, when studying the theory on a lattice. In addition, in both theories one can define a topological charge, which gives rise to distinct topological sectors in configuration space. Configurations that carry a non-trivial topological charge, while minimizing the action of the theory are called instantons. The topological charge allows to introduce a θ-vacuum term, which breaks both parity and charge conjugation symmetry. Both theories undergo a mechanism known as dimensional transmutation, where a theory with only dimensionless parameters acquires a dimensionful scale due to quantization.

The $O(3)$ model is a special case of the $\mathbb{C}P(N-1)$ models [1, 2], since it is equivalent to the $\mathbb{C}P(1)$ model. In these more general models one also observes asymptotic freedom, a non-perturbatively generated mass gap, dimensional transmutation, as well as instanton configurations. Therefore the study of a θ-vacuum angle is also possible. Except for the $\mathbb{C}P(1)$ model, these models are not exactly solvable, but can be studied on a lattice using Monte Carlo methods. Berg and Lüscher came up with a geometric definition of the topological charge on a lattice [3].

On the other hand, the $O(3)$ model is also a special case of the $O(N)$ models, which are asymptotically free theories for $N \geq 3$. These models have a non-perturbatively generated mass gap, but have no instanton configurations, except for the $O(N)$ model in $N-1$ dimensions. These models are exactly solvable in two space-time dimensions [4].

In this sense the 2-d $O(3)$ model is very special, since it is an $O(N)$ model, which allows the introduction of a θ angle. Additionally it is the only $\mathbb{C}P(N-1)$ model that can be solved analytically, at least for $\theta = 0$ and $\theta = \pi$, whereas for other values of θ the model is not integrable [5]. The analytic studies are based on the exact S-matrix theory [6]. For $\theta = 0$, this theory predicts a mass gap $m(\theta = 0) = \frac{8}{e}\Lambda_{\overline{MS}}$ [7], which is generated non-perturbatively. At $\theta = \pi$ a massless theory is predicted, which reduces to the $k = 1$ Wess–Zumino–Novikov–Witten (WZNW) model [8–10] at low energies. This conformal model

describes the interaction of a matrix-valued field $U(x) \in SU(2)$ by the action

$$\begin{aligned} S =& \frac{1}{2g^2} \int \mathrm{d}^2x \ \mathrm{Tr}(\partial_\mu U^\dagger(x) \partial_\mu U(x)) \\ & - \frac{ik}{12\pi} \int_{B^3} \mathrm{d}^3x \ \varepsilon_{\mu\nu\rho} \ \mathrm{Tr}((U(x)^\dagger \partial_\mu U(x))(U(x)^\dagger \partial_\nu U(x))(U(x)^\dagger \partial_\rho U(x))), \end{aligned} \tag{1.1}$$

where the second integration extends over half of a 3-ball, whose border is identified with the compactified two-dimensional space-time.

The 2-d $O(3)$ model with a θ-angle also finds applications in condensed matter physics. A $(1+1)$-d antiferromagnetic quantum spin chain is described by the Hamiltonian

$$H = J \sum_{\langle xy \rangle} \vec{S}_x \cdot \vec{S}_y, \tag{1.2}$$

where the sum goes over all nearest neighbor spin pairs $\langle xy \rangle$ and $\vec{S}_x$ are quantum spin operators satisfying the $SU(2)$ algebra $[S_x^a, S_y^b] = i\delta_{xy}\varepsilon_{abc}S_x^c$. The representation of the spins can be chosen as $S = 1/2, 1, 3/2, \ldots$ Haldane conjectured that such a quantum spin chain has a gap for integer spins S and is gapless for half-integer spins S [11]. It was already known for a long time that for spin $S = 1/2$ the mass gap vanishes [12]. This model can be described by the 2-d $O(3)$ model as a low-energy effective theory with $1/g^2 = S/2$ and where an integer quantum spin chain corresponds to $\theta = 0$ and half-integer spins correspond to $\theta = \pi$.

The exact S-matrix theory can be used to predict quantities even for systems in a finite volume. Balog and Hegedűs [13] provided a prediction for the so-called step scaling function, which was introduced by Lüscher, Weisz, and Wolff [14]. The step scaling function describes the scaling behavior of a renormalized coupling in a finite volume. This allowed to confirm Haldane's conjecture numerically for $\theta = 0$ [15] and within statistical errors also for $\theta = \pi$ [16].

It is easy to show that the action $S[\vec{e}]$ of the 2-d $O(3)$ model (see next section) satisfies the so-called Schwarz inequality

$$S[\vec{e}] \geq \frac{4\pi}{g^2} |Q[\vec{e}]|, \tag{1.3}$$

where $Q[\vec{e}]$ is the topological charge of a configuration $[\vec{e}]$. When implementing this model on the lattice, depending on the action, one may encounter field configurations with non-zero topological charge $Q[\vec{e}]$ that violate the Schwarz inequality. These configurations are known as dislocations. When the action of a dislocation is less than a critical value, a semi-classical argument suggests that the topological susceptibility $\chi_t = \langle Q^2 \rangle / V$ should suffer from an ultra-violet power-law divergence in the continuum limit [17]. On the other hand, it is known that the topological susceptibility in the continuum is only logarithmically divergent, when removing the cut-off. Therefore the observation of a power-law divergence, when using the lattice action, would question the continuum limit of the topological susceptibility. In $\mathbb{C}P(N-1)$ models with $N \geq 3$, this problem does, however, not arise. In the $\mathbb{C}P(2)$ model one can use a modified lattice action [2] to avoid the dislocation problem. In the $\mathbb{C}P(1)$ model (i.e. the $O(3)$ model) using the standard action and the geometric definition of the topological charge [3] the semi-classical argument [17] suggests a power-law divergence of χ_t. Using so-called classically perfect lattice action [18] it possible to remove dislocations by a

delicate fine-tuning. However, it was shown in [19] that the dislocations do not spoil the continuum limit of the topological susceptibility. In this work Bietenholz et. al. have also used a so-called topological action, were all allowed configurations have zero action. Even for this case they observed that the topological susceptibility diverges only logarithmically. As we will see later, even when introducing a non-zero θ-vacuum, the dislocation problem does not spoil the continuum limit. Therefore it does not prevent θ from being physically relevant.

In this work we will use different lattice actions to confirm the exact S-matrix results. Besides the standard action, we use a topological action [19], which constrains the maximal angle between neighboring spins. This action is invariant under small field deformations. Although it does not have the correct naive continuum limit and it violates the Schwarz inequality, we found that this action still yields the correct quantum continuum limit [20,21]. In addition, we combined this action with the standard action and thereby eliminated the lattice spacing effects almost entirely. These optimized actions have also been studied intensively in [22].

In this thesis, we investigate the continuum limit of the step scaling function in the 2-d $O(3)$ model for different θ-vacua. For $\theta > 0$, the system suffers from a sign problem. To obtain high precision Monte-Carlo data, we use a modified Hasenbusch improved estimator [23, 24]. Since we find a different continuum value of the step scaling function for each value of θ, we can conclude that θ indeed is a relevant parameter of the theory which does not get renormalized non-perturbatively. Furthermore, we confirm the result of the conjectured exact S-matrix theory at $\theta = \pi$ [25] with unprecedented precision. For the first time, this numerically confirms the conjectured exact S-matrix of the 2-d $O(3)$ model at $\theta = \pi$ [4] beyond any reasonable doubt. This also confirms the existence of a conformal fixed point at $\theta = \pi$, where the model reduces to the WZNW model at low energies.

This study has been a basis for further investigations to demonstrate walking near the conformal fixed point close to $\theta \approx \pi$ [26]. The essential features of walking technicolor models are shared by this toy model and can be accurately investigated by numerical simulations.

This part of the thesis is organized as follows. We first introduce the 2-d $O(3)$ model in chapter 2, where we also discuss the different actions and the observables, including the step scaling function. In chapter 3 we explain the numerical techniques including Monte Carlo methods, the cluster algorithm [27], and how to handle the sign problem using a modified Hasenbusch estimator. We finish in chapter 4, where we present results of the Monte Carlo simulations.

Chapter 2.

2-d $O(3)$ Model with a θ-Vacuum Angle

2.1. Continuum Theory

Let us write down the action of the 2-d $O(3)$ model in the continuum, which is defined as

$$S[\vec{e}] = \frac{1}{2g^2} \int \mathrm{d}^2x \; \partial_\mu \vec{e}(x) \cdot \partial_\mu \vec{e}(x), \tag{2.1}$$

where g^2 is the coupling constant and $\vec{e}(x)$ is a three-component field of unit-vectors $\vec{e}(x) \in S^2$. The space-time index μ runs over one spacial and one temporal direction, which are treated equally since we are working in Euclidean time. This theory can be quantized using the path integral formalism which leads to the partition function

$$Z = \int \mathcal{D}\vec{e} \exp(-S[\vec{e}]). \tag{2.2}$$

This model has a global $O(3)$ symmetry, which rotates all spins with the same rotation matrix $R \in O(3)$:

$$O(3): \qquad \vec{e}_x \quad \longrightarrow \quad \vec{e}_x{}' = R \; \vec{e}_x \tag{2.3}$$

In addition, we find the discrete global symmetries:

$$\begin{aligned} C: \qquad & \vec{e}_x \quad \longrightarrow \quad \vec{e}_x{}' = -\vec{e}_x, \\ P: \qquad & \vec{e}_{x_1,x_2} \quad \longrightarrow \quad \vec{e}\,'_{x_1,x_2} = \vec{e}_{-x_1,x_2}. \end{aligned} \tag{2.4}$$

The C-symmetry is an element of the $O(3)$ symmetry group.

One can define a topological charge

$$Q[\vec{e}] = \frac{1}{8\pi} \int \mathrm{d}^2x \; \varepsilon_{\mu\nu} \; \vec{e} \cdot (\partial_\mu \vec{e} \times \partial_\nu \vec{e}) \in \mathbb{Z}, \tag{2.5}$$

which is an integer number that describes how many times the sphere S^2 gets covered by $\vec{e}(x)$, when x is integrated over space-time. This quantity gives rise to topologically non-trivial field configurations. A special field configuration are the so-called instantons, which have a non-zero topological charge $Q[\vec{e}]$ and minimize the action $S[\vec{e}]$. From the definition of the action and the topological charge, one can immediately see that the integral

$$I = \int \mathrm{d}^2x \; (\partial_\mu \vec{e} \pm \varepsilon_{\mu\nu} \vec{e} \times \partial_\nu \vec{e})^2 = 4g^2 S[\vec{e}] \pm 16\pi Q[\vec{e}] \geq 0, \tag{2.6}$$

which immediately implies the Schwarz inequality

$$S[\vec{e}] \geq \frac{4\pi}{g^2}|Q[\vec{e}]|. \tag{2.7}$$

Instantons saturate this inequality. Therefore one can read of the (anti)self-duality equation of the instantons in equation (2.6)

$$\partial_\mu \vec{e} = \pm\varepsilon_{\mu\nu}\vec{e} \times \partial_\nu \vec{e}. \tag{2.8}$$

Because of the presence of non-trivial topological sectors, we can define a θ-dependent partition function as

$$Z(\theta) = \int \mathcal{D}\vec{e}\, \exp(-S[\vec{e}])\, \exp(i\theta Q[\vec{e}]). \tag{2.9}$$

It can be seen that the symmetry transformations do not leave the topological charge invariant:

$$\begin{aligned} C: \quad & Q[\vec{e}_x] \quad \longrightarrow \quad -Q[\vec{e}_x], \\ P: \quad & Q[\vec{e}_x] \quad \longrightarrow \quad -Q[\vec{e}_x]. \end{aligned} \tag{2.10}$$

If the θ parameter is not $\theta = 0, \pi$ it breaks the C and P symmetry, which is analogous to the θ-vacuum angle in QCD [28, 29]. The aim of this part of the thesis is to show that the parameter θ is indeed a relevant parameter of the theory, which means that it does not get renormalized non-perturbatively. We will show numerically that for each value of θ there exists a different continuum theory.

2.2. Lattice Implementation

To treat the 2-d $O(3)$ model in perturbation theory, one has to work with a small coupling g. Because this is not always the case, we have to use a non-perturbative method to study this model. We therefore discretize space-time on a lattice, which implies that the field $\vec{e}(x)$ is defined on the sites of the lattice $x_\mu = a(n_1, n_2)$, where a is the lattice spacing and n_μ are integer coordinates (see figure 2.1). To keep this in mind, we denote the position as a subscript to the field variables $\vec{e}_x$.

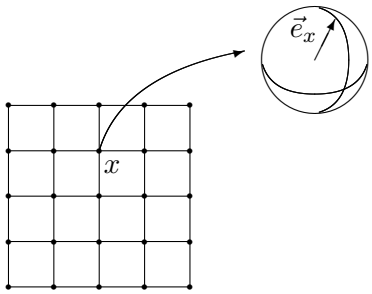

FIGURE 2.1.: In discretized space-time, $\vec{e}_x \in S^2$ is defined on the sites x of the lattice.

One can eliminate the lattice cut-off by taking the so-called continuum limit, which means that one sends the lattice spacing $a \to 0$ to zero in units of a fixed physical correlation length.

The continuum action (2.1) can be discretized by replacing derivatives with finite differences $\partial_\mu \vec{e} \to \frac{1}{a}(\vec{e}_{x+\hat{\mu}} - \vec{e}_x)$

$$S_{\text{standard}}[\vec{e}] = -\frac{1}{g^2} \sum_{\langle xy \rangle} \vec{e}_x \cdot \vec{e}_y, \tag{2.11}$$

where the sum goes over all neighboring sites $\langle xy \rangle$. This is the so-called standard action. In the next section we will also introduce topological actions.

The partition function is again

$$Z = \int \mathcal{D}\vec{e}\, \exp(-S[\vec{e}]), \quad \text{with} \quad \int \mathcal{D}\vec{e} = \left(\prod_x \int_{S^2} \mathrm{d}\vec{e}_x \right). \tag{2.12}$$

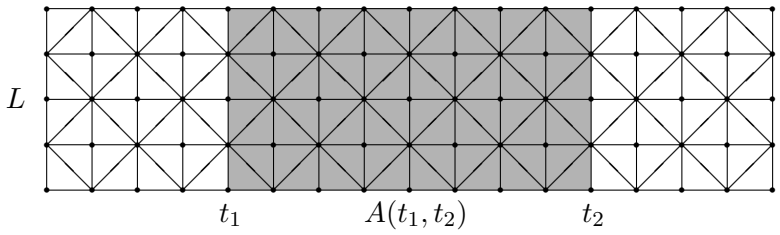

Figure 2.2.: *Triangulated square lattice: the triangles $\langle xyz \rangle$ in the shaded area $A(t_1, t_2)$ carry the topological term $i\theta q_{\langle xyz \rangle}$.*

Also the topological charge $Q[\vec{e}]$ can be implemented in a discretized space-time. In order to do so, we triangulate the lattice as shown in figure 2.2. To each of the triangles $\langle xyz \rangle$, we associate an oriented area $A_{\langle xyz \rangle} = 4\pi q_{\langle xyz \rangle} \in [-2\pi, 2\pi]$ on the sphere S^2, defined by $\vec{e}_x$, $\vec{e}_y$, and $\vec{e}_z$, as it is shown in figure 2.3. If we sum up the normalized areas $q_{\langle xyz \rangle}$ of all triangles, taking into account their orientation, we obtain the topological charge [3]

$$Q[\vec{e}] = \sum_{\langle xyz \rangle} q_{\langle xyz \rangle}. \tag{2.13}$$

Using this definition, the topological charge is again an integer, as long as we sum over all triangles in a periodic space-time lattice. The normalized area $q_{\langle xyz \rangle} \in [-\frac{1}{2}, \frac{1}{2}]$ of one single triangle $\langle xyz \rangle$ can be calculated as

$$R\mathrm{e}^{2\pi i q_{\langle xyz \rangle}} = 1 + \vec{e}_x \cdot \vec{e}_y + \vec{e}_y \cdot \vec{e}_z + \vec{e}_z \cdot \vec{e}_x + i\vec{e}_x \cdot (\vec{e}_y \times \vec{e}_z), \quad R \geq 0. \tag{2.14}$$

Because of the presence of non-trivial topological sectors, we can again define a θ-dependent partition function as

$$Z(\theta) = \int \mathcal{D}\vec{e}\, \exp(-S[\vec{e}])\, \exp(i\theta Q[\vec{e}]), \tag{2.15}$$

where $Q[\vec{e}]$ is now the topological charge defined on the lattice.

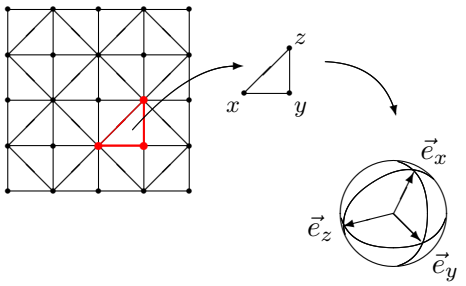

FIGURE 2.3.: Definition of the oriented area $A_{\langle xyz\rangle}$, which gets associated with the triangle $\langle xyz\rangle$.

2.3. Topological and Optimized Constraint Lattice Actions

Besides the standard action we also consider the topological action, that has been introduced in [19]

$$S_{\text{topological}}[\vec{e}] = \sum_{\langle xy\rangle} s(\vec{e}_x, \vec{e}_y), \qquad s(\vec{e}_x, \vec{e}_y) = \begin{cases} 0 & \text{for } \vec{e}_x \cdot \vec{e}_y > \cos\delta \\ \infty & \text{else} \end{cases} . \tag{2.16}$$

Here, we have introduced the maximally allowed angle δ, which plays the role of the coupling constant. The topological action only allows configurations for which the angle between the field variables on neighboring sites x and y is smaller than δ ($\vec{e}_x \cdot \vec{e}_y > \cos\delta$). Otherwise the action is infinite, which means that the corresponding configurations are not allowed. All allowed configurations have the same action $S_{\text{topological}}[\vec{e}] = 0$. As a consequence, this lattice model does not have the correct classical continuum limit, it violates the Schwarz inequality (1.3) between action and topological charge, and it cannot be treated in perturbation theory. Despite these various deficiencies this action still has the correct quantum continuum limit [19].

As will be shown later, the standard action approaches the continuum limit of the step scaling function from above while the topological action approaches it from below. Therefore we combine these two actions in order to reduce the cut-off effects. This we do with an optimized constraint action

$$S_{\text{constraint}}[\vec{e}] = \sum_{\langle xy\rangle} s'(\vec{e}_x, \vec{e}_y), \qquad s'(\vec{e}_x, \vec{e}_y) = \begin{cases} -\frac{1}{g^2}\ \vec{e}_x \cdot \vec{e}_y & \text{for } \vec{e}_x \cdot \vec{e}_y > \cos\delta \\ \infty & \text{else} \end{cases} . \tag{2.17}$$

Here g^2 is again the coupling constant, while δ is a fixed parameter that is tuned to a value which minimizes the cut-off effects. For $\delta = \pi$ the optimized constraint action reduces to the standard action (2.11). On the other hand, if we send $g^2 \to \infty$, we obtain the topological action (2.16).

2.4. Observables

2.4.1. Physical Mass

A standard quantity to measure is the physical mass $m = m(L;\theta)$, which depends on the vacuum angle θ and on the extent L of the lattice in the spatial direction. It can be extracted from the correlation function $C(t_1, t_2; \theta) = \langle \vec{E}(t_1) \cdot \vec{E}(t_2) \rangle_\theta$, which measures the correlation of the averaged spins $\vec{E}$ between two time-slices t_1 and t_2. The averaged spin of one time-slice is defined as

$$\vec{E}(t) = \frac{1}{L} \sum_{x_1} \vec{e}_{(x_1,t)}, \tag{2.18}$$

where $t = x_2$. With this, the correlation function reads

$$C(t_1, t_2; \theta) = \langle \vec{E}(t_1) \vec{E}(t_2) \rangle_\theta = \frac{1}{Z(t_1, t_2; \theta)} \int \mathcal{D}\vec{e}\ \vec{E}(t_1) \cdot \vec{E}(t_2)\ \exp\left(-S[\vec{e}] + i\theta Q(t_1, t_2)\right). \tag{2.19}$$

For technical reasons (see section 3.3) we work with open boundary conditions in the temporal direction and introduce the topological charge $Q(t_1, t_2)$ between the time-slice t_1 and t_2, which is in general a non-integer number. This topological charge $Q(t_1, t_2)$ is the sum of the areas $q_{\langle xyz \rangle}$ corresponding to the triangles that are highlighted in gray in figure 2.3. We also have defined a variant of the partition function as

$$Z(t_1, t_2; \theta) = \int \mathcal{D}\vec{e}\ \exp\left(-S[\vec{e}] + i\theta Q(t_1, t_2)\right). \tag{2.20}$$

For a large separation in time $|t_1 - t_2|$, we expect an exponential fall-off of the correlation function

$$C(t_1, t_2; \theta)\ \sim\ \exp(-m(L;\theta)(t_2 - t_1)), \tag{2.21}$$

from which the mass $m(L;\theta)$ can then be extracted. This requires the lattice to be sufficiently large in the temporal direction. We usually choose $L_t = 10L$. To obtain an estimator for the mass, we calculate the effective mass $m_{\text{eff}}(t)$, which is defined as

$$m_{\text{eff}}(t) = -\log\left(\frac{C(t+1)}{C(t)}\right), \tag{2.22}$$

where $C(t) = \sum_{t_1} C(t_1 + t, t_1; \theta)$ is the averaged correlation function over a certain range of time t_1, which should not get too close to the end of the temporal extent. To calculate the mass $m(L;\theta)$, we average $m_{\text{eff}}(t)$ for sufficiently large t, weighted it by its jackknife error.

In the infinite volume limit $L \to \infty$ the mass is known analytically from the S-matrix theory [4]. For a vanishing θ parameter we have $m(L \to \infty; \theta = 0) = \frac{8}{\mathrm{e}} \Lambda_{\overline{MS}}$, where e is the base of the natural logarithm and $\Lambda_{\overline{MS}}$ is the scale generated by dimensional transmutation in the modified minimal subtraction renormalization scheme. On the other hand, for $\theta = \pi$, one obtains a massless theory: $m(L \to \infty; \theta = \pi) = 0$.

2.4.2. Step Scaling Function

The exact S-matrix theory even predicts physical quantities, in partial the step scaling function, in a finite volume, which is well suited for comparison with numerical data. The step scaling function $\sigma(s, u_0; \theta)$ [14] is defined as follows. Let us choose a rescaling factor s and define the renormalized coupling u_0 as

$$u_0 = m(L; \theta)L. \tag{2.23}$$

Starting on a volume with spacial extent L, one adjusts the coupling g^2 in the action in order to obtain a certain value of the renormalized coupling u_0. Then, one measures the renormalized coupling $u_1 = m(L'; \theta)L'$ on the scaled volume with spacial extent $L' = sL$. Setting the rescaling factor $s = 2$ implies that we measure the quantity

$$\sigma(2, u_0; \theta) = 2m(2L; \theta)L\Big|_{m(L;\theta)L=u_0} \tag{2.24}$$

on a volume which has twice the spacial extent $L' = 2L$ than the original system.

The step scaling function tells us something about the finite-size effects of the system with volume L. For example, if the finite-size effects are very strong, we find that the step scaling function is almost identical to the renormalized coupling ($\sigma(2, u_0; \theta) \approx u_0$). This happens when the box L is small and the correlation length ($\xi = 1/m$) scales roughly with the volume. On the other hand, if finite-size effects are small, the mass is almost independent of the volume L and we find a doubling in the step scaling function ($\sigma(2, u_0; \theta) \approx 2u_0$).

The step scaling function in equation (2.24) is defined in the continuum, but can be generalized to a finite lattice spacing a. The step scaling function $\Sigma(2, u_0, a/L; \theta)$ then tells us how large the renormalized coupling u gets, if we double the volume in the spatial direction ($L \to 2L$), while keeping the lattice spacing a fixed. $\Sigma(2, u_0, a/L; \theta)$ is defined as

$$\Sigma(2, u_0, a/L; \theta) = 2m(2L/a; \theta)L\Big|_{m(L/a;\theta)L=u_0} \tag{2.25}$$

while choosing the coupling g such that $m(L/a; \theta)L = u_0$. In the continuum limit, this definition then corresponds to the step scaling function of equation (2.24)

$$\sigma(2, u_0; \theta) = \lim_{L\to\infty} \Sigma(2, u_0, a/L; \theta). \tag{2.26}$$

When calculating the error of the step scaling function, one has to take into account the error propagation from the uncertainty of the estimate of the coupling g and from the measurement of the masses themselves. This has been done carefully in [30] and is also used here.

The result of the step scaling function for $u_0 = 1.0595$ is known. For zero θ parameter it is $\sigma(2, u_0; \theta = 0) = 1.261210$ [13]. For $\theta = \pi$ it is $\sigma(2, u_0; \theta = \pi) = 1.231064$ [25].

Chapter 3.

Numerical Techniques

3.1. Monte Carlo Methods

3.1.1. Markov Chains and Importance Sampling

In order to calculate expectation values including the correlation function $C(t_1, t_2; \theta)$, we need to evaluate an integral over all possible spin configurations

$$\int \mathcal{D}\vec{e} = \left(\prod_x \int_{S^2} \mathrm{d}\vec{e}_x \right). \tag{3.1}$$

This integral can not be solved analytically. We therefore have to circumvent the integration. Let us set the θ parameter to zero for the moment (we will see how to handle non-zero values of θ in section 3.2 and in section 3.3).

The main idea of the Monte Carlo methods is the so-called importance sampling. This means that, instead of the exact integration, we just sum over certain configurations of this integral and average over them. The configurations $[\vec{e}^{(i)}]$ are chosen according to their probability $p[\vec{e}^{(i)}] = \exp(-S[\vec{e}^{(i)}])$ in order to obtain a correct distribution. Instead of calculating the expectation value as in its definition

$$\langle A \rangle = \frac{1}{Z} \int \mathcal{D}\vec{e}\ A[\vec{e}] \exp\left(-S[\vec{e}]\right) = \frac{1}{Z} \int \mathcal{D}\vec{e}\ A[\vec{e}]\ p[\vec{e}] \tag{3.2}$$

we approximate this integration by summing only over the "most important" configurations

$$\hat{A} = \frac{1}{N} \sum_{i=1}^{N} A[\vec{e}^{(i)}], \tag{3.3}$$

where we call $\hat{A}$ an estimate of $\langle A \rangle$. Here we have chosen a so-called Markov-chain of N configurations. These are N configurations, which are chosen to the their respective weight and labeled with the index (i). Of course, the larger we choose N, the more accurately we can estimate $\langle A \rangle$. If the different configurations in this sum are uncorrelated, one can estimate the mean deviation $\sigma_{\hat{A}}$ of the estimate $\hat{A}$ and the observable $\langle A \rangle$ using the standard deviation of $\hat{A}$ (called σ) as

$$\sigma_{\hat{A}}^2 = \left\langle \left(\hat{A} - \langle A \rangle \right)^2 \right\rangle = \frac{1}{N} \sigma^2. \tag{3.4}$$

Now we use an algorithm that chooses the configurations $[\vec{e}^{(i)}]$ with their correct probability $p[\vec{e}^{(i)}]$. Usually one generates many updates and measures the quantity $A[\vec{e}^{(i)}]$. But how do we get a new configuration $[\vec{e}^{(i+1)}]$ out of an arbitrary configuration $[\vec{e}^{(i)}]$? In order to follow importance sampling, it is best if this algorithm satisfies the following two rules:

Detailed balance: Each two configurations $[\vec{e}^{(i)}]$ and $[\vec{e}^{(i')}]$, have to satisfy detailed balance, which means that

$$p[\vec{e}^{(i)}]\ W([\vec{e}^{(i)}] \to [\vec{e}^{(i')}]) = p[\vec{e}^{(i')}]\ W([\vec{e}^{(i')}] \to [\vec{e}^{(i)}]), \tag{3.5}$$

where $W([\vec{e}^{(i)}] \to [\vec{e}^{(i')}])$ is the transition probability from configuration $[\vec{e}^{(i)}]$ to configuration $[\vec{e}^{(i')}]$. Detailed balance ensures the correct probability distribution in equilibrium because the probability of observing a certain configuration $[\vec{e}^{(i)}]$ is given by

$$\sum_j p[\vec{e}^{(j)}]W([\vec{e}^{(j)}] \to [\vec{e}^{(i)}]) = \sum_j p[\vec{e}^{(i)}]W([\vec{e}^{(i)}] \to [\vec{e}^{(j)}]) = p[\vec{e}^{(i)}], \tag{3.6}$$

where in the first step we have used detailed balance and in the second step we have used that $\sum_j W([\vec{e}^{(i)}] \to [\vec{e}^{(j)}]) = 1$.

Ergodicity: For any given configuration $[\vec{e}^{(i)}]$, the algorithm should be able to reach any other configuration $[\vec{e}^{(i')}]$ with a non-vanishing probability after a finite number of steps.

3.1.2. Metropolis Algorithm

Let us study the most simple algorithm, which obeys detailed balance and ergodicity, known as the Metropolis algorithm. After choosing a certain initial configuration $[\vec{e}^{(0)}]$ (e.g. a trivial one, with all spins aligned in the same direction, or each spin in a random direction), the algorithm runs through the following steps:

i. Pick a random site x and calculate a random rotation matrix R in the vicinity of the unit matrix $\mathbb{1}$.

ii. Rotate the spin at the site x using the rotation matrix R: $\vec{e}_x \to R\vec{e}_x$.

iii. Accept the new configuration $[\vec{e}^{(i+1)}]$ with a certain probability p_{acc}, otherwise undo the rotation R and continue with the previous configuration $[\vec{e}^{(i+1)}] = [\vec{e}^{(i)}]$.

iv. Go back to step 1.

The Metropolis acceptance probability is

$$p_{\text{acc}} = \min\left(1, \frac{p[\vec{e}_{i+1}]}{p[\vec{e}^{(i)}]}\right) \tag{3.7}$$

in order to satisfy detailed balance from equation (3.5). If the averaged acceptance rate is too low, one can choose the rotation matrix R to be closer to the unit matrix $\mathbb{1}$.

Since the probability $p[\vec{e}]$ is nothing else than the exponent of the action, this formula can be represented as

$$p_{\text{acc}} = \min\left(1, \exp(-\Delta S)\right), \tag{3.8}$$

where $\Delta S = S[\vec{e}_{i+1}] - S[\vec{e}^{(i)}]$. Even though $S[\vec{e}]$ depends on all spins of the lattice, ΔS only depends on the rotated spin and on its neighbors. This is a consequence of the fact that we have chosen a local (nearest neighbor) interaction. For the topological action the acceptance probability can only take two values: It is one if the new configuration (after the spin rotation) is allowed, and zero if not.

At the beginning of a simulation, this update algorithm is performed for a certain time without taking any measurements. The reason is that the initial configuration was a completely random or completely ordered one, which is a very unlikely configuration. We thus first have to wait for the system to equilibrate. After this equilibration time, we take measurements (in our case of the correlation function) after every sweep. A sweep is the proposition of N_V new configurations in the Markov chain, where N_V is the number of spins.

If the autocorrelation between two following measurements $A[\vec{e}_i]$ and $A[\vec{e}_{i+1}]$ (e.g. the correlation of the extracted masses of two consecutive measurements) is too big, we can measure the correlation function only after a multiple of sweeps.

This algorithm suffers from the so-called critical slowing down. This means that the larger the correlation length $\xi = \frac{1}{m}$ of the system gets, the longer it takes to obtain an uncorrelated new configuration.

3.1.3. Cluster Algorithm

In order to avoid critical slowing down, the Wolff cluster algorithm has been constructed in [27]. The idea is to update a large cluster of spins collectively instead of just a single spin. If the size of this cluster grows with the correlation length of the system, critical slowing down can be avoided.

A clusters $\mathcal{C}$ is a set of sites x and is constructed as follows. Let us first choose a plane, which is characterized by the vector $\vec{r}$, that is perpendicular to this plane. All the spins $\vec{e}_x$ at sites x, which belong to the cluster $x \in \mathcal{C}$, are then reflected on this plane

$$\vec{e}_x \quad \longrightarrow \quad \vec{e}_x{}' = \vec{e}_x - 2(\vec{e}_x \cdot \vec{r})\vec{r}. \tag{3.9}$$

Under this cluster flip, the change of the action ΔS gets the following contributions. If two sites x and y belong to the cluster $\mathcal{C}$ they do not contribute to a change of the action ΔS under a spin flip, since $\vec{e}_x{}' \cdot \vec{e}_y{}' = \vec{e}_x \cdot \vec{e}_y$. The same is true if both sites do not belong to the cluster. ΔS only gets a contribution, if one site x belongs to the cluster $\mathcal{C}$ and one site y does not. For example, for the standard action the contribution to ΔS is

$$\Delta S = s(\vec{e}_x{}', \vec{e}_y) - s(\vec{e}_x, \vec{e}_y) + (\text{contributions of other links}) = \frac{1}{g^2} 2(\vec{e}_x \cdot \vec{r})(\vec{e}_y \cdot \vec{r}) + \dots \tag{3.10}$$

In order to obey detailed balance, the clusters are formed according to the following rules:

i. Choose a site x at random, add it to the cluster $\mathcal{C}$.

ii. Add all links $\langle xy \rangle$ connecting x with one of its neighbors y to a list ℓ.

iii. Pick the first link $\langle xy \rangle$ of the list ℓ that has not yet been checked.

iv. The link $\langle xy \rangle$ is "activated" with probability

$$p_{\text{bond}} = \max\left(0, 1 - \exp\left(s(\vec{e}_x\,', \vec{e}_y) - s(\vec{e}_x, \vec{e}_y)\right)\right). \tag{3.11}$$

The link $\langle xy \rangle$ is marked as being checked. If the link has not been activated, go back to step iii.

v. If the link $\langle xy \rangle$ has been activated, make sure that both ends x and y belong to the cluster $\mathcal{C}$. If one of the ends did not belong to the cluster before, also add all links connecting the site with its neighbors to the list ℓ. Go back to step iii.

vi. If all links in ℓ are marked as checked, the construction of the cluster is completed.

Note that for the topological action, the bond probability p_{bond} only takes the values 1 or 0.

This cluster algorithm also allows the usage of an improved cluster-estimator of the correlations function. In this thesis, however, we will use another estimator, which is discussed in section 3.3.

3.2. Sign Problem

As soon as we incorporate a non-zero θ parameter, we encounter the so-called sign problem, when performing a Monte Carlo simulation. The reason is that we have interpreted the exponent $\exp(-S[\vec{e}])$ as a weight $p[\vec{e}]$ of a certain configuration $[\vec{e}]$. Since the action $S[\vec{e}]$ is a real-valued function, we always find positive weights $p[\vec{e}]$. If θ is non-zero, the exponent acquires the complex term involving the topological charge $Q[\vec{e}]$ and an expectation value of an observable A has to be calculated as

$$\langle A \rangle_\theta = \frac{1}{Z(\theta)} \int \mathcal{D}\vec{e}\; A[\vec{e}] \exp\left(-S[\vec{e}] + i\theta Q[\vec{e}]\right). \tag{3.12}$$

This exponent can not serve as a weight anymore and we have to find another solution to sample configurations in a Monte Carlo simulation.

For moderate volumes, as the ones investigated here, a possible solution is the so-called reweighting technique [31]. The idea is to sample different configurations, as if θ would be zero, and to shift the complex phase from the topological term in the observable. This is based on the fact that we can express the estimator of the observable A at θ as

$$\langle A \rangle_\theta = \frac{1}{Z(\theta)} \int \mathcal{D}\vec{e}\; A[\vec{e}] \exp\left(i\theta Q[\vec{e}]\right) \exp\left(-S[\vec{e}]\right) = \frac{1}{Z(\theta)} \int \mathcal{D}\vec{e}\; A[\vec{e}] \exp\left(i\theta Q[\vec{e}]\right) p[\vec{e}], \tag{3.13}$$

where again we have chosen $p[\vec{e}] = \exp\left(-S[\vec{e}]\right)$ as if θ would be zero. The partition function can be expressed as

$$Z(\theta) = \int \mathcal{D}\vec{e} \exp(i\theta Q[\vec{e}]) \exp(-S[\vec{e}]) = \int \mathcal{D}\vec{e} \exp(i\theta Q[\vec{e}]) p[\vec{e}] = \langle \exp\left(i\theta Q[\vec{e}]\right) \rangle_0, \tag{3.14}$$

where we have added the subscript $\langle\rangle_0$ to the expectation value to indicate a sampling, which is independent of θ. In this way the expectation value of A can be written as

$$\langle A \rangle_\theta = \frac{\langle A[\vec{e}] \exp\left(i\theta Q[\vec{e}]\right) \rangle_0}{\langle \exp\left(i\theta Q[\vec{e}]\right) \rangle_0}. \tag{3.15}$$

This means that in a Monte Carlo simulation, one updates the configurations $[\vec{e}]$ according to the weights $p[\vec{e}]$ and measures the two quantities $A[\vec{e}]\exp(i\theta Q[\vec{e}])$ and $\exp(i\theta Q[\vec{e}])$ independently. At the end, one averages these two quantities and builds the ratio, which serves as an estimator for the observable A.

In order to estimate the correlation function, we perform exactly this procedure

$$C(t_1,t_2;\theta)=\frac{\left\langle\left(\vec{E}(t_1)\cdot\vec{E}(t_2)\right)\ \exp(i\theta Q(t_1,t_2))\right\rangle_{\theta=0}}{\langle\exp(i\theta Q(t_1,t_2))\rangle_{\theta=0}}=\frac{C(t_1,t_2,0)Z(t_1,t_2,\theta)/Z(0)}{Z(t_1,t_2,\theta)/Z(0)}. \quad (3.16)$$

We have used the topological charge $Q(t_1,t_2)$ between the time-slice t_1 and t_2.

The problem of the reweighting technique is that it suffers from a poor signal-to-noise ratio, because we have a complex phase in the observable which cancels out large parts of the signal. In order to improve the statistics one needs an exponential amount of computer time as a function of the space-time volume.

3.3. Hasenbusch's Improved Estimator

To obtain high accuracy data, despite the sign problem, we use an improved estimator, first proposed by Hasenbusch in [23], which was further developed in [24]. In this work this algorithm is adjusted to address the sign-problem in a system with a non-zero θ parameter.

The original idea [23] is to explicitly integrate out certain rotational degrees of freedom. One rotates all spins after the time-slice t with a rotation matrix $X(t)\in SO(3)$

$$X(t):\ \vec{e}_{(x,t')}\quad\longrightarrow\quad X(t)\vec{e}_{(x,t')}\qquad\text{for all } t'>t. \quad (3.17)$$

Using open boundary conditions in the temporal direction, the contributions to the action $S[\vec{e}]$ and the topological charge $Q[\vec{e}]$ only change on the links between the time-slice t and $t+1$. In order to improve the estimator of the correlation function, one inserts such a rotation on each time-slice and averages over all possible rotation matrices. The correlation of two time-slice averaged spins $\vec{E}(t_1)$ and $\vec{E}(t_2)$ can then be expressed as

$$\vec{E}(t_1)\cdot\vec{E}(t_2)\ \sim\ \vec{E}(t_1)\cdot\langle X(t_1+1)\rangle\langle X(t_1+2)\rangle\cdots\langle X(t_2)\rangle\vec{E}(t_2), \quad (3.18)$$

where

$$\langle X(t)\rangle=\int \mathrm{d}X(t)\exp\left(\mathrm{Tr}\left(X(t)Q(t)^T\right)\right), \quad (3.19)$$

and $\mathrm{d}X(t)$ is the Haar measure of $SO(3)$. The matrix $Q(t)$ is the contribution to the action originating from the links between time-slice t and $t+1$, which for the standard action reads

$$Q_{ij}(t)=\frac{1}{g^2}\sum_x e^i_{(x,t)}e^j_{(x,t+1)}. \quad (3.20)$$

Since the integration over $X(t)$ can not be done analytically, [23] suggests to do this statistically.

In [24] (see appendix E therein) the authors suggest to average only over four different rotation matrices X at each time-slice, which can be done analytically. These four matrices

all do not change the action. The improvement of this estimator of the correlation function is almost equally good as a statistical sampling of these matrices, but the computational effort is drastically reduced. The four matrices can be obtained by first diagonalizing the matrix $Q(t)$ using a singular value decomposition (SVD)

$$Q(t) = U(t)q(t)V(t), \tag{3.21}$$

where $q(t)$ is a diagonal matrix and $U(t)$ and $V(t)$ are the $SO(3)$ SVD-matrices. Equation (3.19) can then be expressed with a new integration variable Y with $X = UYV$ as

$$\langle X(t)\rangle = U(t)\langle Y(t)\rangle V(t), \qquad \text{and} \qquad \langle Y(t)\rangle = \int \mathrm{d}Y(t) \exp\left(\mathrm{Tr}\left(Y(t)q(t)^T\right)\right). \tag{3.22}$$

Note that a choice of $Y(t) = U(t)^T V(t)^T$ corresponds to $X(t) = \mathbb{1}$, which does not change the action, since the rotation of the spins is trivial. It can be seen that there are always four matrices Y_0, Y_1, Y_2, and Y_3, which have the same contribution to the integration in equation (3.22) and are related by

$$Y_1 = W_1^T Y_0 W_1, \qquad Y_2 = W_2^T Y_0 W_2, \qquad Y_3 = W_3^T Y_0 W_3, \tag{3.23}$$

where $W_i \in SO(3)$ are orthogonal matrices with

$$W_1 = \begin{bmatrix} 1 & & \\ & -1 & \\ & & -1 \end{bmatrix}, \quad W_2 = \begin{bmatrix} -1 & & \\ & 1 & \\ & & -1 \end{bmatrix}, \quad W_3 = \begin{bmatrix} -1 & & \\ & -1 & \\ & & 1 \end{bmatrix}. \tag{3.24}$$

Since the four Y_i matrices have the same contribution to the integral, we can just average over these matrices. This average $\frac{1}{4}(Y_0 + Y_1 + Y_2 + Y_3) = (Y_0)_{\mathrm{diag}}$ is the diagonal part of the matrix Y_0. Choosing $Y_0 = U(t)^T V(t)^T$, we calculate an average over X_i matrices, where $X_0 = U(t)U(t)^T V(t)^T V(t) = \mathbb{1}$, $X_1 = U(t)W_1^T U(t)^T V(t)^T W_1 V(t)$, $X_2 = U(t)W_2^T U(t)^T V(t)^T W_2 V(t)$, $X_3 = U(t)W_3^T U(t)^T V(t)^T W_3 V(t)$. We thus end up with an estimator, which comes close to Hasenbusch's original estimator

$$\langle X(t)\rangle \;\approx\; U(t)(U(t)^T V(t)^T)_{\mathrm{diag}} V(t). \tag{3.25}$$

To incorporate a non-zero value of θ one includes the θ term in the sum of the Y matrices. This sum turns out to be

$$\tilde{X}(t) = \sum_i X_i(t) \;\exp\left(i\theta Q\left(t, t+1, X_i\left(t\right)\right)\right), \tag{3.26}$$

where $Q(t, t+1, X_i(t))$ is the topological charge after all the spins $\vec{e}_{(x,t')}$ for $t' > t$ have been rotated with the rotation matrix $X_i(t)$. With this, we obtain improved estimators as

$$\begin{aligned} \left(\vec{E}(t_1)\cdot\vec{E}(t_2)\right)\; \exp(i\theta Q(t_1,t_2)) \;&\sim\; \vec{E}(t_1)\;\tilde{X}(t_1+1)\;\tilde{X}(t_1+2)\cdots\tilde{X}(t_2)\;\vec{E}(t_2) \\ \exp(i\theta Q(t_1,t_2)) \;&\sim\; \Big(\sum_i \mathrm{e}^{i\theta Q(t_1,t_1+1,X_i(t_1+1))}\Big)\cdots\Big(\sum_i \mathrm{e}^{i\theta Q(t_2-1,t_2,X_i(t_2))}\Big) \end{aligned} \tag{3.27}$$

Note that this is just an improved estimator and it does not interfere with the update of the configurations. It can thus not help against critical slowing down. The reason why we are able to estimate high-precision data is that the sign problem is only mild.

Chapter 4.

Numerical Results

4.1. Cut-Off Effects

The 2-d $O(3)$ model has been simulated using Monte Carlo methods (see section 3.1). We compared different lattice actions: the standard action (see section 2.2), the topological action, and constrained action (see section 2.3). To update, we used the cluster algorithm (see section 3.1.3) and to improve the estimator of the correlation function we used Hasenbusch's improved estimator (see section 3.3). After extracting the mass of the correlation function (see section 2.4.1) we calculated the step scaling function (see section 2.4.2). We used lattice sizes up to $L/a = 64$ with $L_t = 10L$ and open boundary conditions in the temporal direction.

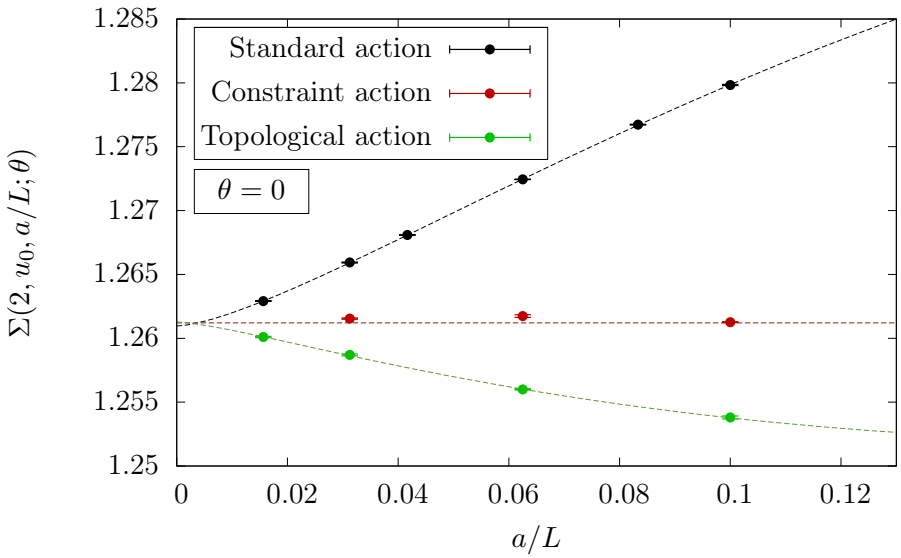

Figure 4.1.: Cut-off dependence of the step scaling function $\Sigma(2, u_0 = 1.0595, a/L; \theta = 0)$ for three different lattice actions: the standard action, the topological lattice action, and the optimized constraint action with $\cos\delta = -0.345$. The fits are based on equation (4.1). The horizontal line represents the analytic continuum results [13].

First, we compare the cut-off behavior of the different lattice actions. It is remarkable that for the standard action the cut-off effects of the step scaling function $\Sigma(2, u_0, a/L; \theta)$ are

known analytically for $\theta = 0$ [32]:

$$\Sigma(2, u_0, a/L; \theta = 0) = \sigma(2, u_0; \theta = 0) + \frac{a^2}{L^2} \left[B \log^3(L/a) + C \log^2(L/a) + \dots \right], \tag{4.1}$$

where B and C are fit parameters and L/a is the number of lattice points in the spatial direction.

By measuring the step scaling function on different lattice sizes L/a, we plot the cut-off behavior of the different lattice actions as it is done in figure 4.1. The curves for the standard action and for the topological action are fits of the function (4.1), where σ, A, and B are fit parameters.

For $\theta = 0$ the continuum limit (horizontal line) is predicted by the exact S-matrix theory to be at $\sigma(2, u_0 = 1.0595; \theta = 0) = 1.2612103$ [13]. As one can see, the standard action approaches this continuum limit from above, while the topological action approaches the continuum limit from below. The maximum angle δ of the constraint action is tuned to the continuum value at a lattice size $L/a = 10$ and takes an optimal value at $\cos(\delta) = -0.345$. Even for finer lattices the cut-off effects of the constraint action are remarkably small and only at the per mill level.

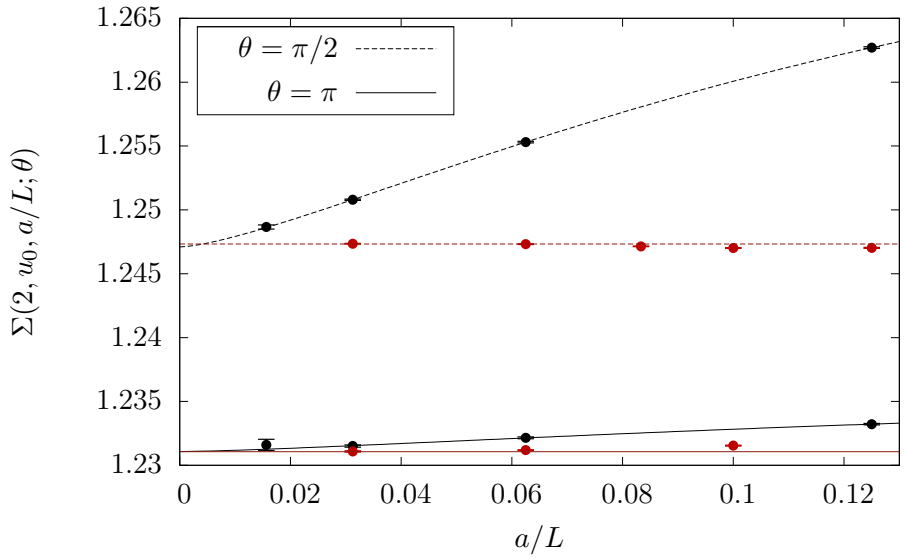

FIGURE 4.2.: Cut-off dependence of the step scaling function $\Sigma(2, u_0 = 1.0595, a/L; \theta)$ for the standard action (black) and the optimized constraint action (red) with $\cos\delta = -0.345$, as well as for $\theta = \frac{\pi}{2}, \pi$. The fits are based on equation (4.1). The horizontal lines represent the analytic continuum results for $\theta = \pi$ [25], and the fitted continuum value for $\theta = \frac{\pi}{2}$.

These calculations have also been performed for $\theta = \pi/2$ and $\theta = \pi$, which is shown in figure 4.2. At $\theta = \pi$ the exact S-matrix theory again predicts a continuum result (horizontal line) of $\sigma(2, u_0 = 1.0595; \theta = \pi) = 1.231064$ [25]. This result is confirmed by extrapolating the results obtained with the standard action or the constraint action. For the constraint action,

we still use the maximal angle δ, which has been tuned at $\theta = 0$. Also in this case the cut-off effects of the constraint action are extremely small.

For $\theta = \pi/2$, we do not have an analytic prediction of the continuum limit and we do not know whether the function (4.1) is still applicable to describe the cut-off effects. Nevertheless, we fit this function to the cut-off effects of the standard action, which gives a small χ^2/d.o.f. Extrapolating to the continuum limit agrees with an estimator of the continuum limit for the constraint action (horizontal line). Again, the constraint action has a maximum angle constraint δ, which has been tuned at $\theta = 0$, but still shows an extremely good cut-off behavior.

4.2. Continuum Mass-Gap

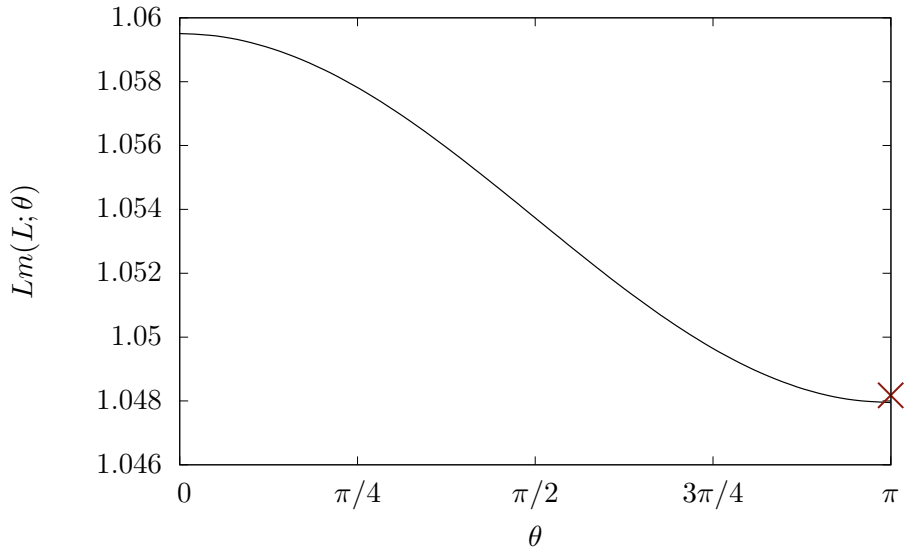

Figure 4.3.: The θ-dependent massgap $Lm(\theta, L)$ at $Lm(0, L) = 1.0595$ using the optimized constraint action for $L = 24a$, compared to the analytic result at $\theta = \pi$ [25] (cross).

Figure 4.1 and 4.2 also show that all continuum limits (at $\theta = 0, \pi/2, \pi$) are significantly different, which means that each value of θ indeed corresponds to a different theory. Hence θ is a relevant parameter that does not renormalize to 0 or π non-perturbatively, as one might have expected due to the presence of dislocations. This can also be seen in figure 4.3, where we plot $m(\theta, L)L$ as a function of θ, keeping the coupling fixed. For $\theta = 0$, we fix the value to $m(0, L)L = 1.0595$, at $\theta = \pi$ one obtains $m(\pi, L)L = 1.048175$ [25].

Chapter 5.

Conclusions and Outlook

We have studied different lattice actions in the 2-d $O(3)$ model. The constraint action combines the standard action with a topological action. The topological action restricts the maximal angle between neighboring spins and is thus invariant under small deformations of the field. In the constraint action this maximal angle is tuned in order to reduce the cut-off effects. Our results show that only a single tuning is necessary (at $L/a = 10,\ \theta = 0$) to once and for all fix this maximal angle. Other lattice sizes or other values of θ have extremely small cut-off effects of the step scaling function which all lie at the per mill level or beyond. An efficient modification of Hasenbusch's improved estimator allowed us to simulate at non-zero values of θ, where a sign problem arises, which, however, turns out to be mild.

We showed that the θ parameter in the 2-d $O(3)$ model is indeed a relevant parameter and does not get renormalized non-perturbatively. We found a different continuum limit for each value of θ (here shown for $\theta = 0, \pi/2, \pi$). Dislocations do not spoil this continuum limit even for $\theta \neq 0$. We confirmed the exact S-matrix conjecture for the step scaling function at $\theta = \pi$, which also implies that the model indeed reduces to the WZNW model at low energies.

A later work [26] has studied the physics of the 2-d $O(3)$ model close to $\theta \approx \pi$, where the physics of a slowly walking coupling has been studied.

We are currently extending the improved actions to gauge theories. Our approach is different from Symanzik's improvement program [33], where one parametrizes the cut-off effects in the framework of effective field theories. This often requires tuning of several parameters, which can be computationally expensive. In our case, we tune just one free parameter against a non-perturbative quantity in the continuum limit. In particular, we have implemented the improved actions for the $SU(2)$ and the $SU(3)$ pure gauge theory in order to drastically reduce cut-off effects. This project is expected to lead to a publication in the near future. It has the potential to significantly improve the accuracy of numerical simulations of QCD and other non-Abelian gauge theories.

Part II.

Quantum Simulation of Non-Abelian Lattice Gauge Theories

Chapter 6.

Introduction

6.1. Motivation

In this second part of the thesis we discuss the quantum simulation of non-Abelian lattice gauge theories. What is actually a non-Abelian gauge theory? Why are these models interesting to study? Why are they so difficult to study? What is a lattice regulator? What is a quantum simulator and how can it help us to learn more about non-Abelian gauge theories? These are questions that we address in this introduction. It is important to have a clear view on the actual problem that we are facing and on the tools we are using to tackle these problems.

In this introduction we start in section 6.2 with a discussion why gauge theories, and here especially non-Abelian gauge theories, are important in particle physics. A prominent non-Abelian gauge theory is the theory of the strong interaction (QCD) in the Standard Model of particle physics. In the next section 6.3 we discuss some effects of the strong interaction, which can not been calculated in perturbation theory. These include confinement and the spontaneous breaking of chiral symmetry. These so-called non-perturbative effects can be studied using lattice gauge theory, which is introduced in section 6.4. We describe Wilson's approach of regularizing gauge theories on a lattice [34]. This method can be used to study equilibrium properties of QCD, such as the hadron spectrum and thermodynamic quantities. On the other hand, Wilson's lattice formulation also has a severe problem when dealing with real-time dynamics, a finite baryon density, or a non-zero θ-vacuum angle, which are discussed in section 6.5. Inspired by applications in condensed matter physics, we suggest to use a quantum simulator to investigate non-perturbative effects that cannot be addressed with a classical computer. In section 6.6 we explain the basic idea of quantum simulating a system using ultra-cold atoms in an optical lattice setup. We finish this introduction by discussing approaches of quantum simulating lattice gauge theories in section 6.7.

In order to implement a system in a quantum simulator, it is advantageous to work with a finite-dimensional Hilbert space. The so-called quantum link models [35–37] are an ideal framework to formulate gauge theories in a finite-dimensional Hilbert space. These models are therefore a key to implementing non-Abelian gauge theories in a quantum simulator and will be discussed in detail in the following chapters. This study will show that the physics of quantum link models is interesting and non-trivial. Furthermore our results can be used to validate future experimental implementation in quantum simulator.

In chapter 7 we review Wilson's approach to lattice gauge theory in the context of QCD and discuss the Hamiltonian formulation of this theory. Quantum link models are then introduced

as an extension of Wilson's lattice gauge theory. We will discuss the gauge symmetry in detail, study the global symmetries of this model, and introduce the concept of staggered fermions.

In the following chapters 8 and 9, we work out quantum link models explicitly for the $U(2)$ and $SO(3)$ gauge groups, respectively. We will show explicitly how quantum link models can be used to implement gauge theories in an optical lattice setup. In addition, we present exact diagonalization results of phenomena including the real-time evolution of a chirally restored hot-spot and the spontaneous breaking of chiral symmetry, as well as its restoration at finite baryon density.

6.2. Non-Abelian Gauge Theories

Gauge theories appear in the context of field theory and describe a special kind of invariance of these models, the so-called gauge symmetry. Gauge transformations relate different field configurations, which correspond to the same physical states. Let us consider classical electrodynamics as an example. Since the electric scalar potential and the magnetic vector potential are not directly observable fields, they can be transformed by gauge transformations, leaving the physical observables (the electric and magnetic field) invariant. We say this model has a gauge symmetry. In contrast to global symmetries, which transform the fields in the same way everywhere in space-time, gauge transformations are local symmetries, which means that the fields are transformed differently at every point in space-time.

In the example of classical electrodynamics, the gauge symmetry is characterized by a real function $\varphi(\vec{x}, t)$. When performing a gauge transformation, temporal or spatial derivatives of this function $\varphi(\vec{x}, t)$ are added to the electric scalar and magnetic vector potential, respectively. Since the gauge transformation is characterized by only one real parameter at every point in space-time $\vec{x}, t$, we talk about a $U(1)$ gauge transformation in electrodynamics. These gauge transformations can be generalized to the non-Abelian case [38], where gauge transformations are characterized by matrix-valued functions $\Omega(\vec{x}, t)$, for example, $SU(N)$ matrices.

The Standard Model of particle physics is such a non-Abelian gauge theory. It is invariant under the $SU(3)_c \times SU(2)_L \times U(1)_Y$ gauge symmetry. The theory involves fermion fields (quarks and leptons), a scalar Higgs field, and gauge fields. Gauge fields are responsible for mediating forces between the fermions, while the Higgs field is responsible for providing a mass to most of the elementary particles. The fermion fields and the gauge fields can undergo gauge transformations, which means that, at every point in space-time, the fields are "rotated" by a matrix $\Omega(\vec{x}, t)$ (see section 7.2). This transformation must leave the physical (observable) quantities invariant. The different forces are described by terms in a Lagrangian functional in the context of quantum field theory. This Lagrangian describes the interactions of the Higgs field, the electroweak force, and the strong force, which is described by quantum chromodynamics (QCD).

6.3. Quantum Chromodynamics and some of its Non-Perturbative Effects

Quantum Chromodynamics (QCD) is a non-Abelian gauge theory with an underlying $SU(3)_c$ gauge symmetry. It is very successful in describing the strong interaction between quarks (fermions) and gluons (vector bosons). This theory is asymptotically free [39,40], which means that the strength of the interaction becomes weaker with increasing momentum transfer. On the other hand, in the low-energy regime, the quarks and gluons couple very strongly to each other. They never occur as free isolated objects, but are always bound into baryons (bound states of 3 quarks, gluons, and a fluctuating number of quark-antiquark pairs, e.g. protons and neutrons) or mesons (bound states of a quark-anti-quark pair, gluons, and a fluctuating number of quark-antiquark pairs, e.g. pions). This phenomenon is known as confinement and is correctly described by QCD, regularized on a space-time lattice.

The study of QCD is affected by various difficulties. One of them is due to ultraviolet (UV) divergences. This problem is encountered, for example, in the path integral formalism, where one integrates over all field configurations. This integration then diverges as one integrates over configurations, which are associated with very high frequency fluctuations of the fields. To address this problem one needs to impose a regularization.

This regularization can be realized in different ways. For example, in perturbation theory, one usually analytically continues the number of space-time dimensions. QCD can then be handled in perturbation theory in the high-energy regime, where the quarks behave almost like free particles (due to asymptotic freedom). This implies that the coupling between quarks and gluons becomes small and one can use perturbation theory and expand quantities in the small coupling in this limit.

Perturbative methods fail when investigating the interaction of quarks in the low-energy regime, because the coupling is very strong in this limit (due to confinement). A non-perturbative approach, which also works for low energies is provided by the lattice regularization (see next section). This means that one replaces the continuous space-time by a discrete set of points and defines the quark fields on the lattice sites and the gluon fields on the links connecting neighboring lattice sites.

Besides confinement, another important non-perturbative effect of QCD is the spontaneous breaking of chiral symmetry. Even though this symmetry is weakly explicitly broken by the mass term of the fermions (see section 7.6.4), the symmetry is still approximately intact for fermions with a small mass. The symmetry is broken spontaneously at low temperatures, leading to (pseudo-)Goldstone bosons, which can be identified as the pions. Because these particles are Goldstone bosons of an (approximate) symmetry, the masses of the pions are small compared to ,e.g., the mass of a nucleon. At high temperatures chiral symmetry is restored, which gives rise to a crossover that separates the low-temperature chirally broken phase from the high-temperature quark-gluon plasma. This crossover has been accurately investigated using Monte Carlo simulations of lattice QCD [41, 42].

6.4. Lattice Field Theory Approach to Non-Abelian Gauge Theories

As described in the last section, some problems in QCD can only be addressed non-perturbatively, which makes it an especially interesting theory to study in the context of lattice field theory. When defining field theories on a lattice, UV divergences are regularized non-perturbatively. By introducing a finite lattice spacing a between nearest-neighbor sites, one automatically eliminates field configurations with frequencies higher than $p > \frac{2\pi}{a}$. Therefore the lattice cut-off serves as a UV regulator and defines the quantum field theory, leading to finite results. Due to the finite volume of the lattice with (anti)periodic boundary conditions, we also have a lower bound of the momentum: $p = \frac{2\pi}{L}$ is the smallest possible non-zero momentum, where L is the extent of the lattice in one of the space-time dimensions. At the end one takes the continuum limit $a \to 0$, while the physical observables should approach a constant. One can also take the infinite volume limit $L \to \infty$.

The non-perturbative physics of a non-Abelian gauge theory is traditionally addressed in the context of Wilson's lattice gauge theory [34]. The fermion fields are then defined on the sites of a 4-d space-time lattice, while the gluon field is represented by parallel transporter matrices residing on the links connecting neighboring lattice sites. Via the path-integral formalism, the lattice formulation of a gauge theory in Euclidean time can be mapped to a problem in statistical mechanics. When the Euclidean action S_E is real, the Boltzmann factor $\exp(-S_E)$ represents a weight, which allows us to use importance sampling to update the field configurations. Statistical methods are then used to compute observables (see section 3.1 in the first part of the thesis). This is a first-principle approach, where all systematic errors (due to the finite lattice spacing a, non-physical masses m, ...) can be controlled rigorously. Lattice gauge theory comes with no assumptions, e.g. on the input parameters (g, m, ...). The parameters can be fixed by matching a quantity with an experimentally measured value.

Lattice gauge theory enables us to address important questions in particle physics. Among other things, it has been very successful in calculating the masses of light hadrons [43, 44]. It can also be used to make predictions about decay constants of light and heavy-light pseudoscalar mesons, semileptonic form factors [45], the running of the coupling, heavier hadrons, excited states, resonances, and flavor physics. Lattice QCD allowed the extraction of quark masses. These masses can be compared with experiments, which confirms QCD as the correct theory of the strong interactions also at low energies.

Lattice gauge theories also find applications in other areas of physics. For example, in condensed matter physics, certain quantum spin liquids are described by a $U(1)$ gauge theory [46]. Also the non-Abelian $SU(2)$ variant of quantum spin liquids has long been debated as a possible connection between the doped Mott insulator and the high-T_c superconducting phase in cuprates [47].

6.5. Limitations of Wilson's Lattice Gauge Theory

We discussed that non-Abelian gauge theories play a central role in the Standard Model of particle physics. For example, the $SU(3)$ gauge theory of the strong interaction gives rise to non-perturbative effects, including chiral symmetry breaking. Monte Carlo based methods allow us to study some of these non-perturbative effects numerically.

Unfortunately, very interesting questions are not accessible by classical simulation methods, due to severe sign problems. The sign problem is encountered, when the Euclidean action S_E is not real, which causes the Monte-Carlo weights of the configurations $\exp(-S_E)$ to be not positive definite. It is possible to absorb the sign (or the complex phase) of the weight in the observable (see section 3.2 in the first part of the thesis) in order to use importance sampling. This procedure, however, leads to a poor signal-to-noise ratio, which requires an exponential amount of computer power to improve the statistics of the Monte Carlo simulation.

Sign problems appear when simulating high-density nuclear matter, for example, in the interior of a neutron star. The nuclear matter in a neutron star is very dense and we might encounter exotic phases like a baryonic superfluid or a color superconductor [48]. In order to study systems at finite densities, one has to add a chemical potential μ, which leads to a complex action problem (a variant of a sign problem). The sign problem also appears when studying non-equilibrium physics, which needs to be calculated in real-time. One example is the real-time evolution of a heavy-ion collision, where the quark-gluon plasma, which is in a chirally symmetric phase, finally hadronizes into mesons and baryons and thus breaks chiral symmetry. As in the context of the classical $O(3)$ model (see first part of the thesis), the study of θ-vacuum effects suffers from a sign problem also in QCD.

For certain simpler models, the sign problem can be solved by expressing the action in other degrees of freedom or by using elaborate update routines [49, 50]. In other cases, we lack new ideas how to circumvent the sign problem. This is a strong motivation to implement non-Abelian gauge theories in a quantum simulator.

6.6. Quantum Simulation, Ultra-Cold Atomic Gases, and Optical Lattices

We have stated that the sign problem in non-Abelian gauge theories is an exponentially hard problem for classical simulations. One idea to circumvent the sign problem is by implementing the system on a quantum simulator. Unlike classical simulations, a quantum simulator does not suffer from a sign problem and can even address the dynamics of the system in real-time.

A quantum simulator is a system, in which quantum objects, e.g. atoms, can be controlled, such that they resemble another quantum system as it was first suggested by Feynman [51]. There are digital and analog quantum simulators. In a digital quantum simulator unitary transformations update the quantum objects step by step. For example, as first suggested by Cirac and Zoller [52], in an ion trap, the internal electronic or nuclear states can be manipulated using laser coupling and interactions between the ions [53]. In principle, such a system would be programmable and could undergo any unitary transformation, at least in its

most general form as a universal quantum simulator.

On the other hand, in an analog quantum simulator the system evolves by its intrinsic dynamics. After an initial state is prepared, the quantum objects interact among themselves, where only certain parameters can be tuned from the outside [54]. For example, a Bose-Einstein condensate of atoms or molecules, which was first realized by Cornell, Wiemann, and Ketterle [55, 56], can be used as an analog quantum simulator. An other example are ultra-cold atomic gases that are trapped in an optical lattice, where a set of laser beams is tuned to form a periodic potential [57]. Individual atoms then find the minima of this potential and thus arrange themselves in the lattice geometry. These potentials are chosen appropriately in order to adjust the interaction parameters between the atoms such that they mimic a certain quantum system that is otherwise difficult to study. When constructing an optical lattice, one can make use of a rich experimental toolbox. Already several systems in condensed matter physics have been emulated in an optical lattice setup, including the bosonic Hubbard model, which was implemented by Greiner et. al. [58].

6.7. Quantum Simulation of Gauge Theories

It is natural to ask whether quantum simulators can be used to study non-Abelian gauge theories. Since these systems embody the quantum nature already in their basic degrees of freedom, one does not encounter a sign problem. Measurements can be performed at arbitrary times, which means that one can even address dynamical questions. Due to its quantum nature, it is most convenient to implement models with a finite-dimensional Hilbert space in a quantum simulator. Our approach to quantum simulate non-Abelian gauge theories is to use quantum link models, which are lattice gauge theories with a finite-dimensional Hilbert space.

Quantum simulators for lattice models with a local $U(1)$ gauge symmetry with [59–61] and without [62–64] coupling to matter fields have already been constructed. Some of these constructions take advantage of the quantum link formulation (see chapter 7), which has a finite dimensional Hilbert space per link. Quantum link models have been introduced for $U(1)$ and $SU(2)$ gauge groups [35–37] and extended to other gauge groups including the QCD gauge group $SU(3)$ [65, 66]. For a detailed review of the recent approaches in quantum simulating lattice gauge theories we refer to [67].

For the first time, we here propose a construction of a quantum simulator for non-Abelian quantum link models with a $U(N)$ [68] or $SO(3)$ [69] gauge symmetry coupled to staggered fermions. Other implementations of non-Abelian gauge theories in optical lattices have been described in [70, 71].

We will show that already a simple realization in $(1+1)$ dimensions shares non-trivial features with QCD, including confinement or spontaneous chiral symmetry breaking and restoration at finite baryon density. Our construction can be realized with ultra-cold alkaline-earth atoms, such as ^{87}Sr or ^{193}Yb, in an optical lattice.

Chapter 7.

From Wilson's Lattice Gauge Theory to Quantum Link Models

7.1. Introduction

In this chapter we motivate quantum link models, which are an alternative formulation of gauge theories on the lattice. We first discuss the standard approach, which was originally suggested by Wilson in section 7.2. We will then discuss staggered fermions, which we will also use in the quantum link formulation, in section 7.3. After that, we discuss the Hamiltonian formulation of Wilson's lattice gauge theory before we ultimately extend this concept to quantum link models in section 7.5. It will become evident that quantum link models are a more general concept, in which the Hamiltonian formulation of Wilson's lattice gauge theory emerges in a certain limit.

7.2. Wilson's Formulation of Lattice Gauge Theory for QCD

7.2.1. The Action of Quantum Chromodynamics in the Continuum

In 1974, Wilson suggested a method how to regularize a gauge theory on the lattice [34]. In this section we summarize how to put QCD on the lattice, following Chapter 2 of Gattringer's and Lang's Book [72]. After that we extend Wilson's lattice gauge theory to more general gauge groups and ultimately to quantum link models.

Before we do that, let us review the QCD action in the continuum. The gauge group of QCD is $SU(3)$. This means that we can transform the fields with a different group element $\Omega(x) \in SU(3)$ at each point x in space-time. We construct the action in the Euclidean path integral formalism, where the space-time coordinates are $x_\mu = (x_1, x_2, x_3, x_4)$ and $x_4 = it$ is the Euclidean time coordinate. Let us introduce the following fields:

Quark fields $\psi^f_{\alpha,c}(x), \overline{\psi}^f_{\alpha,c}(x)$: Since leptons do not take part in the strong interaction, quarks are the only relevant fermions in QCD. The two quark fields are Dirac spinors, which are 4-component Grassmann variables with a Dirac index α. There are six different "flavors" f of quarks, each with a mass m^f. The different flavors are $f \in \{$up, down, strange, charm, bottom, top$\}$. The fermion fields also have a color index c and transform in the

fundamental representation of the $SU(3)$ gauge group:

$$\psi^f_{\alpha,c}(x) \quad \longrightarrow \quad \psi'^f_{\alpha,c}(x) = \Omega(x)_{cd}\psi^f_{\alpha,d}(x), \quad \overline{\psi}^f_{\alpha,c}(x) \quad \longrightarrow \quad \overline{\psi}'^f_{\alpha,c}(x) = \overline{\psi}^f_{\alpha,d}(x)\Omega(x)^\dagger_{dc}, \tag{7.1}$$

where we implicitly summed over the color index d.

Gluon gauge field $A_\mu(x)_{cd}$: The interaction in QCD is mediated by gauge bosons, known as gluons. Because gluons are spin 1 particles, the gluon fields transform as 4-vectors under Euclidean transformations, which means that in 4-d systems with Euclidean space-time, they carry a vector index $\mu \in \{1,2,3,4\}$. In addition they carry two color indices c and d. This gluon field matrix is combined of eight gluon fields $A^a_\mu(x)$ as $A_\mu(x)_{cd} = g_s \sum_{a=1}^{8} A^a_\mu(x)\lambda^a_{cd}/2$, where λ^a are the eight generators (traceless, Hermitian 3×3 matrices, also known as Gell-Mann matrices) of the $SU(3)$ gauge group and g_s is the coupling strength of the gauge fields. This gluon field matrix transforms in the adjoint representation of the $SU(3)$ gauge group, which in matrix form reads

$$A_\mu(x) \quad \longrightarrow \quad A'_\mu(x) = \Omega(x)A_\mu(x)\Omega(x)^\dagger + i(\partial_\mu\Omega(x))\Omega(x)^\dagger. \tag{7.2}$$

Field strength tensor $F_{\mu\nu}(x)_{cd}$: The field strength tensor is responsible for the kinetic energy and the self-interaction of the gauge fields and is defined as

$$F_{\mu\nu}(x) = \partial_\mu A_\nu(x) - \partial_\nu A_\mu(x) + [A_\mu(x), A_\nu(x)]. \tag{7.3}$$

We obtain the gauge transformation rules as:

$$F_{\mu\nu}(x) \quad \longrightarrow \quad F'_{\mu\nu}(x) = \Omega(x)F_{\mu\nu}(x)\Omega(x)^\dagger \tag{7.4}$$

The QCD action takes the form

$$S[\psi,\overline{\psi},A] = \int \mathrm{d}^4x \Big[\sum_f \overline{\psi}^f(x)\left(\gamma_\mu\left(\partial_\mu + iA_\mu(x)\right) + m^f\right)\psi^f(x) + \frac{1}{2g_s^2}\mathrm{Tr}(F_{\mu\nu}(x)F_{\mu\nu}(x))\Big] \tag{7.5}$$

or with all indices written explicitly

$$\begin{aligned} S[\psi,\overline{\psi},A] = \int \mathrm{d}^4x \Big[\sum_f \overline{\psi}^f_{\alpha,c}(x)\Big([\gamma_\mu]_{\alpha,\beta}(\delta_{cd}\partial_\mu + ig_sA^a_\mu(x)\lambda^a_{cd}/2) \\ + m^f\delta_{\alpha\beta}\delta_{cd}\Big)\psi^f_{\beta,d}(x) + \frac{1}{4g_s^2}F^a_{\mu\nu}(x)F^a_{\mu\nu}(x)\Big]. \end{aligned} \tag{7.6}$$

The Euclidean gamma matrices γ_μ obey

$$\{\gamma_\mu,\gamma_\nu\} = 2\delta_{\mu,\nu}\mathbb{1}. \tag{7.7}$$

They are responsible for the mixing of the different Dirac components and ensure the correct behavior under Euclidean space-time rotations. We implicitly summed over repeated indices like Dirac indices $\alpha,\beta \in \{1,2,3,4\}$, vector indices $\mu,\nu \in \{1,2,3,4\}$, color indices $c,d \in \{1,2,3\}$, and the gluon index $a = \{1,2,\ldots,8\}$.

7.2.2. Symmetries of the Continuum QCD Action

We have discussed the behavior of the different fields under $SU(3)$ gauge transformations. It is easy to check that the QCD action (7.5) is invariant under these gauge transformations.

Besides the local gauge symmetry, there are also various global symmetries. One of them is the Euclidean symmetry group (the analog of the Poincaré symmetry in Minkowski space). The Euclidean group operates on the coordinates of the fields, while preserving the Euclidean distance $x_\mu x_\mu$. This symmetry group contains rotations and translations in space-time. Because the QCD action (7.5) is invariant under this symmetry, angular momentum, the energy, and the momenta are conserved. The Euclidean group further contains the discrete parity and time reversal symmetry. Parity inverts the spacial coordinates $\vec{x} \longrightarrow -\vec{x}$, whereas the time reversal inverts the temporal direction $t \longrightarrow -t$. The QCD action is also invariant under charge conjugation, which interchanges the fields of particles and anti-particles.

Another important symmetry of QCD is the chiral symmetry (see section 6.3). Let us first study the chiral symmetry for only one flavor of fermions which transforms the fermion fields as

$$\psi(x) \quad \longrightarrow \quad \psi'(x) = \exp(i\alpha\gamma_5)\psi(x), \qquad \overline{\psi}(x) \quad \longrightarrow \quad \overline{\psi}'(x) = \overline{\psi}(x)\exp(i\alpha\gamma_5), \tag{7.8}$$

where α is a real parameter of the transformation and we have dropped the color, Dirac, and flavor indices. Using that $\gamma_5 = \gamma_1\gamma_2\gamma_3\gamma_4$ anticommutes with γ_μ ($\gamma_\mu\gamma_5 = -\gamma_5\gamma_\mu$), we can check that almost all terms of the action (7.5) are invariant under this transformation. The only term, which breaks this chiral symmetry is the mass term, which transforms as

$$m\overline{\psi}\psi \quad \longrightarrow \quad m\overline{\psi}\exp(2i\alpha\gamma_5)\psi.$$

The reason for this symmetry is that in all terms (apart from the mass term) the "left-handed" and "right-handed" components are independent, which means that they do not couple to each other. Left $(\psi_L, \overline{\psi}_L)$ and right-handed components $(\psi_R, \overline{\psi}_R)$ of the fermion fields are defined using the projection operators

$$P_L = \frac{\mathbb{1} - \gamma_5}{2}, \qquad\qquad P_R = \frac{\mathbb{1} + \gamma_5}{2}$$

to be $\psi_L(x) = P_L\psi(x)$, $\psi_R(x) = P_R\psi(x)$, $\overline{\psi}_L(x) = \overline{\psi}(x)P_R$, and $\overline{\psi}_R(x) = \overline{\psi}(x)P_L$.

For QCD with N_f flavors this symmetry can be extended. Let T^i be the generators of $SU(N_f)$ matrices which act on the flavor index f of the fermion fields ψ^f, $\overline{\psi}^f$. The $SU(N_f)_L \otimes SU(N_f)_R$ chiral symmetry mixes the different flavors of left- and right-handed fermions, respectively, as

$$\begin{aligned} SU(N_f)_L: \quad & \psi_L(x) \quad \longrightarrow \quad \exp(i\alpha_L^i T^i)\psi_L(x), \quad \psi_R(x) \quad \longrightarrow \quad \psi_R(x), \\ SU(N_f)_R: \quad & \psi_L(x) \quad \longrightarrow \quad \psi_L(x), \qquad\qquad\quad \psi_R(x) \quad \longrightarrow \quad \exp(i\alpha_R^i T^i)\psi_R(x). \end{aligned} \tag{7.9}$$

In addition there are also two $U(1)$ chiral symmetries, which transform the fermion fields as

$$\begin{aligned} U(1)_V: \quad & \psi(x) \quad \longrightarrow \quad \exp(i\alpha_V \mathbb{1})\psi(x), \\ U(1)_A: \quad & \psi(x) \quad \longrightarrow \quad \exp(i\alpha_A\gamma_5\mathbb{1})\psi(x). \end{aligned} \tag{7.10}$$

These two symmetries are called vector chiral symmetry (also known as baryon number symmetry) and axial chiral symmetry, because the corresponding Noether currents transform as vectors and pseudo (axial) vectors. This means that in total we encounter an $SU(N_f)_L \otimes SU(N_f)_R \otimes U(1)_V \otimes U(1)_A$ chiral symmetry of the QCD the action (7.5) with N_f massless fermions. The axial $U(1)_A$ symmetry is broken explicitly by an anomaly. By introducing non-zero (but equal) masses m for all fermions, the symmetry gets further explicitly broken down to $SU(N_f)_V \otimes U(1)_V$. Allowing distinct masses for each fermion flavor f reduces the symmetry to $U(1)^{N_f}$.

Due to the small quark masses of $N_f = 2$ (or $N_f = 3$) flavors, the explicit breaking of the $SU(N_f)_L \otimes SU(N_f)_R$ chiral symmetry is small and the symmetry is approximately intact. Nevertheless such a symmetry is not observed in the spectrum. As correctly described by QCD, this symmetry gets spontaneously broken to $SU(N_f)_V$ (for $N_f = 2$ the resulting $SU(2)_V$ symmetry is known as "strong isospin"). This spontaneous breaking (of the approximate symmetry) implies the existence of (pseudo) Goldstone bosons, which we find as the pions.

The $U(1)_V$ symmetry does not get broken and thus gives rise to the baryon number conservation.

7.2.3. Discretization on a Lattice

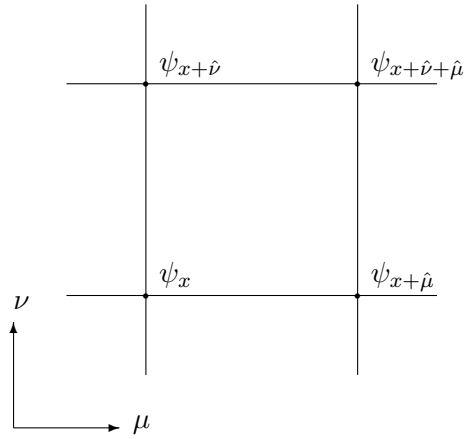

Figure 7.1.: Two dimensional Lattice with a fermion field ψ.

After having discussed the QCD action in the continuum, it can now be discretized on a lattice, as shown in figure 7.1. The fermion fields $\psi(x), \overline{\psi}(x)$ are defined on the sites of the lattice $x = a\,(n_1, n_2, n_3, n_4)$, where a is the lattice spacing and n_μ are integers. To keep this in mind, we denote the position as a subscript to the field variables $\psi_x, \overline{\psi}_x$. To discretize the derivative in a symmetric way one replaces

$$\partial_x \psi(x) \;\sim\; \frac{1}{2a}\left(\psi_{x+\hat{\mu}} - \psi_{x-\hat{\mu}}\right),$$

where $\hat{\mu}$ is a vector (of length a) in the μ-direction. To define a proper lattice action, one

must note that terms like $\overline{\psi}_x \gamma_\mu \psi_{x+\hat{\mu}}$ are not gauge invariant, since they transforms as

$$\overline{\psi}_x \gamma_\mu \psi_{x+\hat{\mu}} \longrightarrow \overline{\psi}_x \Omega_x^\dagger \gamma_\mu \Omega_{x+\hat{\mu}} \psi_{x+\hat{\mu}} = \overline{\psi}_x \Omega_x^\dagger \Omega_{x+\hat{\mu}} \gamma_\mu \psi_{x+\hat{\mu}}.$$

To circumvent this problem one has to introduce a gauge field, which is represented by a matrix-valued field $u_{x,x+\hat{\mu}} \in SU(3)$. This matrix field is associated with the link $x, x+\hat{\mu}$ and therefore known as link variable. It is the fundamental object representing the gauge field and can be thought of as being related to the gauge field $A_\mu(x)$ of the continuum theory as

$$u_{x,x+\hat{\mu}} \sim P \exp\left(i \int_x^{x+\hat{\mu}} A_\mu \, \mathrm{d}s^\mu \right),$$

where P is the path ordering operator and the integral follows a straight line connecting x and $x+\hat{\mu}$. Under a gauge transformation this object transforms as

$$u_{x,x+\hat{\mu}} \longrightarrow u'_{x,x+\hat{\mu}} = \Omega_x u_{x,x+\hat{\mu}} \Omega^\dagger_{x+\hat{\mu}}. \tag{7.11}$$

This is exactly what we need in order to construct a gauge invariant quantity:

$$\frac{1}{2a}\left(\overline{\psi}_x \gamma_\mu u_{x,x+\hat{\mu}} \psi_{x+\hat{\mu}} - \overline{\psi}_x \gamma_\mu u^\dagger_{x-\hat{\mu},x} \psi_{x-\hat{\mu}} \right) \xrightarrow{a\to 0} \overline{\psi}(x) \left(\gamma_\mu \partial_\mu + i A_\mu(x) \right) \psi(x) \tag{7.12}$$

One can show that this expression converges to the correct naive continuum expression when $a \to 0$. The field $\overline{\psi}_x$ at position x is coupled via the matrix field $u_{x,x+\hat{\mu}}$ with its neighbor $\psi_{x+\hat{\mu}}$. Therefore the field $u_{x,x+\hat{\mu}}$ is associated with the link between x and $x+\hat{\mu}$, as shown in figure 7.2.

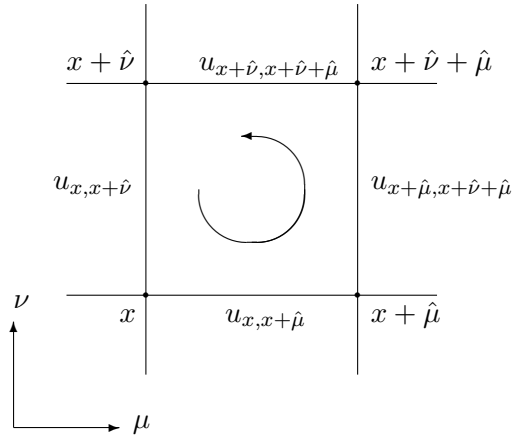

Figure 7.2.: An elementary plaquette of gauge link variables u. The arrow indicates the orientation of the plaquette term.

Also the pure gauge part of the action (involving the field strength tensor) needs to be discretized and expressed in terms of the link variables $u_{x,x+\hat{\mu}}$. One can build a gauge invariant combination of link variables by taking the trace of a product of link variables along a closed loop. The simplest closed loop is an elementary plaquette. One can therefore define the action as a product of four link variables around the plaquette, respecting the orientation (see figure

7.2). It can be shown that this plaquette action converges to its continuum counterpart in the naive continuum limit $a \to 0$:

$$\frac{2}{g_s^2} \sum_{\mu<\nu} \text{Re Tr} \left[\mathbb{1} - u_{x,x+\hat{\mu}} \; u_{x+\hat{\mu},x+\hat{\mu}+\hat{\nu}} \; u^{\dagger}_{x+\hat{\nu},x+\hat{\mu}+\hat{\nu}} \; u^{\dagger}_{x,x+\hat{\nu}} \right] \quad \xrightarrow{a \to 0} \quad \frac{a^4}{4g_s^2} F^a_{\mu\nu}(x) F^a_{\mu\nu}(x). \tag{7.13}$$

Finally, we replace the integral over space-time by a sum over all lattice points

$$\int \mathrm{d}^4 x \; \sim \; \sum_x a^4$$

and we obtain an action, which follow from discretizing the QCD action in a naive way on the lattice:

$$\begin{aligned} S[\psi, \overline{\psi}, u] = a^4 \sum_x \overline{\psi}^f_x \left(\sum_{\mu=1}^{4} \gamma_\mu \frac{u_{x,x+\hat{\mu}} \psi^f_{x+\hat{\mu}} - u^{\dagger}_{x-\hat{\mu},x} \psi^f_{x-\hat{\mu}}}{2a} + m^f \psi^f_x \right) \\ + \frac{2}{g_s^2} \sum_x \sum_{\mu<\nu} \text{Re Tr} \left[\mathbb{1} - u_{x,x+\hat{\mu}} \; u_{x+\hat{\mu},x+\hat{\mu}+\hat{\nu}} \; u^{\dagger}_{x+\hat{\nu},x+\hat{\mu}+\hat{\nu}} \; u^{\dagger}_{x,x+\hat{\nu}} \right] \end{aligned} \tag{7.14}$$

This action is known as the naive fermion action, because it suffers from the so-called fermion doubling problem (see section 7.3.1), where one observes additional fermions in the spectrum. This lattice artifact can be removed, for example, by introducing an additional so-called Wilson term. The Wilson term, on the other hand, brings in new problems, since it breaks chiral symmetry (see section 6.3) explicitly. Another approach is to use staggered fermions, which is what we are going to do in section 7.3.2.

7.3. Staggered Fermions

7.3.1. Fermion Doubling Problem

Let us consider the naive lattice action (7.14). As already mentioned, this action suffers from a fermion doubling problem, which means that we encounter additional particles in the spectrum, which do not appear in the continuum formulation. To see this, we study the free fermion propagator.

The free fermion propagator can be calculated most easily in momentum space. Therefore we Fourier transform the action, while switching off the gauge fields (setting the link variables $u_{x,y}$ to the unit matrix). We define the Fourier transformation of the fermion fields as

$$\psi_p = \sum_x \exp\left(ip_\mu x^\mu\right)\psi_x, \qquad \psi_x = \frac{1}{V}\sum_p \exp\left(-ip_\mu x^\mu\right)\psi_p, \tag{7.15}$$

where $p_\mu = \frac{2\pi k_\mu}{aL_\mu} \in \left\{-\frac{\pi}{a} + \frac{2\pi}{aL_\mu}, \ldots, +\frac{\pi}{a} - \frac{2\pi}{aL_\mu}, \frac{\pi}{a}\right\}$ is the momentum vector in the Brillouin zone and $V = L_1L_2L_3L_4$ is the number of lattice sites. We omitted the flavor index, since we only consider one kind of flavor. Using that

$$\sum_x \exp(-i(p-p')x) = \delta_{p,p'}V,$$

we can express the action (7.14) as

$$S[\psi,\overline{\psi}] = a^4\sum_p \overline{\psi}_p\left(\sum_{\mu=1}^4 \gamma_\mu \frac{i}{a}\sin(ap_\mu) + m\right)\psi_p. \tag{7.16}$$

The part in brackets is the Dirac operator $D(p)$ and its inverse is the fermion propagator in momentum space $\langle\overline{\psi}_{-p}\psi_p\rangle = D(p)^{-1}$. Obviously this operator is diagonal in the momenta p. Therefore, to invert the Dirac operator, we only need to invert the 4×4 matrix of the Dirac operator, which is

$$\langle\overline{\psi}_{-p}\psi_p\rangle = D(p)^{-1} = \frac{m - i/a\sum_\mu \gamma_\mu \sin(p_\mu a)}{m^2 + 1/a^2\sum_\mu \sin^2(p_\mu a)}. \tag{7.17}$$

The poles of the propagator determine the energy of a fermion state. We find poles at

$$0 = (ma)^2 + \sum_\mu \sin^2(p_\mu a) = (ma)^2 + \sum_i \sin^2(p_i a) - \sinh^2(E(\vec{p})a),$$

where we have used that in Euclidean space-time we can express the energy as $p_4 = iE(\vec{p})$ and that $\sin^2(iEa) = -\sinh^2(Ea)$. We therefore read off the dispersion relation of the naive lattice fermions as

$$\sinh^2(E(\vec{p})a) = (ma)^2 + \sum_i \sin^2(p_i a). \tag{7.18}$$

This equation indeed reduces to the dispersion relation in the continuum ($a \to 0$):

$$E(\vec{p})^2 = m^2 + \vec{p}^{\,2}. \tag{7.19}$$

The minimum of the energy is reached for $\vec{p} = 0$, which corresponds to the correct physical fermion state. In equation (7.18), on the other hand, we also find additional minima of the energy. Every state, which has some $p_i = \pi/a$ and some $p_j = 0$ is also a minimum. These states do not disappear in the continuum limit, but are absent in the continuum dispersion relation (7.19). They are called fermion doublers and appear, because we have discretized the fermions on the lattice in a too naive way.

These doubler fermions can be removed by adding an additional term in the action, known as the Wilson term [73]. This term shifts the energy of the doubler fermions, leaving only the $\vec{p} = 0$ state as a minimum of the energy. This shifting term goes to zero in the continuum limit ($a \to 0$), therefore it does not change the continuum limit of the action. The disadvantage of the Wilson term is that it breaks chiral symmetry explicitly. The chiral symmetry is only recovered in the continuum limit through a delicate fine-tuning of the mass parameter, which is seen as unnatural.

In fact, there is even a no-go theorem by Nielsen and Ninomiya [74], which states that any free fermion lattice action, which is local, translation invariant, real, and is invariant under chiral transformations, necessarily suffers from fermion doubling. It should be noted that the theorem does not specify the number of doubler fermions. It is indeed possible to reduce the number of doublers from $2^d - 1$ to 1, but it is impossible to eliminate the doubler fermions completely.

Nevertheless, this problem has been solved quite elegantly, by introducing an additional spatial dimension of finite extent. Both ends of this dimension form a so-called domain wall, where left- and right-handed fermions are localized [75, 76]. By introducing a Wilson term the fermion doublers disappear. Remarkably in this five-dimensional action the chiral symmetry of the light four-dimensional domain wall fermions is not broken when the distance of the domain walls is set to infinity.

Since later we want to implement gauge theories with fermions in an optical lattice setup, we use even another kind of fermions, the so-called staggered fermions. Staggered fermions, which are discussed in the next section, have a simpler structure and reduce the number of fermion doublers by a factor of 4 in 4 dimensions.

7.3.2. Introducing Staggered Fermions

The idea of staggered fermions is to reduce the number of fermionic degrees of freedom in the Dirac space by a process known as spin diagonalization. We will see that after the staggered transformation, the different Dirac components of the fermions decouple [77]. This allows to neglect three of four components, which reduces the number of fermions in the spectrum by a factor of 4. Instead of observing 16 fermion states in 4 dimensions, we only encounter 4 of them which are referred to as different "tastes" of fermions. In addition, there is still a remnant of the chiral symmetry, as we will see in section 7.6.4.

To construct staggered fermions we first define transformed fermion fields $\psi'_x, \overline{\psi}'_x$ as

$$\psi_x = \gamma_1^{x_1}\gamma_2^{x_2}\gamma_3^{x_3}\gamma_4^{x_4}\psi'_x, \qquad \overline{\psi}_x = \overline{\psi}'_x\gamma_4^{x_4}\gamma_3^{x_3}\gamma_2^{x_2}\gamma_1^{x_1}. \tag{7.20}$$

The fermionic part of the naive lattice action (7.14) contains the combinations of the fermion fields $\overline{\psi}_x\gamma_\mu\psi_y$ and $m\overline{\psi}_x\psi_x$, where $y = x + \hat{\mu}$. Using $\gamma_\mu^2 = \mathbb{1}$, these terms can be rewritten in terms of the transformed fermion fields as

$$\begin{aligned}\overline{\psi}'_x\gamma_4^{x_4}\gamma_3^{x_3}\gamma_2^{x_2}\gamma_1^{x_1}\gamma_\mu\gamma_1^{y_1}\gamma_2^{y_2}\gamma_3^{y_3}\gamma_4^{y_4}\psi'_y &= s_{x,y}\overline{\psi}'_x\psi'_y,\\ m\overline{\psi}'_x\gamma_4^{x_4}\gamma_3^{x_3}\gamma_2^{x_2}\gamma_1^{x_1}\gamma_1^{x_1}\gamma_2^{x_2}\gamma_3^{x_3}\gamma_4^{x_4}\psi'_x &= m\overline{\psi}'_x\psi'_x,\end{aligned} \tag{7.21}$$

where $s_{x,x+\hat{\mu}} = (-1)^{x_1+\ldots+x_{\mu-1}}$. In this step the gamma matrices disappeared from the action, implying that the different Dirac components do not mix anymore. In this way, the action describes four identical copies of a one-component fermion. Staggered fermions $\chi, \overline{\chi}$ can now be defined as just one of the four Dirac components of $\psi', \overline{\psi}'$, while ignoring all the other components. This reduces the number of doublers by a factor of four, which means that in 4 dimension we are left with just four fermion states, known as different tastes of the fermions.

The action (7.14) can be rewritten in terms of the staggered fermion fields $\chi, \overline{\chi}$ as

$$\begin{aligned}S[\psi,\overline{\psi},A] = a^4\sum_x \overline{\chi}_x\left(\sum_{\mu=1}^{4}\frac{s_{x,x+\hat{\mu}}u_{x,x+\hat{\mu}}\chi_{x+\hat{\mu}} - s_{x-\hat{\mu},x}u^\dagger_{x-\hat{\mu},x}\chi_{x-\hat{\mu}}}{2a} + m\chi_x\right)\\ + \frac{2}{g^2}\sum_x\sum_{\mu<\nu}\mathrm{Re\ Tr}\left[\mathbb{1} - u_{x,x+\hat{\mu}}\ u_{x+\hat{\mu},x+\hat{\mu}+\hat{\nu}}\ u^\dagger_{x+\hat{\nu},x+\hat{\mu}+\hat{\nu}}\ u^\dagger_{x,x+\hat{\nu}}\right],\end{aligned} \tag{7.22}$$

where $\chi, \overline{\chi}$ are the Grassmann-valued staggered fermion fields, which only have color indices but no Dirac structure. One can think of the Dirac structure to be spread out over the lattice. This will become evident, when we discuss the chiral symmetry transformation of staggered fermions in section 7.6.4.

The action (7.22) can be used to study Euclidean correlators using Monte Carlo simulations. One thereby usually integrates out the staggered fermion degrees of freedom in the partition function, leaving behind a fermion determinant. This is, however, not what we are going to do in this work. In the following we will work in a Hamiltonian formulation. This will allow us to study physical phenomena in real (Minkowski) time.

7.4. Hamiltonian Formulation of Wilson's Lattice Gauge Theory

7.4.1. Gauge Part of the Lagrangian in Temporal Gauge in the Time Continuum

Let us construct the Hamiltonian formulation of the pure gauge part of the action (7.14). To do so, we choose the temporal gauge, which means that we perform a gauge transformation which sets all link variables in the temporal direction to the unit matrix (see figure 7.3):

$$u_{x,x+\hat{4}} \quad \longrightarrow \quad \Omega_x u_{x,x+\hat{4}} \Omega^{\dagger}_{x+\hat{4}} \stackrel{!}{=} \mathbb{1} \tag{7.23}$$

In a system with a finite extent and periodic boundary conditions in the temporal direction, there is only one time-step in which the temporal links can not be set so $\mathbb{1}$. Let us only consider time-steps, where the temporal links were set to $\mathbb{1}$. After choosing the temporal gauge, we can still perform time-independent gauge transformations, leaving the action (7.14) invariant.

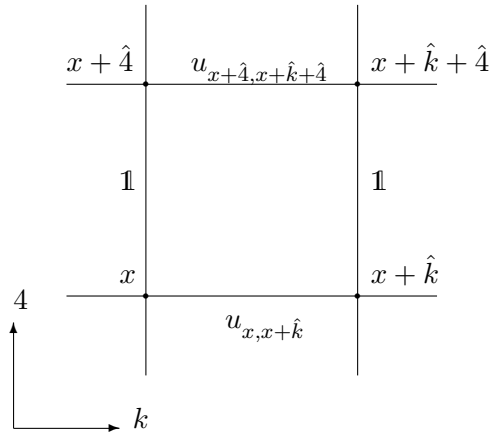

Figure 7.3.: An elementary space-time plaquette of gauge link variables u in the temporal gauge.

To construct the Hamiltonian formulation of lattice gauge theory [78], time and space are considered separately and ultimately the time continuum limit is taken

$$\sum_x a^4 \quad \longrightarrow \quad \int \mathrm{d}x_4 \sum_{\vec{x}} a^3, \tag{7.24}$$

where the sum over all lattice points x in the whole space-time is replaced with a sum over all $\vec{x}$ in one time-slice x_4 combined with an integral over Euclidean time.

The terms of the pure gauge part of the lattice action (7.14), which connect different time-

slices read

$$\frac{2}{g_s^2}\sum_{\vec{x}}\sum_{k=1}^{3}\mathrm{Re\ Tr}\left[\mathbb{1}-u_{x,x+\hat{k}}\ u_{x+\hat{k},x+\hat{k}+\hat{4}}\ u^{\dagger}_{x+\hat{4},x+\hat{k}+\hat{4}}\ u^{\dagger}_{x,x+\hat{4}}\right]$$
$$=\frac{2}{g_s^2}\sum_{\langle xy\rangle}\mathrm{Re\ Tr}\left[\mathbb{1}-u_{x,y}\ u^{\dagger}_{x+\hat{4},y+\hat{4}}\right],$$

where we introduced the sum over all nearest neighbors $\langle xy\rangle$ in one time-slice and $k\in\{1,2,3\}$ is a spatial index. Using the fact that we can rewrite the term

$$-2\mathrm{Re\ Tr}\left[u_{x,y}\ u^{\dagger}_{x+\hat{4},y+\hat{4}}\right]=\mathrm{Tr}\left[(u_{x+\hat{4},y+\hat{4}}-u_{x,y})(u^{\dagger}_{x+\hat{4},y+\hat{4}}-u^{\dagger}_{x,y})\right]+\text{const.},$$

we can take the time continuum limit by rewriting this term as a time-derivative

$$\frac{a^2}{g_s^2}\sum_{\langle xy\rangle}\mathrm{Tr}\left[\frac{u_{x+\hat{4},y+\hat{4}}-u_{x,y}}{a}\frac{u^{\dagger}_{x+\hat{4},y+\hat{4}}-u^{\dagger}_{x,y}}{a}\right]\ \sim\ \mathrm{d}x_4\ \frac{a}{g_s^2}\sum_{\langle xy\rangle}\mathrm{Tr}\left[(\partial_{x_4}u_{x,y})(\partial_{x_4}u^{\dagger}_{x,y})\right]+\text{const.}$$

Now we can write the pure gauge part of the action (7.14) as

$$S[u]=\int\mathrm{d}x_4\ \left\{\frac{a}{g_s^2}\sum_{\langle xy\rangle}\mathrm{Tr}\left[(\partial_{x_4}u_{x,y})(\partial_{x_4}u^{\dagger}_{x,y})\right]-\frac{2}{ag_s^2}\sum_{\square}\mathrm{Re\ Tr}\ u_{\square}\right\},\tag{7.25}$$

where we have ignored constant terms and introduced the sum over all spatial plaquettes $\square$ in a time-slice. $u_{\square}$ is the plaquette matrix from (7.13).

Let us change to real time t (in Minkowski space), by performing the transformation $t=-ix_4$. By defining the action in Minkowski space as $S_M=iS$, the Lagrange function L can be calculated as

$$S_M[u]=\int\mathrm{d}t\ L,\qquad L=\frac{a}{g_s^2}\sum_{\langle xy\rangle}\mathrm{Tr}\left[\dot{u}_{x,y}\dot{u}^{\dagger}_{x,y}\right]+\frac{2}{ag_s^2}\sum_{\square}\mathrm{Re\ Tr}\ u_{\square}.\tag{7.26}$$

In the following, we will be more general by changing the gauge group from $SU(3)$ to $SU(N)$ and by defining the system in d instead of 3 spatial dimensions. We therefore have color indices $c\in\{1,\ldots,N\}$ and vector indices $k\in\{1,\ldots,d\}$ instead of $\mu\in\{1,2,3,4\}$. The link variables are now elements of the group $u_{x,y}\in SU(N)$.

7.4.2. Hamilton Functional

To build a Hamiltonian from a general Lagrange function $L(q_i, \dot{q}_i)$, we need to identify the momenta p_i conjugate to the degrees of freedom q_i. The conjugate momenta are defined as $p_i = \frac{\partial}{\partial \dot{q}_i} L(q_i, \dot{q}_i)$. With this, the variables $\dot{q}_i$ can be expressed as a function of q_i and p_i. Therefore the Hamiltonian $H = p_i \dot{q}_i - L(q_i, \dot{q}_i)$ can then also be written as a function of q and p only. Later, one quantizes the system, by setting up a Hilbert space and promoting p_i and q_i to operators acting in this Hilbert space and obeying canonical commutation relations.

Identifying the correct degrees of freedom in the lattice gauge theory Lagrange function $L(u, u^\dagger, \dot{u}, \dot{u}^\dagger)$ and determining their conjugate momenta is a non-trivial task. Instead of going through the difficult calculation of using generalized Euler angles to parametrize the $SU(N)$ matrices $u_{x,y}$ and associate the canonical conjugate momenta to these angles, we will study the behavior under time-independent gauge transformations. This will allow us to replace $\dot{u}_{x,y}$ and $\dot{u}^\dagger_{x,y}$ in favor of contributions to the conserved charges of gauge transformations. Ultimately, after quantization, the conserved charges of gauge transformations are then identified with contributions to the generators of the gauge symmetry [79]. Let us summarize this procedure:

i. Gauge transformations are a symmetry of the Lagrange function $L(u, u^\dagger, \dot{u}, \dot{u}^\dagger)$, therefore according to Noether's theorem there must be conserved charges. Since gauge transformations are a local symmetry, we obtain a conserved charge at each site x, which we denote as G^a_x.

ii. The G^a_x are functions of $u_{x,y}, u^\dagger_{x,y}, \dot{u}_{x,y}, \dot{u}^\dagger_{x,y}$ and can be used to express the Hamiltonian as a function of the link variables $u_{x,y}, u^\dagger_{x,y}$ and contributions to G^a_x only. These two steps are performed in this section.

iii. After quantization, the operators of the conserved charges are the generators of a symmetry. Therefore the G^a_x become the generators of gauge transformations. Since they are not the canonical conjugate momenta, they do not just obey canonical commutation relations with the link variables. The commutation relation between G^a_x and the link variables $u_{x,y}$ and $u^\dagger_{x,y}$ have to be derived from properties of the gauge transformations. This is what we do in the next section.

Let us consider points i. and ii. in more detail. The aim is to determine the conserved charges of gauge transformations and express the Hamiltonian in terms of contributions to these charges and the link variables. Since gauge transformations at each site x leave the Lagrange function invariant, we can use Noether's theorem, which predicts a conserved charge for each generator G^a_x:

$$G^a_x = \sum_{\langle x' y \rangle} \delta_{x',x} \left(\frac{\partial L}{\partial \dot{u}^{ij}_{x,y}} \delta u^{a,ij}_{x,y} + \frac{\partial L}{\partial \dot{u}^{\dagger ij}_{x,y}} \delta u^{\dagger a,ij}_{x,y} \right), \tag{7.27}$$

where the variation of the link variable $\delta u^a_{x,y}$ will be defined below. Obviously not all the links in the sum over $\langle x' y \rangle$ contribute to this charge, since the variation of most of the link variables are zero. The contributions to the charge G^a_x originate only from variations of links emanating

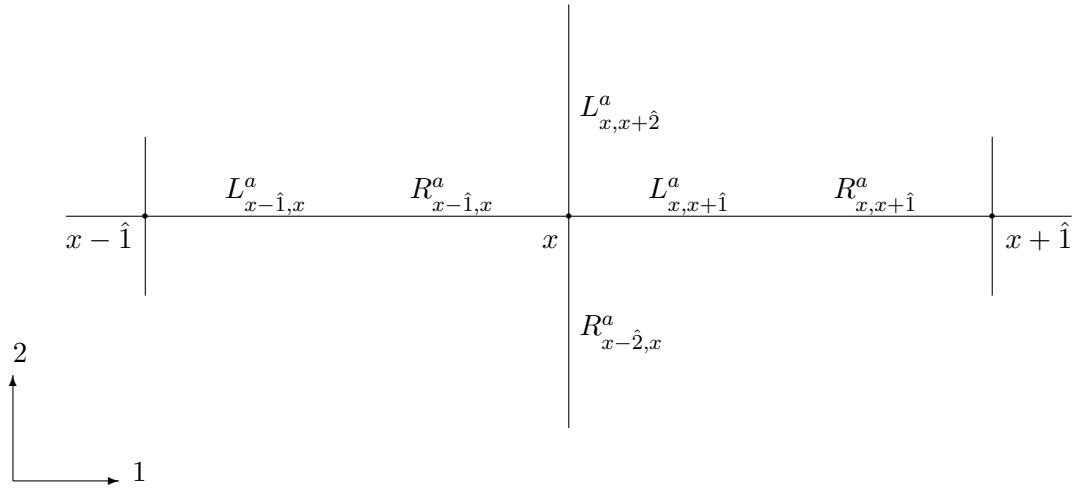

Figure 7.4.: Two links with the associated generators $L^a_{x,y}$ and $R^a_{x,y}$ in the 1-2 plane.

from the site x. In figure 7.4 some of the links, contributing to the conserved charge G^a_x, are shown. G^a_x can be separated into these contributions from each link x', y, denoted as $L^a_{x',y}$ or $R^a_{x',y}$ depending on whether the site x is on the left or the right end of the link x', y (see figure figure 7.4). We therefore split the charge G^a_x into the contributions from each link emanating from the site x as

$$G^a_x = \sum_{k=1}^{d} \left(L^a_{x,x+\hat{k}} + R^a_{x-\hat{k},x} \right). \tag{7.28}$$

To construct $L^a_{x,y}$ and $R^a_{x,y}$, we need to perform a gauge transformation at the site x and calculate the variations of the link variables.

According to section 7.2.3, under gauge transformations the link matrices transform as

$$u^{ij}_{x,y} \quad \longrightarrow \quad u'^{ij}_{x,y} = \Omega^{ik}_x u^{kl}_{x,y} \Omega^{\dagger lj}_y, \tag{7.29}$$

where the $SU(N)$ matrices of the gauge transformations Ω_x and Ω_y can be written as

$$\Omega_x = \exp\left(i\alpha^a_x \lambda^a\right), \qquad \Omega_y = \exp\left(i\alpha^a_y \lambda^a\right). \tag{7.30}$$

λ^a are the generalized $SU(N)$ Gell-Mann matrices. A transformation with infinitesimally small α^a_x can be written as

$$\Omega_x u_{x,y} \Omega^\dagger_y \;\approx\; \left(\mathbb{1} + i\alpha^a_x \lambda^a\right) u_{x,y} \left(\mathbb{1} - i\alpha^a_y \lambda^a\right). \tag{7.31}$$

Let us first study the contribution to the charge G^a_x from a link $(x, x+\hat{k}) = (x, y)$, which we denote as $L^a_{x,y}$. The gauge transformation is performed on the left end of the link, we therefore set $\Omega_y = \mathbb{1}$. With this, the infinitesimal gauge transformation becomes

$$u_{x,y} \quad \longrightarrow \quad u_{x,y} + \alpha^a_x \; \delta u^a_{x,y}, \qquad \text{with} \quad \delta u^{a,ij}_{x,y} = i\lambda^a_{ik} \; u^{kj}_{x,y}. \tag{7.32}$$

The contributions to the conserved charges therefore are

$$L^a_{x,y} = \frac{\partial L}{\partial \dot{u}^{ij}_{x,y}} \delta u^{a,ij}_{x,y} + \frac{\partial L}{\partial \dot{u}^{\dagger ij}_{x,y}} \delta u^{\dagger a,ij}_{x,y} = i \frac{a}{g_s^2} \left(\dot{u}^{\dagger ji}_{x,y} \; \lambda^a_{ik} \; u^{kj}_{x,y} - \dot{u}^{ji}_{x,y} \; u^{\dagger ik}_{x,y} \; \lambda^a_{kj} \right)$$
$$= i \frac{a}{g_s^2} \mathrm{Tr} \left(\dot{u}^\dagger_{x,y} \lambda^a u_{x,y} - \dot{u}_{x,y} u^\dagger_{x,y} \lambda^a \right). \tag{7.33}$$

To obtain the contribution to the charge G^a_x from a link $(x-\hat{k}, x) = (y, x)$, which we denote as $R^a_{y,x}$, we consider a gauge transformation, which acts on the right end of the link only. According to equation (7.31) the variation now becomes

$$\left[\delta u^a_{y,x} \right]_{ij} = -i u^{ik}_{y,x} \lambda^a_{kj} \tag{7.34}$$

and the contribution to the conserved charges $R^a_{y,x}$, can be obtained as

$$R^a_{y,x} = \frac{\partial L}{\partial \dot{u}^{ij}_{y,x}} \delta u^{a,ij}_{y,x} + \frac{\partial L}{\partial \dot{u}^{\dagger ij}_{y,x}} \delta u^{\dagger a,ij}_{y,x} = -i \frac{a}{g_s^2} \left(\dot{u}^{\dagger ji}_{y,x} \; u^{ik}_{y,x} \; \lambda^a_{kj} - \dot{u}^{ji}_{y,x} \; \lambda^a_{ik} \; u^{\dagger kj}_{y,x} \right)$$
$$= -i \frac{a}{g_s^2} \mathrm{Tr} \left(\dot{u}^\dagger_{x,y} u_{x,y} \lambda^a - \dot{u}_{x,y} \lambda^a u^\dagger_{x,y} \right). \tag{7.35}$$

Obviously $L^a_{x,y}$ and $R^a_{x,y}$ are not independent but can be related by

$$u^\dagger_{x,y} L^a_{x,y} \lambda^a u_{x,y} = -R^a_{x,y} \lambda^a. \tag{7.36}$$

With this one can even show that $\sum_a L^a_{x,y} L^a_{x,y} = \sum_a R^a_{x,y} R^a_{x,y}$.

Next, we show that the combination $L^a_{x,y} L^a_{x,y} + R^a_{x,y} R^a_{x,y}$ (summed over the index $a = 1, \ldots, N^2-1$) is exactly what we need to construct the electric contribution to the Hamiltonian. Using the completeness relation of the generalized Gell-Mann matrices

$$\sum_{a=1}^{N^2-1} \lambda^a_{ij} \lambda^a_{kl} = 2\delta_{il}\delta_{jk} - \frac{2}{N} \delta_{ij}\delta_{kl} \tag{7.37}$$

and the identities

$$u^\dagger u = \mathbb{1}, \qquad \dot{u}^\dagger u + u^\dagger \dot{u} = 0 \tag{7.38}$$

we obtain

$$L^a_{x,y} L^a_{x,y} + R^a_{x,y} R^a_{x,y} = -\frac{a^2}{g_s^4} \lambda^a_{ij} \lambda^a_{kl} \Big\{ \left(\dot{u}^{\dagger mi}_{x,y} u^{jm}_{x,y} - \dot{u}^{jm}_{x,y} u^{\dagger mi}_{x,y} \right) \left(\dot{u}^{\dagger nk}_{x,y} u^{ln}_{x,y} - \dot{u}^{ln}_{x,y} u^{\dagger nk}_{x,y} \right)$$
$$+ \left(\dot{u}^{\dagger jm}_{x,y} u^{mi}_{x,y} - \dot{u}^{mi}_{x,y} u^{\dagger jm}_{x,y} \right) \left(\dot{u}^{\dagger ln}_{x,y} u^{nk}_{x,y} - \dot{u}^{nk}_{x,y} u^{\dagger ln}_{x,y} \right) \Big\} \tag{7.39}$$
$$= \frac{16 a^2}{g_s^4} \mathrm{Tr} \left[\dot{u}^\dagger_{x,y} \dot{u}_{x,y} \right].$$

Collecting everything together, we write the Hamiltonian as

$$H = \sum_{\langle xy \rangle} \left\{ \frac{\partial L}{\partial \dot{u}^{ij}_{x,y}} \dot{u}^{ij}_{x,y} + \frac{\partial L}{\partial \dot{u}^{\dagger ij}_{x,y}} \dot{u}^{\dagger ij}_{x,y} \right\} - L$$
$$= \frac{a}{g_s^2} \sum_{\langle xy \rangle} \mathrm{Tr} \left[\dot{u}_{x,y} \dot{u}^\dagger_{x,y} \right] - \frac{2}{a g_s^2} \sum_{\square} \mathrm{Re \; Tr} \; u_\square \tag{7.40}$$
$$= \frac{g_s^2}{16 a} \sum_{\langle xy \rangle} \left(L^a_{x,y} L^a_{x,y} + R^a_{x,y} R^a_{x,y} \right) - \frac{1}{a g_s^2} \sum_{\square} \mathrm{Tr} (u_\square + u^\dagger_\square).$$

7.4.3. Quantizing the Hamiltonian and Deriving Commutation Relations

The Hamiltonian in equation (7.40) is quantized by promoting $u_{x,y}$ and G_x to operators. The Hilbert space is the direct product space, containing square-integrable functions of $SU(N)$ matrices for each link x, y. We can choose a basis in which the operator $u_{x,y}$ is diagonal. After this quantization the operators G_x^a are the generators of gauge transformations, operating in the Hilbert space. As for the conserved charges, also the generators of gauge transformations can be broken down to operators $L_{x,y}^a$ and $R_{x,y}^a$, which are associated with the left and right end of a link x, y: $L_{x,y}^a$ generate gauge transformations on the left end of the link (at the site x), while $R_{x,y}^a$ do so on the right end of the link (at the position y, see figure 7.4).

Since $L_{x,y}^a$ and $R_{x,y}^a$ are now operators, they no longer commute with the operators of the link variables $u_{x,y}$. To determine the corresponding commutation relations, we study the operator definition of $L_{x,y}^a$ and $R_{x,y}^a$. Both operators generate $SU(N)$ gauge transformations, therefore they obey

$$[L_{x,y}^a, L_{x,y}^b] = 2if^{abc}L_{x,y}^c, \quad [R_{x,y}^a, R_{x,y}^b] = 2if^{abc}R_{x,y}^c, \tag{7.41}$$

where f^{abc} are the structure constants of $SU(N)$. Since we can apply the transformation independently on the left or on the right side, $L_{x,y}^a$ and $R_{x,y}^a$ commute

$$[L_{x,y}^a, R_{x,y}^b] = 0, \tag{7.42}$$

as do operators on different links. The operators $L_{x,y}^a$ generate gauge transformation on the left end of the link x, y, which reads according to equation (7.29)

$$\exp\left(-i\alpha_x^a L_{x,y}^a\right) u_{x,y} \exp\left(i\alpha_x^a L_{x,y}^a\right) = \exp\left(i\alpha_x^a \lambda^a\right) u_{x,y}.$$

This equation, explicitly written with all the matrix indices, reads

$$\exp\left(-i\alpha_x^a L_{x,y}^a\right) u_{x,y}^{ij} \exp\left(i\alpha_x^a L_{x,y}^a\right) = \left[\exp\left(i\alpha_x^a \lambda^a\right)\right]_{ik} u_{x,y}^{kj},$$

where from now on we use indices like i, j for the color degrees of freedom. Expanding this equation to first order in α_x^a leads to

$$\begin{aligned}\left(\mathbb{1} - i\alpha_x^a L_{x,y}^a\right) u_{x,y}^{ij} \left(\mathbb{1} + i\alpha_x^a L_{x,y}^a\right) + \mathcal{O}(\alpha^2) &= u_{x,y}^{ij} + i\alpha_x^a \lambda_{ik}^a u_{x,y}^{kj} + \mathcal{O}(\alpha^2) \\ u_{x,y}^{ij} - i\alpha_x^a \left[L_{x,y}^a, u_{x,y}^{ij}\right] + \mathcal{O}(\alpha^2) &= u_{x,y}^{ij} + i\alpha_x^a \lambda_{ik}^a u_{x,y}^{kj} + \mathcal{O}(\alpha^2)\end{aligned}$$

and we obtain the commutation relation

$$\left[L_{x,y}^a, u_{x,y}^{ij}\right] = -\lambda_{ik}^a u_{x,y}^{kj}, \tag{7.43}$$

which is consistent in all orders in α_x^a.

In a similar fashion using

$$\exp\left(-i\alpha_y^a R_{x,y}^a\right) u_{x,y} \exp\left(i\alpha_y^a R_{x,y}^a\right) = u_{x,y} \exp\left(-i\alpha_y^a \lambda^a\right),$$

we get for the commutation relation for the operator R^a:

$$\left[R_{x,y}^a, u_{x,y}^{ij}\right] = u_{x,y}^{ik} \lambda_{kj}^a. \tag{7.44}$$

Operators on different links commute with each other.

As in equation (7.36), the operators $L_{x,y}^a$ and $R_{x,y}^a$ are not independent. In fact they also satisfy $\sum_a L_{x,y}^a L_{x,y}^a = \sum_a R_{x,y}^a R_{x,y}^a$.

7.4.4. Gauss Law

The physical Hilbert space only contains gauge invariant states. Because we want gauge variant states to be eliminated from the Hilbert space, the Gauss law is implemented. To see that, we study the gauge transformations in more details. As stated earlier, the operators $L^a_{x,y}$ and $R^a_{x,y}$ generate gauge transformations on the left and on the right end of a link x, y and are associated with the left and right end of the link, as shown in figure 7.4.

Applying a gauge transformation at the position x, of course, not only transforms the link variable $u_{x,x+\hat{1}}$ but also all other link variables emanating from the site x. If, for example, the link variable $u_{x,x+\hat{1}}$ gets transformed as

$$u_{x,x+\hat{1}} \quad \longrightarrow \quad u'_{x,x+\hat{1}} = \exp\big(-i\alpha^a_x L^a_{x,x+\hat{1}}\big) u_{x,x+\hat{1}} \exp\big(i\alpha^a_x L^a_{x,x+\hat{1}}\big),$$

also all other link variables including $u_{x-\hat{1},x}, u_{x,x+\hat{2}}, \ldots$ need to be transformed as

$$\begin{aligned}
u_{x-\hat{1},x} \quad &\longrightarrow \quad u'_{x-\hat{1},x} = \exp\big(-i\alpha^a_x R^a_{x-\hat{1},x}\big) u_{x-\hat{1},x} \exp\big(i\alpha^a_x R^a_{x-\hat{1},x}\big) \\
u_{x,x+\hat{2}} \quad &\longrightarrow \quad u'_{x,x+\hat{2}} = \exp\big(-i\alpha^a_x L^a_{x,x+\hat{2}}\big) u_{x,x+\hat{2}} \exp\big(i\alpha^a_x L^a_{x,x+\hat{2}}\big) \\
u_{x-\hat{2},x} \quad &\longrightarrow \quad u'_{x-\hat{2},x} = \exp\big(-i\alpha^a_x R^a_{x-\hat{2},x}\big) u_{x-\hat{2},x} \exp\big(i\alpha^a_x R^a_{x-\hat{2},x}\big).
\end{aligned}$$

This has to be done in every spatial direction and therefore one defines generators of gauge transformations at the site x as

$$G^a_x = \sum_{k=1}^{d} \left(L^a_{x,x+\hat{k}} + R^a_{x-\hat{k},x} \right). \tag{7.45}$$

The operators G^a_x generate a local $su(N)$ algebra

$$[G^a_x, G^b_y] = 2i\delta_{xy} f^{abc} G^c_x. \tag{7.46}$$

The unitary operator, representing a general gauge transformation in the Hilbert space is defined as

$$V = \prod_x \exp\left(i\alpha^a_x G^a_x\right). \tag{7.47}$$

From now on sums and products, like the one here, are meant to extend over all spacial sites x and do not include a sum or product over time-slices. Since the generators $L^a_{x,y}$ and $R^a_{x,y}$ associated with different links commute with each other, the transformation rule of a link variable is

$$\begin{aligned}
u_{x,y} \quad \longrightarrow \quad u'_{x,y} &= V^\dagger u_{x,y} V = \exp\left(-i\left(\alpha^a_x L^a_{x,y} + \alpha^a_y R^a_{x,y}\right)\right) u_{x,y} \exp\left(i\left(\alpha^a_x L^a_{x,y} + \alpha^a_y R^a_{x,y}\right)\right) \\
&= \exp\left(i\alpha^a_x \lambda^a\right) u_{x,y} \exp\left(-i\alpha^a_y \lambda^a\right).
\end{aligned} \tag{7.48}$$

One can show that we have constructed a Hamiltonian, which is gauge invariant ($V^\dagger H V = H$). Therefore all generators G^a_x commute with the Hamiltonian ($[G^a_x, H] = 0$). We can thus choose a basis in the Hilbert space by classifying the different states by their G^a_x quantum numbers. Later one can diagonalize each sector of the Hamiltonian H in this basis individually.

Let us consider the states $|\psi\rangle$, which are elements of the Hilbert space on which the operators act. Let us choose a basis in which the states are classified by their quantum numbers with respect to the generators of gauge transformations G_x^a. In this basis, there are certain states for which

$$G_x^a|\psi\rangle = 0 \qquad \text{for all } a, \tag{7.49}$$

which are gauge invariant, because they obey $V^\dagger|\psi\rangle = |\psi\rangle$. Only the gauge invariant states are physical.

Equation (7.49) is known as the Gauss law. One can think of the operators $L_{x,y}^a$ and $R_{x,y}^a$ acting on the Hilbert space of square-integrable functions in $SU(N)$. These operators generate an $su(N)$ algebra on the left and on the right end of every link x, y. Due to the Gauss law (conditions (7.49) and (7.45)), applying the generators of the $su(N)$ algebra to the states of the links adjacent to a site x have to add up to zero. This means that they need to form an $su(N)$ singlet (also known as a color-singlet).

7.4.5. Hamilton Formulation of $U(N)$ Gauge Theories

So far, we have considered a pure lattice gauge theory with an $SU(N)$ gauge group. Nevertheless, the lattice Hamiltonian formulation can also be realized for other gauge groups, including $U(N)$. In chapter 8, we will study a model with a $U(N)$ gauge symmetry and in chapter 9 we will discuss an $SO(3)$ gauge theory, which are both not more complicated to formulate.

The most simple case is probably the study of a $U(1)$ gauge group. This is a special case, because in $U(1)$ the link variables $u_{x,y}$ and the gauge transformation "matrices" Ω_x and Ω_y are just complex phases: $\Omega_x = \exp(i\alpha_x)$, $\Omega_y = \exp(i\alpha_y)$. Applying a gauge transformation at the left or at the right end of the link therefore only changes the phase of the link variable $u_{x,y} \in U(1)$

$$u_{x,y} \quad \longrightarrow \quad u'_{x,y} = \Omega_x u_{x,y} \Omega_y^\dagger = \exp\left(i\left(\alpha_x - \alpha_y\right)\right) u_{x,y}.$$

There are again conserved charges due to local gauge invariance, which we denote as G_x. These charges can be broken down to contributions from the links emanating from the site x as

$$G_x = \sum_{k=1}^{N} \left(E_{x-\hat{k},x} - E_{x,x+\hat{k}} \right). \tag{7.50}$$

$E_{x,y}$ can be constructed as the contribution to the conserved charge G_x according to Noether's theorem in the same way as we did it in the non-Abelian case:

$$E_{x,y} = -i\frac{a}{g^2}\left(\dot{u}_{x,y}^* u_{x,y} - \dot{u}_{x,y} u_{x,y}^*\right) \tag{7.51}$$

One can show that the term $E_{x,y}E_{x,y}$ is again proportional to the $\dot{u}\dot{u}^*$ term in the Lagrange function. Therefore the Hamiltonian can be written as

$$H = \frac{g^2}{4a} \sum_{\langle xy \rangle} E_{x,y}^a E_{x,y}^a - \frac{1}{ag^2} \sum_{\square} \left(u_\square + u_\square^*\right). \tag{7.52}$$

After quantization, $E_{x,y}$ are promoted to operators. Instead of two generators $L_{x,y}$ and $R_{x,y}$, only the generator $E_{x,y}$ is needed. Using equation (7.50) and defining $W = \prod_x \exp(i\alpha_x G_x)$, the link variables indeed transform as

$$\begin{aligned} u_{x,y} \quad \longrightarrow \quad W^\dagger u_{x,y} W &= \exp\left(i\left(\alpha_x - \alpha_y\right) E_{x,y}\right) u_{x,y} \exp\left(-i\left(\alpha_x - \alpha_y\right) E_{x,y}\right) \\ &= \exp\left(i\left(\alpha_x - \alpha_y\right)\right) u_{x,y}. \end{aligned}$$

The commutation relation of the link field $u_{x,y}$ and its conjugate momentum $E_{x,y}$ can be derived from

$$\exp\left(i\left(\alpha_x - \alpha_y\right) E_{x,y}\right) u_{x,y} \exp\left(-i\left(\alpha_x - \alpha_y\right) E_{x,y}\right) = \exp\left(i\left(\alpha_x - \alpha_y\right)\right) u_{x,y},$$

which reads on a link x, y

$$[E_{x,y}, u_{x,y}] = u_{x,y}, \tag{7.53}$$

while operators on different links commute.

The Gauss law ($G|\psi\rangle = 0$) is intuitive to understand. On each link, we have an integer quantum numbers, representing the electric flux. At each site x, the sum of the fluxes of all emanating links have to add up to zero.

To build a general $U(N)$ lattice gauge theory, one notes that $U(N)$ is nothing else than the direct product of the two gauge groups $U(N) = SU(N) \otimes U(1)$. Therefore, one has generators $L^a_{x,y}$ and $R^a_{x,y}$ of $SU(N)$ and $E_{x,y}$, which is the generator of the $U(1)$ symmetry.

7.4.6. Staggered Fermions in the Hamiltonian Formulation

In the Hamiltonian formulation, we can no longer use the Grassmann valued variables $\overline{\chi}^i_x, \chi^i_x$ of the staggered fermions (see section 7.3.2). Instead, fermion creation $\psi^{i\dagger}_x$ and annihilation operators ψ^i_x, which act in a Hilbert space, have to be introduced. Since they generate and annihilate staggered fermions, they do not have a Dirac index, they only have the $SU(N)$ color index i. These operators obey the usual anti-commutation relations of fermion operators

$$\{\psi^{i\dagger}_x, \psi^{j\dagger}_y\} = \{\psi^i_x, \psi^j_y\} = 0, \qquad \{\psi^i_x, \psi^{j\dagger}_y\} = \delta_{xy}\delta_{ij}. \tag{7.54}$$

A careful analysis [77] shows that the $U(N)$ Hamiltonian, including fermions, can be written as

$$\begin{aligned} H = &- t \sum_x \sum_{k=1}^{d} \left(s_{x,x+\hat{k}} \psi^\dagger_x u_{x,x+\hat{k}} \psi_{x+\hat{k}} + \text{H.c.} \right) + m \sum_x s_x \psi^\dagger_x \psi_x \\ &+ \frac{g^2}{2} \sum_{\langle xy \rangle} \left(L^a_{x,y} L^a_{x,y} + R^a_{x,y} R^a_{x,y} \right) + \frac{g'^2}{2} \sum_{\langle xy \rangle} E^a_{x,y} E^a_{x,y} - \frac{2}{4g^2} \sum_{\square} \text{Re Tr } u_{\square}, \end{aligned} \tag{7.55}$$

where we have redefined the coupling constants t, g, and g' and a new staggered sign factor had to be introduced as $s_x = (-1)^{x_1 + \cdots + x_d}$. For a $U(N)$ gauge symmetry, these new coupling parameters g and g' do not directly correspond to g_s from the Lagrange function.

Let us study how the fermion operators transform under gauge transformations. Since the fermions are in the fundamental representation of $SU(N) \otimes U(1)$ they transform as

$$\begin{aligned} SU(N): &\qquad \psi^i_x \longrightarrow V^\dagger \psi^i_x V = \left[\exp\left(i\alpha^a_x \lambda^a \right) \right]^{ij} \psi^j_x, \\ U(1): &\qquad \psi^i_x \longrightarrow W^\dagger \psi^i_x W = \exp\left(i\alpha_x \right) \psi^i_x. \end{aligned} \tag{7.56}$$

The generators of the $SU(N)$ gauge transformation, G^a_x, and the generator of the additional $U(1)$ symmetry, G_x, can be extended in order to transform the fermions correctly. These generators can be expressed in terms of the flux operators L^a, R^a, E, and the fermion field operators ψ^i, $\psi^{\dagger i}$ as

$$\begin{aligned} SU(N): &\qquad G^a_x = \psi^{\dagger i}_x \lambda^a_{ij} \psi^j_x + \sum_{k=1}^{d} \left(L^a_{x,x+\hat{k}} + R^a_{x-\hat{k},x} \right), \\ U(1): &\qquad G_x = \psi^{\dagger i}_x \psi^i_x + \sum_{k=1}^{d} \left(E_{x-\hat{k},x} - E_{x,x+\hat{k}} \right). \end{aligned} \tag{7.57}$$

It is straight forward to check that by using the site based generators of gauge transformations

$$V = \prod_x \exp\left(i\alpha^a_x G^a_x \right), \qquad W = \prod_x \exp\left(i\alpha_x G_x \right), \tag{7.58}$$

equation (7.56) is satisfied.

These operators leave the Hamiltonian invariant $[G^a_x, H] = [G_x, H] = 0$. Again, the physical states $|\psi\rangle$ have to be gauge invariant, which means

$$G^a_x |\psi\rangle = 0, \qquad G_x |\psi\rangle = 0. \tag{7.59}$$

This implies that the links emanating from a site x have to form a color-singlet state together with the fermion at the site x.

7.5. Quantum Link Formulation of Lattice Gauge Theory

7.5.1. What is a Quantum Link Model?

In the previous section, we have worked out the gauge invariant Hamiltonian (7.40) of Wilson's lattice gauge theory. As we have seen, the momenta conjugate to the gauge link variables $u_{x,y}$ and $u^\dagger_{x,y}$ are the operators $L^a_{x,y}$ and $R^a_{x,y}$, which generate $SU(N)$ gauge transformations on the left and on the right end of the link x, y, respectively. These so-called $SU(N)$ electric flux operators $L^a_{x,y}$ and $R^a_{x,y}$ ($a = 1, \ldots, N^2 - 1$) are associated with the left and right end of the link (see figure 7.5). The two operators generate an $su(N)_L \oplus su(N)_R$ algebra on each link (see equation (7.60)). For models with an additional $U(1)$ gauge symmetry, we also encounter the generator $E_{x,y}$, representing the Abelian $U(1)$ electric flux. In case the Hamiltonian is also invariant under this additional $U(1)$ symmetry, we also encounter the commutation relations for $E_{x,y}$. The commutation relations of all these operators have been derived as

$$\begin{array}{llll} [R^a, R^b] = 2if^{abc}R^c, & [R^a, u^{ij}] = u^{ik}\lambda^a_{kj}, & [L^a, u^{ij}] = -\lambda^a_{ik}u^{kj}, & [E, u^{ij}] = u^{ij}, \\ [L^a, L^b] = 2if^{abc}L^c, & [R^a, L^b] = 0, & [E, R^a] = 0, & [E, L^a] = 0, \end{array} \quad (7.60)$$

for operators on the same link, while operators associated with different links commute. Here, λ^a are the $SU(N)$ Gell-Mann matrices and f^{abc} are the $SU(N)$ structure constants.

The states on each link are elements of the Hilbert space of square-integrable wave functions of $SU(N)$ (or $U(N)$) matrices. This Hilbert space is infinite-dimensional. Quantum link models, on the other hand, operate in a finite-dimensional Hilbert space per link.

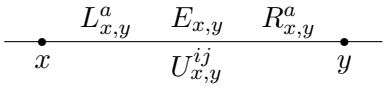

Figure 7.5.: The quantum link operator $U_{x,y}$ and the electric flux operators defined on the link x, y.

Quantum link models are an alternative formulation of lattice gauge theory, where the elements the link matrices are replaced by non-commuting operators acting in a new Hilbert space. We can thus reduce the number of states per link to a finite number, which is allows the implementation in a quantum simulator [60,67,68]. Due to their finite dimensional Hilbert space, quantum link models can also be addressed using exact diagonalization methods [60, 68, 69] (see chapter 8 and 9) and even allow to use cluster algorithms to improve quantum Monte Carlo methods [80, 81]. This allows to study phenomena that can not be addressed in the context of standard lattice gauge theory.

Quantum link models are an extension of ordinary Wilson-type lattice gauge theory, in the same way as quantum spin models are an extension of classical spin models. It is well known how to extend classical spin models to a quantized version by introducing a spin operator for each spin component. The spin operator replaces the ordinary $\mathbb{C}$ number, therefore giving up the commutativity of the different components of the spin. In a similar way, we can introduce quantum operators for each element of the link matrix $U^{ij}_{x,y}$, replacing the $\mathbb{C}$ number by an

operator, which we call a quantum link operator. We thus give up the commutativity of the elements of the link matrices $U^{ij}_{x,y}$ and $U^{ij\dagger}_{x,y}$.

To realize the physics in a finite-dimensional Hilbert space, one quantizes the elements of the link matrices $u^{ij}_{x,y}$ in a similar fashion as we quantize the elements of a classical spin by forming quantum spin operators. These newly quantized link variables are then denoted as U^{ij}_{xy}. As in Wilson's lattice gauge theory, these operators build up a Hamiltonian, which evolves the system in real-time. To take the continuum limit of this lattice gauge theory, one can introduce an additional spatial dimension of finite extent (similar to the procedure in [37]). For example, to regularize QCD in $(3+1)$ dimensions in a quantum link model, one uses a $(4+1)$ dimensional system. The extent of the extra dimension resembles the inverse coupling constant $1/g_s^2$ of the corresponding $(3+1)$-d lattice gauge theory. Hence, varying the extent of the extra dimension allows one to approach the continuum limit, in case the system is in the Coulomb phase. In this limit dimensional reduction to four dimensions occurs. Since the symmetries, including gauge symmetry, stay intact, universality implies that quantum link models correspond to the same continuum field theory as its classical counterpart.

In this work, however, we will not attempt to take the continuum limit of full QCD in $(3+1)$ dimensions. We rather study the intrinsic nature of quantum link models in lower dimensions. Therefore we will not introduce extra dimensions and perform dimensional reductions. As it will turn out, already quantum link models in low dimensions show interesting physics like confinement [60], spontaneous chiral symmetry breaking [68] (see section 8), and restoration at finite baryon density [69] (see section 9).

7.5.2. $U(1)$ Quantum Link Model

Hamiltonian and Commutation Relations

For pedagogical reasons, we first discuss quantum link models with a $U(1)$ gauge symmetry, in order to illustrate the basic idea. In section 7.5.3, we extend this formalism to $SU(N)$ and $U(N)$ gauge groups, which contain further technical difficulties.

The objects, which build up the Hamiltonian are the quantum link operators $U_{x,y}$ and its conjugate momenta $E_{x,y}$, associated with each link x, y. As in Wilson's lattice gauge theory (see section 7.4.5), the $E_{x,y}$ are responsible for the transformation of the link operators $U_{x,y}$ under $U(1)$ gauge transformations:

$$\begin{aligned} U_{x,y} \quad \longrightarrow \quad U'_{x,y} &= \exp\left(i\left(\alpha_x - \alpha_y\right) E_{x,y}\right) U_{x,y} \exp\left(-i\left(\alpha_x - \alpha_y\right) E_{x,y}\right) \\ &= \exp\left(i\alpha_x\right) U_{x,y} \exp\left(-i\alpha_y\right). \end{aligned}$$

This transformation rule leads us to the commutation relation:

$$[E_{x,y}, U_{x,y}] = U_{x,y}. \tag{7.61}$$

The Hermitian conjugate of this equation is

$$[E_{x,y}, U^\dagger_{x,y}] = -U^\dagger_{x,y}, \tag{7.62}$$

since the generators of gauge transformations are Hermitian operators $E^\dagger_{x,y} = E_{x,y}$.

As for Wilson's lattice gauge theory, we define the $U(1)$ Hamiltonian as

$$H = \frac{g^2}{4a} \sum_{\langle xy \rangle} E^a_{x,y} E^a_{x,y} - \frac{1}{ag^2} \sum_{\square} \left(U_{\square} + U^{\dagger}_{\square} \right), \tag{7.63}$$

where the plaquette operator in the spatial k-l plane is defined as

$$U_{\square} = U_{x,x+\hat{k}} U_{x+\hat{k},x+\hat{k}+\hat{l}} U^{\dagger}_{x+\hat{l},x+\hat{k}+\hat{l}} U^{\dagger}_{x,x+\hat{l}}. \tag{7.64}$$

Compared to equation (7.52), we have replaced the link variables $u_{x,y}$ and $u^*_{x,y}$ with quantum link operators $U_{x,y}$ and $U^{\dagger}_{x,y}$, which are non-commuting operators.

Embedding Algebra $su(2)$

The simplest way to satisfy the two commutation relations (7.61) and (7.62) is by representing the three operators by spin operators

$$U_{x,y} = S^+_{x,y}, \quad U^{\dagger}_{x,y} = S^-_{x,y}, \quad E_{x,y} = S^3_{x,y}, \tag{7.65}$$

since spin operators satisfy

$$[S^3, S^+] = S^+, \quad [S^3, S^-] = -S^-.$$

With this replacement, we can calculate the commutation relation among the quantum link operators

$$[U_{x,y}, U^{\dagger}_{x,y}] = [S^+_{x,y}, S^-_{x,y}] = 2S^3_{x,y} = 2E_{x,y}. \tag{7.66}$$

The quantum link operators can be expressed as: $U_{x,y} = S^1_{x,y} + iS^2_{x,y}$, $U^{\dagger}_{x,y} = S^1_{x,y} - iS^2_{x,y}$. The three Hermitian operators $S^1_{x,y}, S^2_{x,y}, S^3_{x,y}$ generate an $su(2)$ algebra on each link x, y. By choosing an irreducible representation of $su(2)$ on a link, the Hilbert space is only finite-dimensional. Choosing a basis, where $S^3_{x,y}$ is a diagonal operator, each basis state can be characterized by its eigenvalue with respect to $S^3_{x,y}$. In the context of $su(2)$, we usually talk about spin. We can think of the degrees of freedom as being spins, one associated with each link. These spin states represent the electric flux. In this basis, $U_{x,y}$ is a spin raising operator (or flux raising operator), $U^{\dagger}_{x,y}$ is a flux lowering operator, $E_{x,y}$ is the diagonal flux operator.

In quantum link models, the Hilbert space is restricted to states of exactly one representation of these operators. We can choose among different representations:

- The fundamental (two-dimensional) spin representation, is the spin (or flux) 1/2 representation. The fluxes of each link x, y can either be up $|\uparrow\rangle_{x,y}$ or down $|\downarrow\rangle_{x,y}$. Two sample configurations are illustrated in figure 7.6, where flux up states are represented by an arrow in the right or upwards direction, flux down states are represented by left or down arrows.

  The quantum link operators act as raising and lowering operators $U_{x,y}|\uparrow\rangle_{x,y} = 0$, $U^{\dagger}_{x,y}|\uparrow\rangle_{x,y} = |\downarrow\rangle_{x,y}$, $U_{x,y}|\downarrow\rangle_{x,y} = |\uparrow\rangle_{x,y}$, $U^{\dagger}_{x,y}|\downarrow\rangle_{x,y} = 0$, while the generator of gauge transformations is diagonal in this basis: $E_{x,y}|\uparrow\rangle_{x,y} = \frac{1}{2}|\uparrow\rangle_{x,y}, E_{x,y}|\downarrow\rangle_{x,y} = -\frac{1}{2}|\downarrow\rangle_{x,y}$.

In this representation, the term $E_{x,y}E_{x,y} = 1/4$ is a trivial constant and can therefore be omitted in the Hamiltonian. Only the plaquette term is then responsible for the dynamics. From the definition of the plaquette (7.64), it can be seen that the plaquette operators raise the flux on two links and lower the flux on the two other links around a plaquette. Figure 7.6 illustrates the action of $U_\square$, which raises the flux on the link x_1, x_2 and x_2, x_3 and lowers the flux on the links x_4, x_3 and x_1, x_4. $U_\square^\dagger$ does the exact opposite. The operators $U_\square$ and $U_\square^\dagger$ annihilate any other configuration of fluxes around a plaquette.

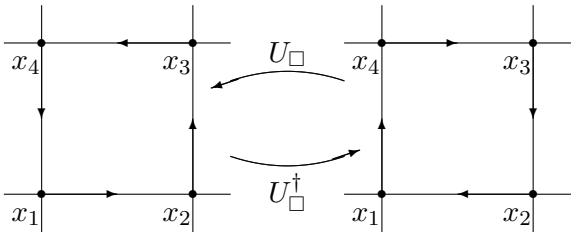

Figure 7.6.: The plaquette operators $U_\square$ and $U_\square^\dagger$ flip the electric flux around the plaquette.

- In any higher-dimensional representation (for example the three-dimensional flux 1 representation), there is an interplay between the two terms in the Hamiltonian. The $E_{x,y}E_{x,y}$ term favors links with a flux that is close to zero. The plaquette term again raises and lowers fluxes around a plaquette.

Gauss Law

As in section 7.4.5, the operator generating gauge transformations at the site x is defined as

$$G_x = \sum_{k=1}^{d} \left(E_{x-\hat{k},x} - E_{x,x+\hat{k}} \right). \tag{7.67}$$

A general gauge transformation can again be parametrized as $W = \prod_x \exp(i\alpha_x G_x)$, which transforms quantum link operators as

$$\begin{aligned} U_{x,y} \quad \longrightarrow \quad W^\dagger U_{x,y} W &= \exp\left(i\left(\alpha_x - \alpha_y\right) E_{x,y}\right) U_{x,y} \exp\left(-i\left(\alpha_x - \alpha_y\right) E_{x,y}\right) \\ &= \exp\left(i\alpha_x\right) U_{x,y} \exp\left(-i\alpha_y\right). \end{aligned}$$

Since the Hamiltonian is gauge invariant ($[G_x, H] = 0$), the generators of gauge transformations G_x and the Hamiltonian can be diagonalized simultaneously. The eigenstates of G_x with zero eigenvalue are the gauge invariant states, because then $W^\dagger|\psi\rangle = |\psi\rangle$.

As in section 7.4.5, we reduce the Hilbert space to the gauge invariant states, requiring $G_x|\psi\rangle = 0$ at any site x. This condition causes the "continuity of flux". This means that (as long as we do not have fermions in the system) at every site x, the number of "incoming" fluxes is the same as the number of "outgoing" fluxes. Incoming flux is the sum of fluxes of links on the "left" of the site x (links $x - \hat{k}, x$), whereas outgoing flux is the sum of fluxes of links on the "right" of the site x (links $x, x + \hat{k}$). This condition is known as the Gauss law.

In the illustrations, this means that at every site the number of incoming arrows is the same as the number of outgoing arrows. A sample configuration for a flux 1/2 system satisfying Gauss's law, is shown in figure 7.7.

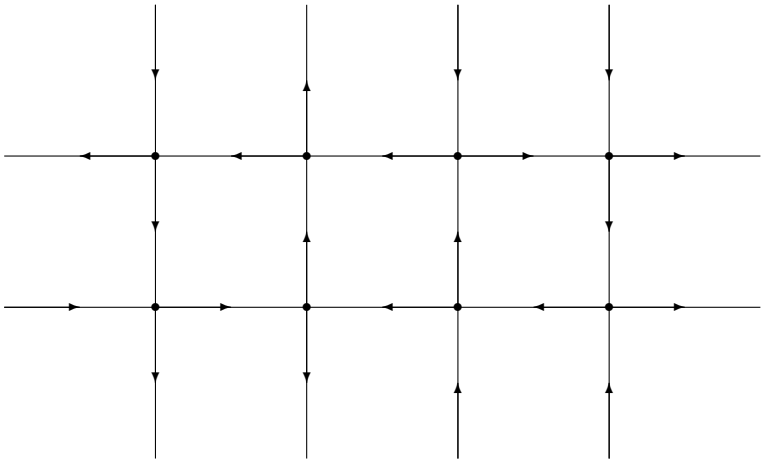

Figure 7.7.: A sample configuration for a flux 1/2 system, which fulfills the Gauss law at every site.

Study

The $U(1)$ quantum link model coupled to dynamical staggered fermions (see section 7.5.4) has been studied in [60]. This study addresses interesting physical phenomena like string breaking and the evolution after a quench, which are both inaccessible to classical simulation methods.

The string breaking happens, when an external $\bar{Q}Q$ pair is separated over a long distance, while a dynamical $q\bar{q}$ pair is crated. The electric flux profile is the order parameter of the breaking, which can be observed in real-time. The large value of the electric flux, which is due to the confining string of the static $\bar{Q}Q$ pair spontaneously breaks down when a dynamical $q\bar{q}$ pair is generated.

The real-time evolution after a quench happens in nature for example after a heavy-ion collision when the quark-gluon plasma returns to the ordinary hadronic vacuum and thus breaks the chiral symmetry spontaneously. In this work the spontaneous breaking of the parity symmetry was studied by preparing a parity-invariant initial state in which we find a staggered electric flux configuration. When approaching the true vacuum this state will spontaneously break parity, which can also be observed in real-time.

7.5.3. $SU(N)$ and $U(N)$ Quantum Link Models

Hamiltonian and Commutation Relations

The objects which build up the Hamiltonian with an $SU(N)$ gauge symmetry are the quantum link operators $U^{ij}_{x,y}$, which are $N \times N$ matrices of operators, as well as the operators $L^a_{x,y}$ and $R^a_{x,y}$. For a Hamiltonian with an additional $U(1)$ gauge symmetry, there is also the operator $E_{x,y}$. As in Wilson's lattice gauge theory (see section 7.4.3), $L^a_{x,y}$, $R^a_{x,y}$, and $E_{x,y}$ are responsible for the transformation of the link operators $U^{ij}_{x,y}$ under gauge transformations (7.76). The transformation rules lead us to the same commutation relation as the ones derived in section 7.4.3:

$$[R^a_{x,y}, U^{ij}_{x,y}] = U^{ik}_{x,y}\lambda^a_{kj}, \qquad [L^a_{x,y}, U^{ij}_{x,y}] = -\lambda^a_{ik}U^{kj}_{x,y}, \qquad [E_{x,y}, U^{ij}_{x,y}] = U^{ij}_{x,y}. \tag{7.68}$$

The Hermitian conjugate of these equations are

$$[R^a_{x,y}, U^{ij\dagger}_{x,y}] = -U^{ik\dagger}_{x,y}\lambda^a_{jk}, \qquad [L^a_{x,y}, U^{ij\dagger}_{x,y}] = \lambda^a_{ki}U^{kj\dagger}_{x,y}, \qquad [E_{x,y}, U^{ij\dagger}_{x,y}] = -U^{ij\dagger}_{x,y}. \tag{7.69}$$

Combining the Hamiltonian of $SU(N)$ lattice gauge theory from section 7.4.3 with the $U(1)$ quantum link Hamiltonian, one gets

$$H = \frac{g^2}{2}\sum_{\langle xy\rangle}\left(L^a_{x,y}L^a_{x,y} + R^a_{x,y}R^a_{x,y}\right) + \frac{g'^2}{2}\sum_{\langle x,y\rangle}E^2_{x,y} - \frac{1}{4g^2}\sum_{\square}\left(\mathrm{Tr}U_{\square} + \mathrm{H.c.}\right), \tag{7.70}$$

where we have redefined the coupling constants g and g'. The trace of the plaquette operator in the k-l plane is defined as

$$\mathrm{Tr}U_{\square} = U^{ij}_{x,x+\hat{k}}U^{jm}_{x+\hat{k},x+\hat{k}+\hat{l}}U^{nm\dagger}_{x+\hat{l},x+\hat{k}+\hat{l}}U^{in\dagger}_{x,x+\hat{l}}. \tag{7.71}$$

We have replaced the elements of the link variables $u^{ij}_{x,y}$ and $u^{ij*}_{x,y}$ with quantum link operators $U^{ij}_{x,y}$ and $U^{ij\dagger}_{x,y}$, which are non-commuting operators. $U^{ij\dagger}_{x,y}$ is meant to be the Hermitian conjugate of the operator $U^{ij}_{x,y}$, indices are not interchanged. $L^a_{x,y}$ and $R^a_{x,y}$ are the generators of $SU(N)$ gauge transformations on a link x, y from the left and from the right, respectively. $E_{x,y}$ are the generators of an additional $U(1)$ gauge symmetry.

In the form (7.72), the Hamiltonian is invariant under $SU(N)\otimes U(1)$ gauge transformations. If the system should only be invariant under $SU(N)$ gauge transformation, the additional $U(1)$ symmetry can be broken by adding a determinant term to the Hamiltonian:

$$\begin{aligned} H = &\frac{g^2}{2}\sum_{\langle xy\rangle}\left(L^a_{x,y}L^a_{x,y} + R^a_{x,y}R^a_{x,y}\right) + \frac{g'^2}{2}\sum_{\langle x,y\rangle}E^2_{x,y} \\ &- \frac{1}{4g^2}\sum_{\square}\left(\mathrm{Tr}U_{\square} + \mathrm{H.c.}\right) - \gamma\sum_{\langle x,y\rangle}\left(\det U_{x,y} + \mathrm{H.c.}\right). \end{aligned} \tag{7.72}$$

For $\gamma \neq 0$, this Hamiltonian is still invariant under $SU(N)$ gauge transformation, but not under the additional $U(1)$ symmetry, generated by the operators $E_{x,y}$.

Embedding Algebra $su(2N)$

The simplest way to satisfy the commutation relations (7.68) and (7.69) is by embedding the quantum link operators and the generators of $U(N)$ gauge transformations in an $su(2N)$ algebra. In appendix A we present the generators of an $su(2N)$ algebra and show that they can be combined in order to represent quantum link operators and the generators of gauge transformations, satisfying the above commutation relations. We further present the explicit matrix representation for the fundamental representation of the $su(2N)$ algebra.

As shown in appendix A, by embedding the quantum link operators in the $su(2N)$ algebra, they satisfy the commutation relations (7.68) and (7.69), as well as commutation relations among the quantum link operators

$$[U^{ij}, U^{kl\dagger}] = 2(\tfrac{4}{N}\delta_{ik}\delta_{jl}E + \delta_{ik}\lambda^a_{lj}R^a - \delta_{jl}\lambda^a_{ik}L^a), \qquad [U^{\dagger ij}, U^{kl\dagger}] = [U^{ij}, U^{kl}] = 0. \tag{7.73}$$

By choosing an irreducible representation of $su(2N)$ on each link, the link Hilbert space is only finite-dimensional. There are $(N-1)$ operators among the $L^a_{x,y}$ and $(N-1)$ operators among the $R^a_{x,y}$, which are diagonal, so together with the diagonal operator $E_{x,y}$, we have $(2N-1)$ diagonal operators. This means that there are $(2N-1)$ quantum numbers, which are the eigenvalues with respect to each of these diagonal operators. These quantum numbers again represent the electric fluxes. We thus have $(2N-1)$ independent fluxes per link. This is in close analogy to the $U(1)$ quantum link model (see section 7.5.2), where we just encountered one flux variable. Again, the quantum link operators $U^{ij}_{x,y}$ and $U^{ij\dagger}_{x,y}$ raise or lower some of the fluxes.

In appendix A we have given an explicit expression for the operators in the fundamental representation, which is $2N$-dimensional. The $2N$ basis vectors at each link x, y are the eigenstates of the diagonal operators among the $L^a_{x,y}$ and $R^a_{x,y}$ and of $E_{x,y}$. The terms $L^a_{x,y}L^a_{x,y} + R^a_{x,y}R^a_{x,y}$ and $E_{x,y}E_{x,y}$ are all proportional to the unit matrix in the fundamental representation and have thus no effect on the dynamics. It can further be shown that the γ-term in the Hamiltonian (7.72) is always zero in the fundamental representation. This term is responsible for breaking explicitly the additional $U(1)$ gauge symmetry. Therefore, in order to work with an $SU(N)$ (instead of a $U(N)$) gauge symmetry, one has to work with higher-dimensional representations. The smallest representation, for which $\det(U_{x,y}) \neq 0$, is a $[(2N)!/(N!)^2]$-dimensional representation [65].

Gauss Law

As already discussed, we consider quantum link models with an $SU(N)$ or a $U(N)$ gauge symmetry. In section 7.4.4, we introduced the site based generators of $SU(N)$ gauge transformations G^a_x, where a is the index of the generator ($a = 1, 2, \ldots, N^2-1$). These operators obey $[G^a_x, G^b_y] = 2i\delta_{xy}f^{abc}G^c_x$. The G_x are again the generators of the additional $U(1)$ gauge

symmetry. Generators of the $SU(N)$ and $U(N)$ gauge transformations read

$$\begin{aligned} SU(N): \qquad & G^a_x = \sum_k \left(L^a_{x,x+\hat{k}} + R^a_{x-\hat{k},x} \right), \\ U(1): \qquad & G_x = \sum_k \left(E_{x-\hat{k},x} - E_{x,x+\hat{k}} \right). \end{aligned} \tag{7.74}$$

A general $U(N)$ gauge transformation can then be parametrized by the unitary operators

$$V = \exp\left(i \sum_x \alpha^a_x G^a_x \right), \qquad W = \exp\left(i \sum_x \alpha_x G_x \right). \tag{7.75}$$

At each site x, these operators generate gauge transformations, which affect all the links $x, x+\hat{k}$ and $x-\hat{k}, x$ emanating from the point x:

$$\begin{aligned} SU(N): \quad U^{ij}_{x,y} \quad \longrightarrow \quad V^\dagger U^{ij}_{x,y} V &= \exp\big(-i\left(\alpha^a_x L^a_{x,y} + \alpha^a_y R^a_{x,y}\right)\big) U^{ij}_{x,y} \exp\big(i\left(\alpha^a_x L^a_{x,y} + \alpha^a_y R^a_{x,y}\right)\big) \\ &= \big[\exp\big(i\alpha^a_x \lambda^a\big)\big]^{ik} U^{kl}_{x,y} \big[\exp\big(-i\alpha^a_y \lambda^a\big)\big]^{lj}, \\ U(1): \quad U^{ij}_{x,y} \quad \longrightarrow \quad W^\dagger U^{ij}_{x,y} W &= \exp\left(i\left(\alpha_x - \alpha_y\right) E_{x,y}\right) U^{ij}_{x,y} \exp\left(-i\left(\alpha_x - \alpha_y\right) E_{x,y}\right) \\ &= \exp\left(i\alpha_x\right) U^{ij}_{x,y} \exp\left(-i\alpha_y\right). \end{aligned} \tag{7.76}$$

The $SU(N)$ transformations indeed leave the Hamiltonian invariant ($[G^a_x, H] = 0$). For a $U(N)$ quantum link Hamiltonian, also the additional $U(1)$ transformation commutes with the Hamiltonian ($[G_x, H] = 0$). This allows us define a basis with respect to the operators G^a_x (and G_x) before diagonalizing the Hamiltonian. We then only choose the physical states, which are gauge invariant. These are the singlet states of G^a_x (and G_x), which means that we require the Gauss law

$$G^a_x |\psi\rangle = 0, \qquad (G_x |\psi\rangle = 0). \tag{7.77}$$

The reason is that then $W^\dagger |\psi\rangle = |\psi\rangle$ (and $V^\dagger |\psi\rangle = |\psi\rangle$).

By imposing the Gauss law, the dimension of the physical Hilbert space is reduced. This again, leads to a "continuity of flux" at every site x. This is exactly what we already experienced when imposing the Gauss law in the $U(1)$ quantum link model (see section 7.5.2) except that now we encounter flux from the Abelian and the non-Abelian generators.

7.5.4. Staggered Fermions in Quantum Link Models

In the quantum link model, staggered fermions are introduced in the same way as for ordinary lattice gauge theory in the Hamiltonian formalism (see section 7.4.6).

Again, the creation $\psi^{\dagger i}_x$ and annihilation operators ψ^i_x obey the usual anti-commuting relations

$$\{\psi^i_x, \psi^j_y\} = \{\psi^{\dagger i}_x, \psi^{\dagger j}_y\} = 0, \qquad \{\psi^i_x, \psi^{\dagger j}_y\} = \delta_{xy}\delta_{ij}. \tag{7.78}$$

These operators act on a Hilbert space and have a color index i. The Dirac structure is spread out over the space-time lattice. The quantum link model Hamiltonian (7.72) together with

the fermionic part reads

$$\begin{aligned} H = &- t \sum_x \sum_{k=1}^{d} \left(s_{x,x+\hat{k}} \psi_x^\dagger U_{x,x+\hat{k}} \psi_{x+\hat{k}} + \text{H.c.} \right) + m \sum_x s_x \psi_x^\dagger \psi_x \\ &+ \frac{g^2}{2} \sum_{\langle xy \rangle} \left(L_{x,y}^a L_{x,y}^a + R_{x,y}^a R_{x,y}^a \right) + \frac{g'^2}{2} \sum_{\langle x,y \rangle} E_{x,y}^2 \\ &- \frac{1}{4g^2} \sum_{\square} \left(\text{Tr} U_{\square} + \text{H.c.} \right) - \gamma \sum_{\langle x,y \rangle} \left(\det U_{x,y} + \text{H.c.} \right), \end{aligned} \tag{7.79}$$

where $s_x = (-1)^{x_1 + \cdots + x_d}$ and $s_{x,x+\hat{k}} = (-1)^{x_1 + \cdots + x_{k-1}}$, g, g' are gauge couplings, and m is the mass parameter of the fermions. We have also introduced the hopping parameter t.

As for the Hilbert space of the fermions, also the Hilbert space on which the quantum link operators U^{ij}, $U^{ij\dagger}$ and the generators of gauge transformation L^a, R^a, and $E_{x,y}$ act is finite-dimensional. In section 7.5.3 these operators have been discussed in detail.

For $\gamma = 0$, this Hamiltonian is invariant under $SU(N) \otimes U(1) = U(N)$ gauge transformations. Again, the site-based generators of gauge transformations are defined as

$$V = \prod_x \exp\left(i \alpha_x^a G_x^a \right), \qquad W = \prod_x \exp\left(i \alpha_x G_x \right) \tag{7.80}$$

and transform the quantum link operators $U_{x,y}^{ij}$ and the fermion field operators ψ_x^i as

$$\begin{aligned} SU(N): \quad & V^\dagger U_{x,y}^{ij} V = \left[\exp\left(i \alpha_x^a \lambda^a \right) \right]^{ik} U_{x,y}^{kl} \left[\exp\left(-i \alpha_y^a \lambda^a \right) \right]^{lj}, \quad V^\dagger \psi_x^i V = \left[\exp\left(i \alpha_x^a \lambda^a \right) \right]^{ij} \psi_x^j, \\ U(1): \quad & W^\dagger U_{x,y}^{ij} W = \exp\left(i \alpha_x \right) U_{x,y}^{ij} \exp\left(-i \alpha_y \right), \qquad W^\dagger \psi_x^i W = \exp\left(i \alpha_x \right) \psi_x^i. \end{aligned} \tag{7.81}$$

In order for the fermion field operators ψ_x^i to transform correctly under gauge transformations, the generators of gauge transformations are expressed in terms of the flux operators L^a, R^a, E, and the fermion field operators ψ^i, $\psi^{\dagger i}$ as

$$\begin{aligned} SU(N): \quad & G_x^a = \psi_x^{\dagger i} \lambda_{ij}^a \psi_x^j + \sum_k \left(L_{x,x+\hat{k}}^a + R_{x-\hat{k},x}^a \right), \\ U(1): \quad & G_x = \psi_x^{\dagger i} \psi_x^i + \sum_k \left(E_{x-\hat{k},x} - E_{x,x+\hat{k}} \right). \end{aligned} \tag{7.82}$$

The $SU(N)$ transformations indeed leave the Hamiltonian invariant ($[G_x^a, H] = 0$). For a $U(N)$ quantum link Hamiltonian, also the additional $U(1)$ transformation commutes with the Hamiltonian ($[G_x, H] = 0$). Again, the physical states $|\psi\rangle$ have to be gauge invariant, which means

$$G_x^a |\psi\rangle = 0, \qquad (G_x |\psi\rangle = 0). \tag{7.83}$$

The Gauss law of the non-Abelian generators (left part of 7.83) requires at every site x that the sum of all fluxes of each links emanating from the site x have to form a color-singlet state together with the fermion at the site x.

We will work out the fundamental representation of a $U(2)$ quantum link Hamiltonian with fermions and quantum link operators in $(1+1)$ dimensions explicitly and discuss all the gauge invariant states in section 8.3.

7.6. Global Symmetries of Quantum Link Models

Besides the local gauge symmetry, which has been discussed in the previous sections, the Hamiltonian of quantum link models is also invariant under certain global symmetries. A prominent global symmetry in field theory is the Euclidean group (see section 7.2.2), which gets, however, explicitly broken by the lattice. Only a discrete subgroup thereof remains a symmetry of the Hamiltonian. This subgroup consists of

- the spacial translations,
- rotations by 90°,
- charge conjugation,
- and the parity transformation.

Chiral symmetry poses a delicate problem, when implementing gauge theories on the lattice. Staggered fermions still have a remnant of chiral symmetry, which is in the Hamiltonian formulation reduced to

- a $\mathbb{Z}_2$ chiral symmetry.

For an $SU(N)$ quantum link model, we further have

- an additional global $U(1)$ symmetry,

which is responsible for a conservation of baryon number. For $U(N)$ quantum link models this $U(1)$ symmetry is a local symmetry and thus Gauss' law eliminates baryons from the physical Hilbert space.

Some of these symmetries are important for our applications in the following chapters and are therefore discussed in more details in this section.

7.6.1. Spatial Translations

When we introduced staggered fermions in section 7.3.2, we noted that the Dirac components got spread out over the lattice. Simply shifting the whole system by one lattice spacing means that we are considering a different Dirac component of the fermions. The Hamiltonian is therefore not invariant under this transformation. This becomes evident when we look at the mass term of the Hamiltonian (7.79), which is not invariant against a translation by one lattice spacing due to the staggered phase factor $s_x = (-1)^{x_1+\cdots+x_d}$.

A correct translation operation T_k (translating in the k-direction) has to transform the system by two lattice spacings. This means that the fermion field operators ψ_x and the quantum link operators $U_{x,y}$ have to be transformed as

$$T_k: \qquad {}^{T_k}U_{x,y} = U_{x+2\hat{k},y+2\hat{k}}, \qquad {}^{T_k}\psi_x = \psi_{x+2\hat{k}}. \tag{7.84}$$

Also the generators of gauge transformations $L^a_{x,y}, R^a_{x,y}, E_{x,y}$ have to be transformed as

$$T_k: \qquad {}^{T_k}L^a_{x,y} = L^a_{x+2\hat{k},y+2\hat{k}}, \qquad {}^{T_k}R^a_{x,y} = R^a_{x+2\hat{k},y+2\hat{k}}, \qquad {}^{T_k}E_{x,y} = E_{x+2\hat{k},y+2\hat{k}}. \tag{7.85}$$

Note that the lattice is periodic, therefore all coordinates are given modulo the number of lattice sites in the k-direction, denoted as L_k. It is easy to check that this transformation leaves the Hamiltonian (7.79) invariant.

Let us consider a periodic lattice with L_k sites in the k-direction. $L_k/2$ consecutive translations T_k (in the k-direction by two lattice spacings) shift the system once around the lattice ending at the original position, which implies that $T_k^{L_k/2} = \mathbb{1}$. Therefore the eigenvalues of T_k are complex phases:

$$T_k|\psi\rangle = \exp\left(ip_k\right)|\psi\rangle \tag{7.86}$$

We find that for

$$\begin{aligned} L_k/2 \text{ even}: \qquad & p_k \in \left\{0, \pm\tfrac{4\pi}{L_k}, \pm\tfrac{8\pi}{L_k}, \ldots, \pi\right\}, \\ L_k/2 \text{ odd}: \qquad & p_k \in \left\{0, \pm\tfrac{4\pi}{L_k}, \pm\tfrac{8\pi}{L_k}, \ldots, \pm\pi\tfrac{L_k-2}{L_k}\right\}. \end{aligned} \tag{7.87}$$

p_k is known as the momentum (or true momentum) of the translation eigenstate $|\psi\rangle$. Since T_k is a symmetry, the eigenstates of the Hamiltonian can simultaneously be diagonalized with respect to T_k. Therefore each eigenstate of the Hamiltonian has a definite momentum p_k in each direction.

7.6.2. Charge Conjugation

What we define here as a charge conjugation operation C_k is in fact a combination of a charge conjugation and a flavor transformation in the k-direction (see 7.6.4). A charge conjugation transforms particles into antiparticles and changes the representation of the generators of the embedding $su(2N)$ algebra (see appendix A) to its conjugate representation. The fermion operators and the operators of the embedding $su(2N)$ algebra of therefore transform as

$$\begin{aligned} C_k: \quad & {}^{C_k}U^{ij}_{x,y} = U^{ij\dagger}_{x+\hat{k},y+\hat{k}}, \qquad {}^{C_k}\psi^i_x = (-1)^{x_1+\cdots+x_k}\psi^{i\dagger}_{x+\hat{k}}, \\ & {}^{C_k}L^a_{x,y} = -L^{a*}_{x+\hat{k},y+\hat{k}}, \quad {}^{C_k}R^a_{x,y} = -R^{a*}_{x+\hat{k},y+\hat{k}}, \qquad {}^{C_k}E_{x,y} = -E_{x+\hat{k},y+\hat{k}}. \end{aligned} \tag{7.88}$$

Note that the hopping term (the one with the parameter t) in the Hamiltonian (7.79) transforms to its Hermitian conjugate. Note further, that we can choose a representation in which the matrix of the operator $\sum_a L^a L^a + R^a R^a$ is real and therefore not affected by complex conjugation.

Two consecutive charge conjugation operations correspond to a spatial translation, which implies that $C_k^2 = T_k$. We can therefore separate the eigenvalue of C_k into a momentum p_k and a charge parity sign $c_k \in \{+1, -1\}$:

$$C_k|\psi\rangle = (-1)^{c_k}\exp(ip_k/2)|\psi\rangle \qquad \Longrightarrow \qquad C_k^2|\psi\rangle = \exp(ip_k)|\psi\rangle = T_k|\psi\rangle \tag{7.89}$$

When charge conjugation C_k is a symmetry, the eigenstates of the Hamiltonian can simultaneously be diagonalized with respect to C_k. Each eigenstate of the Hamiltonian has then a definite charge conjugation parity c_k in each k-direction.

There is, however, a subtlety with these charge conjugation symmetries, because we have transformed the quantum link operators and the generators of gauge transformations to operators in the conjugate representation. Only for representations which are equivalent to their conjugate representation charge conjugation is a symmetry. Such representations of the $su(2N)$ algebra exist. One of them corresponds to a Young tableau with N vertically aligned boxes. This is a $\frac{(2N)!}{(N!)^2}$-dimensional representation of the embedding $su(2N)$ algebra. This will become evident when we talk about the rishon representation in section 8.2.1. Only for a representation with exactly N rishons, the operators are transformed to the same representation.

7.6.3. Parity Transformation

In odd dimensions d, a parity transformation P inverts all coordinates. The inversion has an additional consequence on the generators of gauge transformations: The operators generating gauge transformations on the left end of a link are now associated with the right end of a link and vice versa. Therefore the operators of the Hamiltonian transform as

$$\begin{aligned} P: \qquad & {}^{P}U^{ij}_{x,y} = U^{ji\dagger}_{-y,-x}, \qquad {}^{P}\psi^{i}_{x} = \psi^{i}_{-x}, \\ & {}^{P}L^{a}_{x,y} = R^{a}_{-y,-x}, \qquad {}^{P}R^{a}_{x,y} = L^{a}_{-y,-x}, \qquad {}^{P}E_{x,y} = -E_{-y,-x}. \end{aligned} \tag{7.90}$$

Note the periodicity of the lattice: A coordinate $-x$ corresponds to the lattice site $(-x_1 + L_1, -x_2 + L_2, \ldots, -x_d + L_d)$. Note further that the hopping term in the Hamiltonian (7.79) transforms to its Hermitian conjugate.

For a system in even dimensions d, this kind of parity transformation corresponds to a rotation of the system by 180°. This is not what we mean, when we talk about parity transformations. Instead we would therefore consider a reflection, for example, on the 2-axis as a parity transformation P.

Two consecutive parity transformations flip the system back in the original state, which implies that $P^2 = \mathbb{1}$. Therefore the eigenvalues of P are $p \in \{+1, -1\}$:

$$P|\psi\rangle = p|\psi\rangle \tag{7.91}$$

Since parity P is a symmetry, the eigenstates of the Hamiltonian can simultaneously be diagonalized with respect to P. Therefore each eigenstate of the Hamiltonian has a definite parity p. Note that a parity transformation does not commute with, for example, a translation. Therefore the states can not simultaneously be associated with the parity p and momentum p_k quantum numbers.

7.6.4. Chiral Transformation

In section 7.2.2 we have introduced the chiral symmetry as an operation which mixes the different flavor components of the fermions separately for the left and right-handed chirality. Since we are working with staggered fermions, the different flavors are identified with the different "tastes" of the staggered fermions. These tastes correspond to the different fermion doublers and are (together with the Dirac components) spread out over the lattice. Therefore, a chiral transformation has to move the fermions in some way over the lattice. We see that the mass term breaks explicitly a symmetry which shifts the system by one lattice spacing. This is exactly what we expect to happen for the chiral symmetry. On the other hand, the symmetry of shifting the system consecutively by one lattice spacing in an even number of different directions corresponds to a "taste symmetry".

Let us define the shift symmetry by one lattice spacing in the k-direction. The operators transform as

$$\begin{aligned} S_k: \qquad & {}^{S_k}U^{ij}_{x,y} = U^{ij}_{x+\hat{k},y+\hat{k}}, \qquad {}^{S_k}\psi^i_x = (-1)^{x_{k+1}+\cdots+x_d}\psi^i_{x+\hat{k}}, \\ & {}^{S_k}L^a_{x,y} = L^a_{x+\hat{k},y+\hat{k}}, \qquad {}^{S_k}R^a_{x,y} = R^a_{x+\hat{k},y+\hat{k}}, \qquad {}^{S_k}E_{x,y} = E_{x+\hat{k},y+\hat{k}}. \end{aligned} \tag{7.92}$$

For massless fermions ($m = 0$), we find an exact chiral symmetry, which is broken explicitly by the lattice from $SU(N_f)_L \otimes SU(N_f)_R \otimes U(1)_V$ (see section 7.2.2) to a $(\mathbb{Z}_2)^d$ chiral symmetry. Since in this case, this shift transformation S_k is a symmetry, the eigenstates of the Hamiltonian can simultaneously be diagonalized with respect to S_k. Two consecutive shift transformations correspond to a spatial translation, i.e. $S_k^2 = T_k$. We can therefore associate each eigenstate of the Hamiltonian with a definite so-called fake momentum in the k-direction, denoted as p'_k which is $p'_k = \pm p_k/2$:

$$S_k|\psi\rangle = \exp(ip'_k)|\psi\rangle \qquad \Longrightarrow \qquad S_k^2|\psi\rangle = \exp(ip_k)|\psi\rangle = T_k|\psi\rangle \tag{7.93}$$

For a non-zero mass m term in the Hamiltonian $m\sum_x(-1)^{x_1+\cdots x_d}\psi^{i\dagger}_x\psi^i_x$ the chiral symmetry is broken explicitly to a $(\mathbb{Z}_2)^{d-1}$ taste symmetry.

As it is encountered in nature (see section 7.2.2), we try to find a spontaneous breaking of the chiral symmetry in the massless case ($m = 0$). A spontaneously broken symmetry gives rise to two degenerate vacuum states, which can be observed when diagonalizing the Hamiltonian. Since we work in a finite spatial volume V, this degeneracy is not exact. The energy difference of the two lowest states in the spectrum $\Delta E = E_1 - E_0$ scales as

$$\Delta E \sim \exp\left(-\alpha V\right), \tag{7.94}$$

where α is some constant.

Chapter 8.

Application I: $U(N)$ Quantum Link Model

8.1. Motivating the $U(N)$ Quantum Link Model

$U(N)$ quantum link models are ideal toy models to study phenomena including spontaneous breaking of the chiral symmetry in a gauge theory. Due to their finite-dimensional Hilbert space per link, these models can be quantum simulated by implementing them in ultra-cold matter in an optical lattice, which is explained in section 8.2. In section 8.3 all operators appearing in the $U(2)$ quantum link model are constructed explicitly. Results of exact diagonalization calculations are presented, which show the spontaneous breaking of the chiral symmetry even already in $(1+1)$ dimensions. These results can be used to validate an implementation in a quantum simulator.

8.2. Implementation of $U(N)$ Quantum Link Models in an Optical Lattice

8.2.1. Rishon Representation

For implementing quantum link models in a quantum simulator it turns out to be advantageous to use the so called rishon representation. This representation is based on the fact that the quantum link operators can be represented as fermion bi-linears. These fermions are called rishons. An optical lattice setup can then be used to simulate the dynamics of these rishons, by studying the fermions evolving on an optical lattice setup.

Rishons are fermions associated with the left and right end of a link. In d dimensions, the creation $c^{i\dagger}_{x,\pm k}$ and annihilation operators $c^{i}_{x,\pm k}$ obey the usual anti-commuting relations

$$\{c^{i}_{x,\pm k}, c^{j}_{y,\pm l}\} = \{c^{i\dagger}_{x,\pm k}, c^{j\dagger}_{y,\pm l}\} = 0, \qquad \{c^{i}_{x,\pm k}, c^{j\dagger}_{y,\pm l}\} = \delta_{xy}\delta_{\pm k,\pm l}\delta_{ij}, \tag{8.1}$$

where $i, j \in \{1, \ldots, N\}$ are color indices and k, l label the spacial direction. The quantum link operators and the link based generators of gauge transformations can be expressed in terms of these rishon creation and annihilation operators as

$$\begin{aligned} R^{a}_{x,x+\hat{k}} &= c^{i\dagger}_{x+\hat{k},-k}\ \lambda^{a}_{ij}\ c^{j}_{x+\hat{k},-k}, & L^{a}_{x,x+\hat{k}} &= c^{i\dagger}_{x,+k}\ \lambda^{a}_{ij}\ c^{j}_{x,+k}, \\ E_{x,x+\hat{k}} &= \frac{1}{2}\left(c^{i\dagger}_{x+\hat{k},-k}c^{i}_{x+\hat{k},-k} - c^{i\dagger}_{x,+k}\ c^{i}_{x,+k}\right), & U^{ij}_{x,x+\hat{k}} &= c^{i}_{x,+k}\ c^{j\dagger}_{x+1,-k}. \end{aligned} \tag{8.2}$$

This representation fulfills the commutation relations of the quantum link model (7.68) and (7.73), as it can be checked straightforwardly. Figure 8.1 sketches for example how the quantum link operator $U_{x,y}$ in one dimension is replaced with the rishons $c_{x,+}$ and $c_{y,-}$ associated with the left and right end of the link x, y.

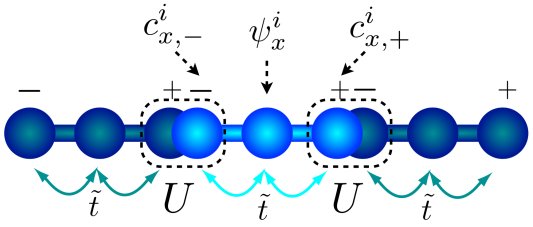

FIGURE 8.1.: A superlattice with rishon and fermion sites. Quantum link operators U can be represented in terms of rishon operators c, $c^\dagger$.

The quantum link Hamiltonian can be expressed in terms of the rishons. We leave out the part with the electric flux operators, since we will not need it in the future to study interesting dynamics. The fermionic and plaquette part of the Hamiltonian (7.79) then reads

$$\begin{aligned} H =& -t\sum_{\langle xy\rangle}\left(s_{x,y}\psi^{i\dagger}_x U^{ij}_{x,y}\psi^j_y + \text{H.c.}\right) + m\sum_x s_x\psi^{i\dagger}_x\psi^i_x - \frac{1}{4g^2}\sum_\square(\text{Tr}U_\square + \text{H.c.}) \qquad (8.3)\\ =& -t\sum_{\langle x,y=x+\hat{k}\rangle}\left(s_{x,y}\psi^{i\dagger}_x c^i_{x,+k}\; c^{j\dagger}_{y,-k}\psi^j_y + \text{H.c.}\right) + m\sum_x s_x\psi^{i\dagger}_x\psi^i_x - \frac{1}{4g^2}\sum_\square(\text{Tr}U_\square + \text{H.c.}), \end{aligned}$$

where the plaquette term in the k-l plane can be expressed as

$$\begin{aligned} \text{Tr}U_\square &= U^{ij}_{x,x+\hat{k}}U^{jm}_{x+\hat{k},x+\hat{k}+\hat{l}}U^{nm\dagger}_{x+\hat{l},x+\hat{k}+\hat{l}}U^{in\dagger}_{x,x+\hat{l}}\\ &= (c^i_{x,+k}c^{j\dagger}_{x+\hat{k},-k})(c^j_{x+\hat{k},+l}c^{m\dagger}_{x+\hat{k}+\hat{l},-l})(c^m_{x+\hat{k}+\hat{l},-k}c^{n\dagger}_{x+\hat{l},+k})(c^n_{x+\hat{l},-l}c^{i\dagger}_{x,+l}). \qquad (8.4) \end{aligned}$$

Let us study the terms involving rishons in more details. The hopping term, proportional to t, induces a hop of a fermion from site y to x and simultaneously induces a hop of a rishon from $(x, +k)$ to $(y, -k)$. This term therefore describes the hopping of different kinds of fermions, one fermion hopping from y to x, while another one (the rishon) hops from x to y. The plaquette term, on the other hand, only involves the rishons. On each link at the boundary of a plaquette it induces a hop of a rishon from one end of the link to the other end (see figure 8.2).

The hopping of the rishons underlies certain constraints. In particular, the Hamiltonian (8.3) conserves the total number of rishons per link. We identify the number of rishons on each link as

$$\mathcal{N}_{x,x+\hat{k}} = c^{i\dagger}_{x,+k}c^i_{x,+k} + c^{i\dagger}_{x+\hat{k},-k}c^i_{x+\hat{k},-k} \qquad (8.5)$$

and notice that this operator commutes with the Hamiltonian. The number of rishons per link is fixed by choosing a certain representation of the embedding quantum link algebra $su(2N)$ (see section 7.5.3). For example, in the fundamental representation, which is $2N$-dimensional (corresponding to a Young tableau with one box), we find one rishon per link. The reason

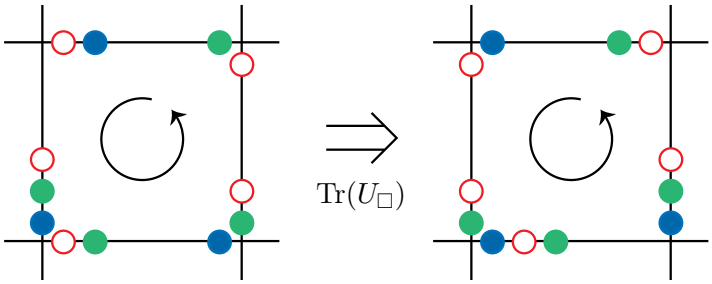

Figure 8.2.: The plaquette term lets the rishons hop around the plaquette.

for this is that one rishon can be found in one of $2N$ states: The rishon can have N different colors and sit either on the left end of the link (at $(x, +k)$) or on the right end of the link (at $(x + \hat{k}, -k)$). For two rishons we find $N(2N-1)$ possible ways for them to arrange on the left or right end of the link, corresponding to an $N(2N-1)$-dimensional representation of the quantum link algebra (corresponding to a Young tableau with two vertically aligned boxes). It turns out that a representation with $\mathcal{N} = n$ rishons corresponds to a Young tableau with n vertically aligned boxes.

In order to study the Gauss law, we represent the generators of gauge transformations in terms of the rishon operators:

$$\begin{aligned} SU(N): \quad G^a_x &= \psi^{\dagger i}_x \lambda^a_{ij} \psi^j_x + \sum_k \left(L^a_{x,x+\hat{k}} + R^a_{x-\hat{k},x} \right) \\ &= \psi^{\dagger i}_x \lambda^a_{ij} \psi^j_x + \sum_k \left(c^{i\dagger}_{x,+k} \lambda^a_{ij} c^j_{x,+k} + c^{i\dagger}_{x,-k} \lambda^a_{ij} c^j_{x,-k} \right), \\ U(1): \quad G_x &= \psi^{\dagger i}_x \psi^i_x + \sum_k \left(E_{x-\hat{k},x} - E_{x,x+\hat{k}} \right) \\ &= \psi^{\dagger i}_x \psi^i_x + \sum_k \frac{1}{2} \left(c^{i\dagger}_{x,-k} c^i_{x,-k} - c^{i\dagger}_{x-\hat{k},+k} c^i_{x-\hat{k},+k} - c^{i\dagger}_{x+\hat{k},-k} c^i_{x+\hat{k},-k} + c^{i\dagger}_{x,+k} c^i_{x,+k} \right). \end{aligned} \tag{8.6}$$

In order for a state $|\psi\rangle$ to be gauge invariant under $U(N)$ gauge transformations, we require the Gauss law $G^a|\psi\rangle = 0$ and $G|\psi\rangle = 0$. From equation (8.6) we see that the Gauss law for the $SU(N)$ generators require that at every site x the rishons and the fermions need to form a color singlet state. The physical meaning of the Gauss law of the $U(1)$ generator is less obvious. Let us first study the electric flux operator $E_{x,x+\hat{k}}$ from equation (8.2). This flux operator measures the difference of the number of rishons on the right end of the link minus the number of rishons on the left end of the link. The Gauss law of the $U(1)$ generator requires that at every site x on both links, the link $x - \hat{k}, x$ and the link $x, x + \hat{k}$, this difference of rishons is constant, unless there is a fermion on the site x.

In section 7.5.3 we explained that it is also possible to study $SU(N)$ quantum link models with no additional $U(1)$ symmetry by introducing the γ-term. This term involves the determinant of the quantum link operator and thus breaks the additional $U(1)$ symmetry. It is also possible to represent this term using rishons [65]. We will, however, not study this term in more details.

8.2.2. Gauge Invariant Operators

In the previous section the Gauss law in the rishon representation was interpreted as a requirement to find color singlet combinations of fermions and rishons at every site x. Since the Hamiltonian transforms gauge invariant states into other gauge invariant states, it is obvious to ask whether the Hamiltonian of equation (8.3) itself can also be expressed entirely in terms of gauge invariant operators. This is indeed possible by defining the following gauge invariant operators

$$Q_{x,\pm k} = \psi^i_x c^{i\dagger}_{x,\pm k}, \qquad M_x = \psi^{i\dagger}_x \psi^i_x, \qquad \Phi_{x,\pm k,\pm l} = c^{i\dagger}_{x,\pm k} c^i_{x,\pm l}. \tag{8.7}$$

$Q^\dagger_{x,\pm k}$ ($Q_{x,\pm k}$) create (annihilate) fermions, while annihilating (creating) a rishon. $Q^\dagger_{x,\pm k}$ and $Q_{x,\pm k}$ are called constituent quark operators. The so-called meson operator M_x counts the number of fermions at the site x. The glueball operator $\Phi_{x,\pm k,\pm l}$ lets a rishon hop from the link $x, x \pm \hat{l}$ to the link $x, x \pm \hat{k}$. This allows us to write the Hamiltonian of equation (8.3) in terms of the gauge invariant operators

$$\begin{aligned} H =& -t \sum_{\langle x,y=x+\hat{k}\rangle} \left(s_{x,y} \psi^{i\dagger}_x c^i_{x,+k}\ c^{j\dagger}_{y,-k} \psi^j_y + \text{H.c.} \right) + m \sum_x s_x \psi^{i\dagger}_x \psi^i_x - \frac{1}{4g^2} \sum_\square \left(\text{Tr} U_\square + \text{H.c.} \right), \\ =& -t \sum_{\langle x,y=x+\hat{k}\rangle} \left(s_{x,y} Q^\dagger_{x,+k}\ Q_{y,-k} + \text{H.c.} \right) + m \sum_x s_x M_x - \frac{1}{4g^2} \sum_\square \left(\text{Tr} U_\square + \text{H.c.} \right), \end{aligned} \tag{8.8}$$

where the plaquette term in the k-l plane can be expressed as

$$\begin{aligned} \text{Tr} U_\square &= (c^i_{x,+k} c^{j\dagger}_{x+\hat{k},-k})(c^j_{x+\hat{k},+l} c^{m\dagger}_{x+\hat{k}+\hat{l},-l})(c^m_{x+\hat{k}+\hat{l},-k} c^{n\dagger}_{x+\hat{l},+k})(c^n_{x+\hat{l},-l} c^{i\dagger}_{x,+l}) \\ &= -\Phi_{x,+l,+k} \Phi_{x+\hat{k},-k,+l} \Phi_{x+\hat{k}+\hat{l},-l,-k} \Phi_{x+\hat{l},+k,-l}. \end{aligned} \tag{8.9}$$

8.2.3. Symmetry Transformations

The symmetry transformations discussed in section 7.6 can also be implemented on the rishons and be used to study the transformation properties of the gauge invariant operators.

Spatial Translations Spatial translations just shift the rishons by two lattice spacings in the k-direction

$$T_k: \qquad {}^{T_k}c^i_{x,+l} = c^i_{x+2\hat{k},+l}, \qquad {}^{T_k}c^i_{x,-l} = c^i_{x+2\hat{k},-l}, \tag{8.10}$$

which leads to the transformation rules (7.84) and (7.85). This implies that the gauge invariant operators transform as

$$T_k: \quad {}^{T_k}Q_{x,\pm l} = Q_{x+2\hat{k},\pm l}, \quad {}^{T_k}M_x = M_{x+2\hat{k}}, \quad {}^{T_k}\Phi_{x,\pm l,\pm l'} = \Phi_{x+2\hat{k},\pm l,\pm l'}. \tag{8.11}$$

Charge Conjugation The charge conjugation maps particles to anti-particles, therefore we transform the rishons as

$$C_k: \qquad {}^{C_k}c^i_{x,+l} = c^{i\dagger}_{x+\hat{k},+l}, \qquad {}^{C_k}c^i_{x,-l} = -c^{i\dagger}_{x+\hat{k},-l}, \tag{8.12}$$

which leads to the transformation rules of equation (7.88). Note that by performing a charge conjugation, we transform to operators to the conjugate representation. For the rishons this implies that the number of rishons $\mathcal{N}_{x,y}$ does not stay constant, but transforms as

$$^{C_k}\mathcal{N}_{x,y} = 2N - \mathcal{N}_{x,y}. \tag{8.13}$$

This means that only for a representation with $\mathcal{N}_{x,y} = N$ (N rishons per link), the operators are transformed to the same representation. This representation corresponds to a Young tableau of N vertically aligned boxes, which has $\frac{(2N)!}{(N!)^2}$ dimensions.

The gauge invariant operators transform as

$$\begin{aligned} C_k: \qquad & ^{C_k}Q_{x,\pm l} = \mp(-1)^{x_1+\cdots+x_k} Q^\dagger_{x+\hat{k},\pm l}, \qquad & ^{C_k}M_x = N - M_{x+\hat{k}}, \\ & ^{C_k}\Phi_{x,\pm l,\pm l'} = \mathrm{sign}(\pm l)\ \mathrm{sign}(\pm l') \left(N\delta_{\pm l,\pm l'} - \Phi_{x+\hat{k},\pm l',\pm l}\right). \end{aligned} \tag{8.14}$$

Parity Transformation The parity transformation inverts all coordinates of the operators and interchanges the operator on the left end of the link with the ones on the right end. Therefore the rishons transform as

$$P: \qquad ^{P}c^i_{x,+l} = c^i_{-x,-l}, \qquad ^{P}c^i_{x,-l} = c^i_{-x,+l}, \tag{8.15}$$

which leads to the transformation rules of equation (7.90). This implies that the gauge invariant operators transform as

$$P: \qquad ^{P}Q_{x,\pm l} = Q_{-x,\mp l}, \qquad ^{P}M_x = M_{-x} \qquad ^{P}\Phi_{x,\pm l,\pm l'} = \Phi_{-x,\mp l,\mp l'}. \tag{8.16}$$

Chiral Transformation A chiral translation shifts the rishons by one lattice spacings in the k-direction

$$S_k: \qquad ^{S_k}c^i_{x,+l} = c^i_{x+\hat{k},+l}, \qquad ^{S_k}c^i_{x,-l} = c^i_{x+\hat{k},-l}, \tag{8.17}$$

which leads to the transformation rules of equation (7.92). This implies that the gauge invariant operators transform as

$$S_k: \quad ^{S_k}Q_{x,\pm l} = (-1)^{x_{k+1}+\cdots x_x} Q_{x+\hat{k},\pm l}, \quad ^{S_k}M_x = M_{x+\hat{k}}, \quad ^{S_k}\Phi_{x,\pm l,\pm l'} = \Phi_{x+\hat{k},\pm l,\pm l'}. \tag{8.18}$$

8.2.4. Microscopic Atomic Hamiltonian

Now we are ready to describe the implementation of the quantum link Hamiltonian with ultracold atoms in an optical lattice setup. The implementation can be realized with a single species of alkaline-earth atoms (e.g. ^{87}Sr or ^{173}Yb), representing either the rishons or the staggered fermions, depending on their location in an optical superlattice [68]. We choose alkaline-earth atoms because they have a large nuclear spin I in which the color degrees of freedom can be encoded. Due to their large size (compared to the nucleus), the interaction of alkaline-earth atoms is almost independent of the nuclear spin. This guarantees the color-independent interactions of fermions and rishons.

The rishon representation allowed us to rewrite the quantum link Hamiltonian as a system of hopping fermions in equation (8.3). For simplicity, let us restrict ourselves to a system in $(1+1)$ dimensions. Instead of an actual hop of a fermion from $x+1$ to x and a hop of the rishon from $(x,+)$ to $(x+1,-)$ (see figure 8.1), it is more convenient to move the alkaline-earth atom from $x+1$ to the rishon position $(x+1,-)$, while moving another atom from the rishon position $(x,+)$ to the fermion position x. An optical superlattice guarantees this behavior by restricting some atoms only to move within the bright part in figure 8.1 and some atoms only within the darker region.

These dynamics can be described by the following microscopic atomic Hamiltonian:

$$\widetilde{H} = U\sum_x (\mathcal{N}_{x,x+1} - n)^2 - \tilde{t}\sum_x \left(\psi_x^{i\dagger} c_{x,+}^i + \psi_x^{j\dagger} c_{x,-}^j + \text{H.c.}\right) + m\sum_x s_x \psi_x^{i\dagger}\psi_x^i. \tag{8.19}$$

The $\tilde{t}$ term allows the hop of a fermion to a rishon position, while the U term keeps the number of rishons $\mathcal{N}_{x,x+1}$ on each link constant to n rishons, as long as U is chosen to be sufficiently large. By identifying $t = \tilde{t}^2/U$, we recover the quantum link Hamiltonian in terms of the rishons of equation (8.3) in $(1+1)$ dimensions in second order perturbation theory.

To implement this system in an optical lattice setup one needs only one species of fermions, which hop between neighboring sites, keeping the total number of rishons per link constant. Instead of a complicated interaction between the fermionic degrees of freedom (ψ) and the bosonic degrees of freedom ($U_{x,y}$), all the degrees of freedom can be represented by just one kind of fermions hopping in an optical lattice. The hopping of these fermions is restricted to a certain range on the lattice. Depending on the position of a fermion, it represents the fermion ψ or a rishon c (see figure 8.1). In our proposed implementation we use alkaline-earth atoms (e.g. ^{87}Sr or ^{173}Yb). The color degrees of freedom are encoded in the Zeeman levels of these atoms, where due to their nuclear spin I, we have an $SU(2I+1)$ symmetry in which the gauge group $SU(N)$ or $U(N)$ can be embedded.

8.3. $U(2)$ Quantum Link Model in $(1+1)$ Dimensions

8.3.1. Hamiltonian

The quantum link Hamilton in the rishon representation in $(1+1)$ dimensions reads

$$\begin{aligned} H &= -t \sum_x \left(\psi_x^{i\dagger} c_{x,+}^i \; c_{x+1,-}^{j\dagger} \psi_{x+1}^j + \text{H.c.} \right) + m \sum_x (-1)^x \psi_x^{i\dagger} \psi_x^i \\ &= -t \sum_x \left(Q_{x,+}^\dagger \; Q_{x+1,-} + \text{H.c.} \right) + m \sum_x (-1)^x M_x. \end{aligned} \tag{8.20}$$

Because we are in $(1+1)$ dimensions, the plaquette term is absent. Let us quickly review all ingredients of this Hamiltonian: The term proportional to the hopping parameter t is responsible for the interaction between the fermionic and the gauge degrees of freedom. The gauge fields are represented in terms of rishons, where $c^{i\dagger}$ and c^i are the creation and annihilation operators of the rishons (see section 8.2.1). They are associated with the left and right end of a link (see figure 8.1). The operators $\psi^{i\dagger}$ and ψ^i create and annihilate staggered fermions of color i (see section 7.3.2) and mass m. In section 8.2.2 we have defined the gauge invariant operators $Q_{x,\pm} = \psi_x^i c_{x,\pm}^{i\dagger}$ and $M_x = \psi_x^{i\dagger} \psi_x^i$.

To investigate whether this model actually shows interesting physics, we now present some exact diagonalization results for a $(1+1)$-dimensional system with a $U(2)$ gauge symmetry. We first show the spontaneous breaking of the chiral symmetry, before we study the evolution process of a chirally restored hot-spot in real-time.

In the $U(2)$ quantum link model, two fermions can form a bosonic baryon described by the creation operator $\varepsilon_{i,j} \psi^{i\dagger} \psi^{j\dagger}$. This is in contrast to QCD, where three fermions (quarks) build up a fermionic baryon.

It turns out that, in its original form, the Hamiltonian of equation (8.20) does not break chiral symmetry spontaneously. It is only possible to induce an explicit breaking for non-zero masses $m \neq 0$. To find spontaneously broken chiral symmetry (for $m = 0$), we extend the Hamiltonian by a 4-fermi interaction. This can be done by introducing an additional term, which favors a staggered pattern

$$H = -t \sum_x \left(Q_{x,+}^\dagger \; Q_{x+1,-} + \text{H.c.} \right) + m \sum_x (-1)^x M_x + G \sum_x (M_x - 1)^2. \tag{8.21}$$

This G-term is invariant under the various symmetries, including the chiral symmetry (see section 8.2.3). This means that the chiral symmetry is not broken explicitly. Nevertheless, the G-term with $G < 0$ disfavors the states $|2\rangle_x$ and $|3\rangle_x$ explicitly. This eventually leads to a ground state, which can be qualitatively illustrated as a "cartoon-state" $|414\ldots41\rangle = |4\rangle_0 |1\rangle_1 |4\rangle_2 \cdots |4\rangle_{L-2} |1\rangle_{L-1}$ or a "cartoon-state" $|141\ldots14\rangle$. Both of these states break the chiral symmetry spontaneously.

8.3.2. Gauss Law

The physical states $|\psi\rangle$ have to be gauge invariant under $U(2)$ gauge transformations, i.e. $G_x^a|\psi\rangle = G_x|\psi\rangle = 0$ (see section 7.5.3 and 8.2.1). If we work in the fundamental representation (corresponding to one rishon per link), we see that only four states at each site x are gauge invariant:

$$|1\rangle_x = \frac{1}{\sqrt{2}}\left(c^{\dagger 1}_{x,-}c^{\dagger 2}_{x,+} - c^{\dagger 2}_{x,-}c^{\dagger 1}_{x,+}\right)|0\rangle_x, \qquad |2\rangle_x = \frac{1}{\sqrt{2}}\left(c^{\dagger 2}_{x,-}\psi^{\dagger 1}_x - c^{\dagger 1}_{x,-}\psi^{\dagger 2}_x\right)|0\rangle_x,$$
$$|3\rangle_x = \frac{1}{\sqrt{2}}\left(c^{\dagger 2}_{x,+}\psi^{\dagger 1}_x - c^{\dagger 1}_{x,+}\psi^{\dagger 2}_x\right)|0\rangle_x, \qquad |4\rangle_x = \psi^{\dagger 2}_x\psi^{\dagger 1}_x|0\rangle_x. \tag{8.22}$$

These states are illustrated in figure 8.3. In state $|1\rangle_x$, there are two rishons close to the site x, one on the link to the left and one on the link to the right of the site x. The two rishons form a color-singlet. In state $|2\rangle_x$ and $|3\rangle_x$, there is one fermion at the site x and one rishon on the link to the left (right) of the site x. The fermion and the rishon form a color-singlet. In state $|4\rangle_x$ two fermions on the site x form a color-singlet.

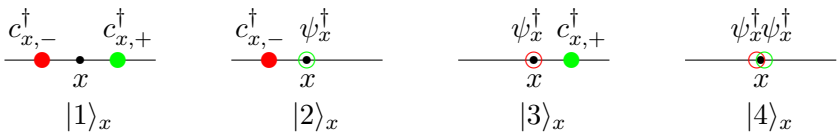

FIGURE 8.3.: Illustration of the four different gauge invariant states in a $(1+1)$-dimensional $U(2)$ quantum link model. The filled circles represent rishons, while the empty circles represents the fermions ("quarks"). The two objects must be of opposite color in order to form a color-singlet.

One can use the states $\{|1\rangle_x, |2\rangle_x, |3\rangle_x, |4\rangle_x\}$ as a basis at each site x. By acting with the operators $Q_{x,\pm}$ and M_x on these basis states one obtains

$$M_x = \begin{bmatrix} 0 & 0 & 0 & 0 \\ 0 & 1 & 0 & 0 \\ 0 & 0 & 1 & 0 \\ 0 & 0 & 0 & 2 \end{bmatrix}, \quad Q_{x,+} = \begin{bmatrix} 0 & 1 & 0 & 0 \\ 0 & 0 & 0 & 0 \\ 0 & 0 & 0 & \sqrt{2} \\ 0 & 0 & 0 & 0 \end{bmatrix}, \quad Q_{x,-} = \begin{bmatrix} 0 & 0 & 1 & 0 \\ 0 & 0 & 0 & \sqrt{2} \\ 0 & 0 & 0 & 0 \\ 0 & 0 & 0 & 0 \end{bmatrix}. \tag{8.23}$$

Because we have four possible states at each site x, we might naively expect the dimension of the Hilbert space to scale as 4^L with the number L of lattice sites. However, there is a reduction of the Hilbert space: since we deal with a representation with just one rishon per link, the rishon is restricted to be either on the left or on the right end of the link. This restricts the states of neighboring sites to only two possibilities. For example a state $|1\rangle_x$ corresponds to two rishons next to the site x. This means that on the link $x, x+1$, the rishon is on the left side, which forbids the states $|1\rangle_{x+1}$ or $|2\rangle_{x+1}$ at the site $x+1$, since both require the rishon to be on the right side of the link $x, x+1$. On the other hand, $|1\rangle_x$ requires the rishon to be on the right side of the link $x-1, x$, which forbids the states $|1\rangle_{x-1}$ and $|3\rangle_{x-1}$ at the site $x-1$.

One can convince oneself that only the following combinations of neighboring states are

allowed:

$$\begin{aligned} &|1\rangle_x|3\rangle_{x+1}, \quad &&|2\rangle_x|2\rangle_{x+1}, \quad &&|3\rangle_x|3\rangle_{x+1}, \quad &&|4\rangle_x|2\rangle_{x+1}, \\ &|1\rangle_x|4\rangle_{x+1}, \quad &&|2\rangle_x|1\rangle_{x+1}, \quad &&|3\rangle_x|4\rangle_{x+1}, \quad &&|4\rangle_x|1\rangle_{x+1}. \end{aligned} \tag{8.24}$$

This means that for each state only two possible neighboring states are allowed. Therefore the dimension of the total Hilbert space only scales as 2^L.

8.3.3. Spontaneous Chiral Symmetry Breaking

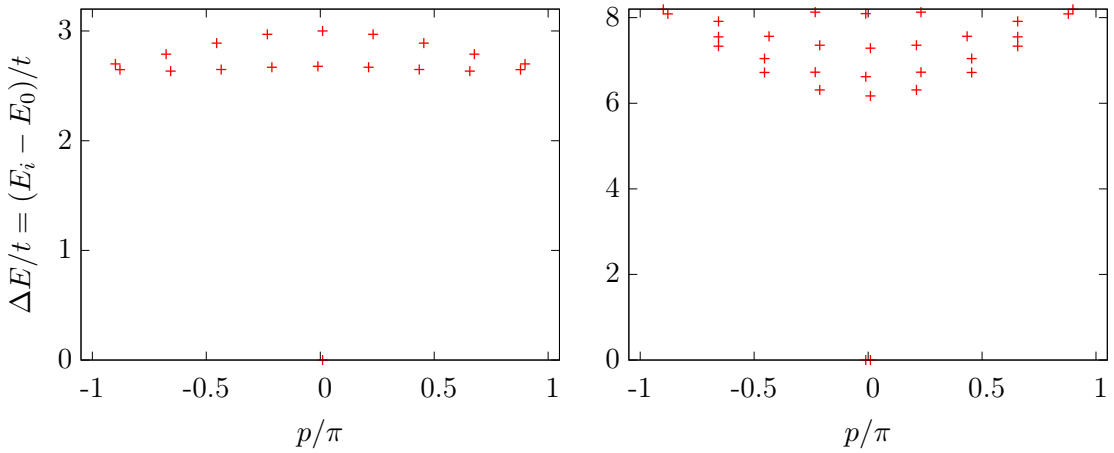

Figure 8.4.: Spectrum of the quantum link Hamiltonian for a system size $L = 18$ in the chirally symmetric phase ($G/t = 0$, left) and a phase, where chiral symmetry is broken spontaneously ($G/t = -6$, right).

Let us study the spectrum of this $U(2)$ quantum link Hamiltonian. As discussed in section 7.6.4, in a system in which a discrete $\mathbb{Z}_2$ chiral symmetry is broken spontaneously, we should find an almost degenerate spectrum, as long as the system is in a finite volume. This means that the spectrum always contains pairs of states, which have almost the same energy. These pairs of states are related by the spontaneously broken chiral symmetry and the energy difference ΔE between those two states decreases exponentially with the volume L.

In figure 8.4 we show the spectrum of the quantum link Hamiltonian obtained by exact diagonalization for $L = 18$. We plot the energy (in units of the hopping parameter t) of the lowest few eigenstates against the true momentum p (see section 7.6.1). In order to distinguish degenerate states, we slightly move the symbols in the plot to the left and to the right in a staggered fashion. The energy is normalized to be zero for the ground state. In the left plot (for a zero four fermi-parameter $G/t = 0$ in units of the hopping parameter t), we do not find an almost degenerate spectrum, since the different states do not appear in pairs. Already the first exited state has a non-zero true momentum p. We conclude that, in this case, the chiral symmetry is not spontaneously broken. On the other hand, in the right plot (for a parameter $G/t = -6$), we find a spectrum where the states always appear in pairs. We assume that the chiral symmetry is broken spontaneously in this case.

To verify the spontaneous chiral symmetry breaking, we study the scaling behavior of the energy difference of the two lowest energy states $\Delta E = E_1 - E_0$ as a function of the volume. In case of a spontaneously broken symmetry, this energy difference should vanish exponentially with the volume L of the system. In figure 8.5 we show these energy differences for $G/t = -6$, which indeed confirms spontaneous chiral symmetry breaking.

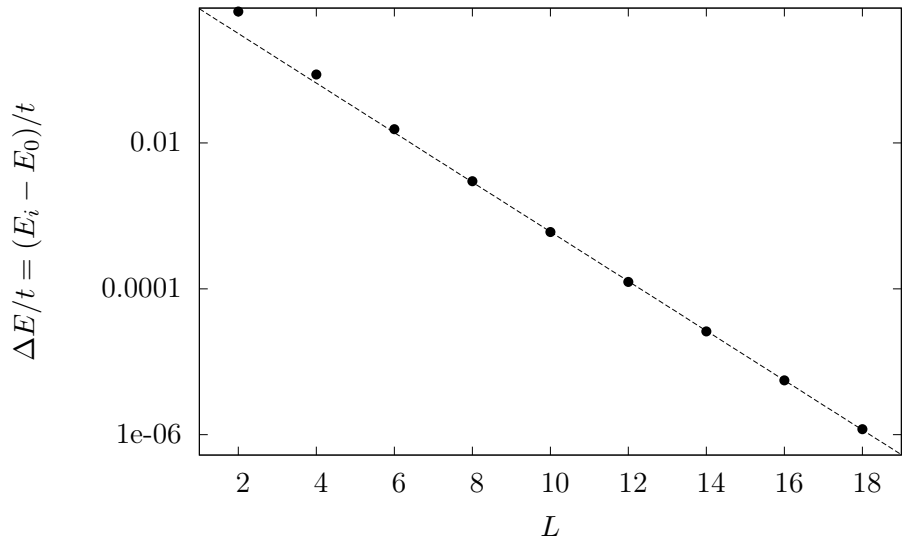

FIGURE 8.5.: The exponential scaling of the energy difference for $G/t = -6$ of the almost degenerate vacua indicates spontaneous chiral symmetry breaking.

The spontaneous chiral symmetry breaking would be interesting to observe in an experimental realization of this model in a quantum simulator. The results can then also be used to validate the implementation.

8.3.4. Real-Time Evolution

The expansion of a chirally restored hot-spot in a chirally broken background is calculated in real-time. To do this, we prepare the system in an initial configuration, where the chiral symmetry is broken everywhere (background vacuum) except at two points (hot-spot, here at $x = 5, 6$) where chiral symmetry is restored. To measure the chiral symmetry breaking locally, we define the chiral condensate as

$$(\bar{\psi}\psi)_x = (-1)^x \cdot (1 - M_x). \tag{8.25}$$

It is easy to see that the states $|2\rangle_x$ and $|3\rangle_x$ lead to a vanishing chiral condensate, whereas the states $|1\rangle_x$ and $|4\rangle_x$ have a non-zero expectation value of the chiral condensate

$$(\bar{\psi}\psi)_x|1\rangle_x = (-1)^x|1\rangle_x \qquad (\bar{\psi}\psi)_x|4\rangle_x = (-1)^{x+1}|4\rangle_x. \tag{8.26}$$

The hot-spot mimics, for example, the quark-gluon plasma in a heavy-ion collision. In our example in figure 8.6, we prepare an initial state $|\psi_0\rangle = |141413341414\rangle$. This is done by

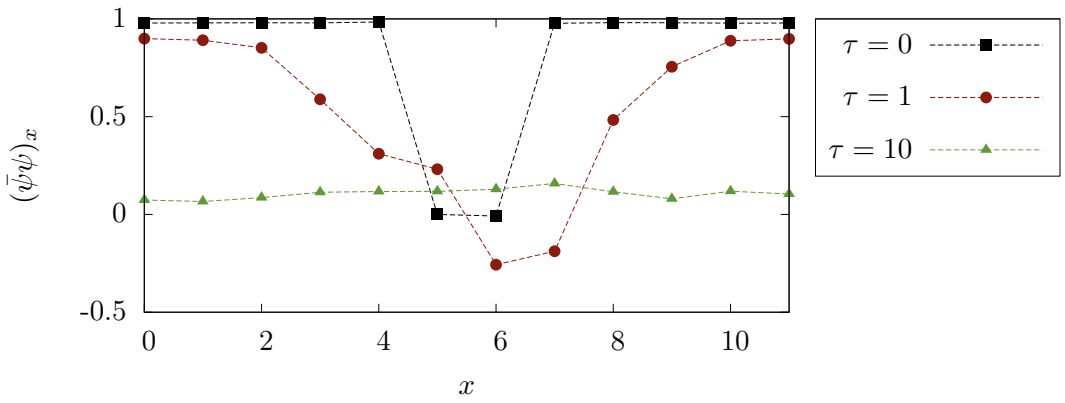

Figure 8.6.: Spatial dependance of the chiral order parameter for various real times $\tau = 0, 1, 10$. We have chosen $m/t = 0.001, G/t = -6$ and diagonalized an $L = 12$ system.

diagonalizing the Hamiltonian of a $L = 12$ system (using the lowest 100 eigenstates) and projecting the desired initial state $|\psi_0\rangle$ onto the eigenstates. After certain time-intervals ($\tau = 0, \tau = 1, \tau = 10$, measured in units of the inverse hopping parameter $1/t$) we measure the order parameter of the chiral symmetry breaking, the chiral condensate $(\bar{\psi}\psi)_x$. In the plot shown in figure 8.6, we see how with increasing time the symmetric phase is spreading out on the lattice until the system equilibrates in a chirally symmetric phase.

Since we only consider a finite volume, the system can not "cool down" to the chirally broken vacuum state. Instead it equilibrates in a high-temperature state with vanishing chiral condensate.

Chapter 9.

Application II: $SO(3)$ Quantum Link Model

9.1. Motivating the $SO(3)$ Quantum Link Model

After having studied $SU(N)$ and $U(N)$ quantum link models, here we extend our work to an $SO(3)$ quantum link model [66]. This model is interesting, since it has a global (instead of a local) $U(1)$ symmetry, which gives rise to a conserved baryon number B. The fermions in this model transform in the vector representation of $SO(3)$, which means that they are triplets and can therefore couple to a triplet "gluon" to form a color-neutral "baryon". Therefore the "baryons" in this model are fermions as they are in QCD. This is in contrast to the $U(2)$ quantum link model from the previous chapter, where two fermions coupled to each other to build a bosonic "baryon". We can further combine a fermion with an anti-fermion to form a color-neutral "meson" and a pair of "gluons" can form a "glueball".

We will introduce two four-fermion coupling parameters G and V for which we investigate the phase diagram. We search for phases, where chiral symmetry is spontaneously broken. By introducing a finite baryon density, we can study whether chiral symmetry gets restored.

In other regions of the phase diagram we find a massless phase.

It is also possible to study some aspects of "nuclear" physics by measuring binding energies at finite baryon densities. For example the lowest states in the baryon number $B = 2$ or $B = 3$ sectors correspond to bound states of "deuterium" or "tritium". These results will be published in [69].

This chapter is organized as follows: We first introduce $SO(3)$ quantum link models by discussing the Hamiltonian and the embedding $so(6)$ algebra in section 9.2. This algebra can be represented by two spinors per link, which is explained in section 9.3 and works very similar to the rishon representation for $U(N)$ quantum link models (see section 8.2.1). After that we present exact diagonalization results for a system in $(1+1)$ dimensions in section 9.4.

9.2. Introducing the $SO(3)$ Quantum Link Model

9.2.1. Hamiltonian and Commutation Relations

Let us denote the quantum link operators of $SO(3)$ gauge models as $O^{ab}_{x,y}$ $(a, b \in \{1, 2, 3\})$. These are 3×3 matrices, where each element is a Hermitian operator acting in a Hilbert space. In close analogy to the previous sections, we define the link-based generators of $SO(3)$ gauge

transformations as $L^a_{x,y}$ and $R^a_{x,y}$, which obey

$$[R^a_{x,y}, R^b_{x,y}] = 2i\varepsilon_{abc} R^c_{x,y}, \qquad [L^a_{x,y}, L^b_{x,y}] = 2i\varepsilon_{abc} L^c_{x,y}, \qquad [R^a_{x,y}, L^b_{x,y}] = 0 \tag{9.1}$$

for operators on the same link, while operators associated with different links commute. They transform the quantum link operators as

$$\begin{aligned} SO(3): \qquad O^{ab}_{x,y} \quad \longrightarrow \quad & \exp\big(-i\big(\alpha^{a'}_x L^{a'}_{x,y} + \alpha^{a'}_y R^{a'}_{x,y}\big)\big) O^{ab}_{x,y} \exp\big(i\big(\alpha^{a'}_x L^{a'}_{x,y} + \alpha^{a'}_y R^{a'}_{x,y}\big)\big) \\ & = \big[\exp\big(i\alpha^{a'}_x t^{a'}\big)\big]^{ac} O^{cd}_{x,y} \big[\exp\big(-i\alpha^{a'}_y t^{a'}\big)\big]^{db}, \end{aligned} \tag{9.2}$$

where $t^a_{bc} = -2i\varepsilon_{abc}$ form the 3×3 matrix representation of the $SO(3)$. From these transformation rules we can derive the commutation relations (similar to section 7.4.3) as

$$[L^a_{x,y}, O^{bc}_{x,y}] = -t^a_{bd} O^{dc}_{x,y}, \qquad [R^a_{x,y}, O^{bc}_{x,y}] = O^{bd}_{x,y} t^a_{dc}. \tag{9.3}$$

It will turn out that, besides the operators $L^a_{x,y}$ and $R^a_{x,y}$, also the operators $O^{ab}_{x,y}$ are all Hermitian.

Let us also add staggered fermions (see section 7.4.6) to the system. The fermion creation and annihilation operators $\psi^{a\dagger}_x$ and ψ^a_x transform under the $SO(3)$ vector representation

$$SO(3): \qquad \psi^a_x \quad \longrightarrow \quad \big[\exp\big(i\alpha^{a'}_x t^{a'}\big)\big]^{ab} \psi^b_x, \qquad \psi^{a\dagger}_x \quad \longrightarrow \quad \psi^{b\dagger}_x \big[\exp\big(-i\alpha^{a'}_x t^{a'}\big)\big]^{ba}. \tag{9.4}$$

With this we define the $SO(3)$ quantum link model Hamiltonian with staggered fermions

$$\begin{aligned} H = & -t \sum_x \sum_{k=1}^{d} \Big(s_{x,x+\hat{k}} \psi^\dagger_x O_{x,x+\hat{k}} \psi_{x+\hat{k}} + \text{H.c.} \Big) + m \sum_x s_x \psi^\dagger_x \psi_x \\ & + \frac{g^2}{2} \sum_{\langle xy \rangle} \big(L^a_{x,y} L^a_{x,y} + R^a_{x,y} R^a_{x,y} \big) - \frac{1}{4g^2} \sum_{\square} \text{Tr} O_{\square}, \end{aligned} \tag{9.5}$$

where $s_x = (-1)^{x_1 + \cdots + x_d}$ and $s_{x,x+\hat{k}} = (-1)^{x_1 + \cdots + x_{k-1}}$. The trace of the plaquette operator in the k-l plane is defined as

$$\text{Tr} O_{\square} = O^{ab}_{x,x+\hat{k}} O^{bc}_{x+\hat{k},x+\hat{k}+\hat{l}} O^{cd}_{x+\hat{l},x+\hat{k}+\hat{l}} O^{da}_{x,x+\hat{l}}. \tag{9.6}$$

Let us contrast $SO(3)$ quantum link models with the previously discussed $U(2)$ quantum link model. For the $U(2)$ quantum link model, we found that the link-based generators of $U(2)$ gauge transformations (the seven generators $L^a_{x,y}$, $R^a_{x,y}$, and $E_{x,y}$) and the quantum link operators $U^{ij}_{x,y}$ and $U^{ij\dagger}_{x,y}$ (corresponding to eight Hermitian operators $M^{ij}_{x,y}$ and $N^{ij}_{x,y}$) generate the link-based $su(4)$ algebra. As it will turn out, it is possible to embed the six generators of $SO(3)$ gauge transformations ($L^a_{x,y}$ and $R^a_{x,y}$) and the nine quantum link operators $O^{ab}_{x,y}$ in an $so(6)$ algebra. Even though both embedding algebras are generated by 15 Hermitian operators and, in fact, $so(6) = su(4)$, the quantum link models are very different. The $SO(3)$ quantum link operators are for themselves Hermitian operators $O^{ab\dagger}_{x,y} = O^{ab}_{x,y}$ and are generators of the $so(6)$ algebra as will be explained in the next section.

9.2.2. Embedding Algebra $so(6)$

The simplest way to satisfy the commutation relations of equations (9.1) and (9.3) is by embedding the quantum link operators and the link-based generators of $SO(3)$ gauge transformations in an $so(6)$ algebra. We write down the explicit 6-dimensional vector-representation of the generators of the $so(6)$ algebra and show that they are exactly the quantum link operators and the generators of gauge transformations, satisfying the above commutation relations.

The algebra $so(6)$ has 15 Hermitian generators, where 6 generators are the generators of the subalgebra $so(3) \oplus so(3)$. We identify these operators with $L^a_{x,y}$ and $R^a_{x,y}$, which generate the $so(3)_L \oplus so(3)_R$ subalgebra. In the vector-representation of $so(6)$, we can write these operators explicitly as

$$L^a_{x,y} = \begin{bmatrix} 0 & 0 \\ 0 & t^a \end{bmatrix}, \qquad R^a_{x,y} = \begin{bmatrix} t^a & 0 \\ 0 & 0 \end{bmatrix}, \tag{9.7}$$

where again $t^a_{bc} = -2i\varepsilon_{abc}$ are 3×3 matrices generating an $so(3)$ algebra. The remaining 9 Hermitian generators can be written as:

$$O^{ab}_{x,y} = \begin{bmatrix} 0 & 2iD^{(ab)} \\ -2iD^{(ba)} & 0 \end{bmatrix}, \tag{9.8}$$

where $D^{(ab)}_{cd} = \delta_{ad}\delta_{bc}$ are 3×3 matrices with all elements being zero, except the one in the column a, row b, which is equal to 1. It is straightforward to show that this representation satisfies the commutation relations (9.1) and (9.3). Also commutation relations among the quantum link operators can be derived as

$$[O^{ab}, O^{cd}] = -\delta_{ac}t^e_{bd}R^e - \delta_{bd}t^e_{ac}L^e. \tag{9.9}$$

By choosing an irreducible representation of $so(6)$ on each link, the link Hilbert space is finite-dimensional.

9.2.3. Gauss Law

A general $SO(3)$ gauge transformation can be parametrized by the unitary operator

$$V = \prod_x \exp\left(i\alpha^a_x G^a_x\right), \tag{9.10}$$

where the site-based generators of $SO(3)$ gauge transformations G^a_x obey

$$[G^a_x, G^b_y] = 2i\delta_{x,y}\varepsilon_{abc}G^c_x.$$

Similar to the generators of $SU(N)$ gauge transformations (see section 8.3.2), we define the generators of $SO(3)$ as

$$G^a_x = \psi^{\dagger b}_x t^a_{bc}\psi^c_x + \sum_k \left(L^a_{x,x+\hat{k}} + R^a_{x-\hat{k},x}\right). \tag{9.11}$$

In this way, the fermion field operators ψ^a_x and the quantum link operators $O^{ab}_{x,y}$ transform correctly under gauge transformations

$$SO(3): \quad V^\dagger O^{ab}_{x,y} V = \left[\exp\left(i\alpha^{a'}_x t^{a'}\right)\right]^{ac} O^{cd}_{x,y} \left[\exp\left(-i\alpha^{a'}_y t^{a'}\right)\right]^{db}, \quad V^\dagger \psi^a_x V = \left[\exp\left(i\alpha^{a'}_x t^{a'}\right)\right]^{ab} \psi^b_x.$$

These $SO(3)$ gauge transformations indeed leave the Hamiltonian invariant ($[G^a_x, H] = 0$). The physical states $|\psi\rangle$ have to be gauge invariant, which means

$$G^a_x |\psi\rangle = 0, \tag{9.12}$$

because then $V^\dagger|\psi\rangle = |\psi\rangle$. This Gauss law requires at every site x that the states on the link emanating from the site x have to form a color-singlet together with the fermion at the site x.

We will work out the fundamental representation of an $SO(3)$ quantum link Hamiltonian with fermions and quantum link operators in $(1+1)$ dimensions explicitly and discuss all the gauge invariant states in section 9.4.2.

9.3. Implementation of the $SO(3)$ Quantum Link Model

9.3.1. Spinor Representation

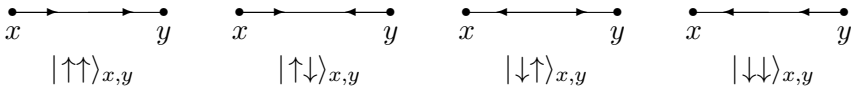

FIGURE 9.1.: Four states of the fundamental representation of the embedding $so(6)$ algebra, represented in terms of two spin-$\frac{1}{2}$ objects at the left and at the right end of the link.

When studying $U(N)$ or $SU(N)$ quantum link models, we realized that the embedding $su(2N)$ algebra can be represented as a bi-linear of fermionic rishon operators, associated with the left and the right end of the link (see section 8.2.1). In a similar way, the embedding $su(6)$ algebra of $SO(3)$ quantum link models can be represented by a bi-linear of spin operators. We can associate spin operators with the left and the right end of the link $x, x+\hat{k}$ and identify

$$O^{ab}_{x,x+\hat{k}} = \sigma^a_{x,+k} \otimes \sigma^b_{x+\hat{k},-k}, \qquad L^a_{x,x+\hat{k}} = \sigma^a_{x,+k} \otimes \mathbb{1}, \qquad R^a_{x,x+\hat{k}} = \mathbb{1} \otimes \sigma^a_{x+\hat{k},-k}. \tag{9.13}$$

which indeed satisfy the equations (9.1), (9.3), and (9.9). This is the fundamental representation of $so(6)$, which is 4-dimensional. Choosing the basis, in which σ^3 is a diagonal operator, we can identify the four basis states per link as $\{|\uparrow\uparrow\rangle_{x,y}, |\uparrow\downarrow\rangle_{x,y}, |\downarrow\uparrow\rangle_{x,y}, |\downarrow\downarrow\rangle_{x,y}\}$ as illustrated in figure 9.1.

From now on we omit the tensor product sign $\otimes$.

The quantum link Hamiltonian can be expressed in terms of the spin operators. We leave out the part with the operator $\sum_a L^a L^a + R^a R^a$, since in the fundamental representation it is proportional to the unit matrix. The fermionic and plaquette part of the Hamiltonian (9.5)

then reads

$$\begin{aligned} H =& -t\sum_{\langle xy\rangle}\Big(s_{x,y}\psi^{a\dagger}_x O^{ab}_{x,y}\psi^b_y + \text{H.c.}\Big) + m\sum_x s_x\psi^{a\dagger}_x\psi^a_x - \frac{1}{4g^2}\sum_\square \text{Tr}O_\square, \\ =& -t\sum_{\langle x,y=x+\hat{k}\rangle}\Big(s_{x,y}\psi^{a\dagger}_x\sigma^a_{x,+k}\ \sigma^b_{y,-k}\psi^b_y + \text{H.c.}\Big) + m\sum_x s_x\psi^{a\dagger}_x\psi^a_x - \frac{1}{4g^2}\sum_\square \text{Tr}O_\square, \end{aligned} \tag{9.14}$$

where the plaquette term in the k-l plane can be expressed as

$$\begin{aligned} \text{Tr}O_\square &= O^{ab}_{x,x+\hat{k}}O^{bc}_{x+\hat{k},x+\hat{k}+\hat{l}}O^{cd}_{x+\hat{l},x+\hat{k}+\hat{l}}O^{da}_{x,x+\hat{l}} \\ &= (\sigma^a_{x,+k}\sigma^b_{x+\hat{k},-k})(\sigma^b_{x+\hat{k},+l}\sigma^c_{x+\hat{k}+\hat{l},-l})(\sigma^c_{x+\hat{k}+\hat{l},-k}\sigma^d_{x+\hat{l},+k})(\sigma^d_{x+\hat{l},-l}\sigma^a_{x,+l}). \end{aligned} \tag{9.15}$$

The Gauss law ($G^a_x|\psi\rangle = 0$) requires that the $2d$ spin states, which touch the site x, form a singlet together with the fermion at the site x.

9.3.2. Gauge Invariant Operators

As for $U(N)$ quantum link models, it is also possible to express the Hamiltonian of the $SO(3)$ quantum link model entirely in terms of gauge invariant operators. For this purpose we define the following operators

$$B_{x,\pm k} = \psi^a_x\sigma^a_{x,\pm k}, \qquad M_x = \psi^{a\dagger}_x\psi^a_x, \qquad \Phi_{x,\pm k,\pm l} = \sigma^a_{x,\pm k}\sigma^a_{x,\pm l}. \tag{9.16}$$

Because both, the "quarks" (i.e. the adjoint fermions ψ^a_x) and the "gluons" ($\sigma^a_{x,\pm k}$) are color-triplets, they can form a color neutral "baryon" state. The operators $B^\dagger_{x,\pm k}$ and $B_{x,\pm k}$ can be understood as "baryon" creation and annihilation operators. The operator M_x counts the number of fermions at the site x. The operator

$$B = \sum_x\left(M_x - \frac{3}{2}\right) \tag{9.17}$$

counts the total number of baryons in the system. Since the baryon number is a conserved quantity, it commutes with the Hamiltonian ($[B, H] = 0$) and the system can be diagonalized in each "baryon" sector individually. $\Phi_{x,\pm k,\pm l}$ is known as the glueball operator. This allows us to write the Hamiltonian (9.14) in terms of the gauge invariant operators

$$\begin{aligned} H =& -t\sum_{\langle x,y=x+\hat{k}\rangle}\Big(s_{x,y}\psi^{a\dagger}_x\sigma^a_{x,+k}\ \sigma^b_{y,-k}\psi^b_y + \text{H.c.}\Big) + m\sum_x s_x\psi^{a\dagger}_x\psi^a_x - \frac{1}{4g^2}\sum_\square \text{Tr}O_\square \\ =& -t\sum_{\langle x,y=x+\hat{k}\rangle}\Big(s_{x,y}B^\dagger_{x,+k}\ B_{y,-k} + \text{H.c.}\Big) + m\sum_x s_x M_x - \frac{1}{4g^2}\sum_\square \text{Tr}O_\square, \end{aligned} \tag{9.18}$$

where the plaquette term in the k-l plane can be expressed as

$$\begin{aligned} \text{Tr}O_\square &= (\sigma^a_{x,+k}\sigma^b_{x+\hat{k},-k})(\sigma^b_{x+\hat{k},+l}\sigma^c_{x+\hat{k}+\hat{l},-l})(\sigma^c_{x+\hat{k}+\hat{l},-k}\sigma^d_{x+\hat{l},+k})(\sigma^d_{x+\hat{l},-l}\sigma^a_{x,+l}) \\ &= \Phi_{x,+l,+k}\Phi_{x+\hat{k},-k,+l}\Phi_{x+\hat{k}+\hat{l},-l,-k}\Phi_{x+\hat{l},+k,-l}. \end{aligned} \tag{9.19}$$

The commutation relations among the different gauge invariant operators are

$$\begin{aligned} [M_x, M_y] &= 0, & [B_{x,\pm k}, M_y] &= \delta_{xy} B_{x,\pm k}, \\ \{B_{x,\pm k}, B_{y,\pm l}\} &= \delta_{xy}\delta_{\pm k,\pm l}\; 2i\varepsilon_{abc}\; \psi^a_x\; \psi^b_x\; \sigma^c_{x,\pm k}, \\ \{B^\dagger_{x,\pm k}, B_{y,\pm l}\} &= \delta_{xy}\left[2i\delta_{\pm k,\pm l}\varepsilon_{abc}\; \psi^{a\dagger}_x\; \psi^b_x\; \sigma^c_{x,\pm k} + \Phi_{x,\pm k,\pm l}\right]. \end{aligned} \tag{9.20}$$

Note that $\Phi_{x,\pm k,\pm k} = 3 \cdot \mathbb{1}$.

9.3.3. Symmetry Transformations

The symmetry transformations have been discussed for $U(N)$ quantum link models in section 7.6 and in section 8.2.3. In this section we work out the symmetries of $SO(3)$ quantum link models and study the transformation properties of the various operators.

Spatial Translations Spatial translations shift the whole system by two lattice spacings in the k-direction:

$$\begin{aligned} T_k: \quad & {}^{T_k}O_{x,y} = O_{x+2\hat{k},y+2\hat{k}}, \quad {}^{T_k}\psi_x = \psi_{x+2\hat{k}}, \\ & {}^{T_k}L^a_{x,y} = L^a_{x+2\hat{k},y+2\hat{k}}, \quad {}^{T_k}R^a_{x,y} = R^a_{x+2\hat{k},y+2\hat{k}}, \quad {}^{T_k}\sigma^a_{x,\pm l} = \sigma^a_{x+2\hat{k},\pm l}, \\ & {}^{T_k}B_{x,\pm l} = B_{x+2\hat{k},\pm l}, \quad {}^{T_k}M_x = M_{x+2\hat{k}}, \quad {}^{T_k}\Phi_{x,\pm l,\pm l'} = \Phi_{x+2\hat{k},\pm l,\pm l'}. \end{aligned} \tag{9.21}$$

This transformation is a symmetry of the Hamiltonian and leads to the conservation of the true momentum p_k. This symmetry can be used to prediagonalize the Hamiltonian with respect to the true momentum p_k and calculate the spectrum for each momentum sector individually (see section 9.4.4).

Charge Conjugation Besides shifting the system by one lattice spacing in the k-direction, the charge conjugation maps particles to anti-particles and performs a special gauge transformation, which is constant in space and can be characterized by the gauge transformation matrix

$$C = \begin{bmatrix} -1 & & \\ & 1 & \\ & & -1 \end{bmatrix}. \tag{9.22}$$

In the fundamental representation, the operators of the quantum link model transform as

$$\begin{aligned} C_k: \quad & {}^{C_k}O^{ab}_{x,y} = C^{ac}O^{cd}_{x+\hat{k},y+\hat{k}}C^{db} = O^{ab*}_{x+\hat{k},y+\hat{k}}, \quad {}^{C_k}\psi^a_x = (-1)^{x_1+\cdots+x_k}C^{ab}\psi^{b\dagger}_{x+\hat{k}}, \\ & {}^{C_k}L^a_{x,y} = C^{ab}L^b_{x+\hat{k},y+\hat{k}} = -L^{a*}_{x+\hat{k},y+\hat{k}}, \quad {}^{C_k}R^a_{x,y} = C^{ab}R^b_{x+\hat{k},y+\hat{k}} = -R^{a*}_{x+\hat{k},y+\hat{k}}, \\ & {}^{C_k}\sigma^a_{x,\pm l} = C^{ab}\sigma^b_{x+\hat{k},\pm l} = \sigma^{a*}_{x+\hat{k},\pm l}, \quad {}^{C_k}M_x = 3 - M_{x+\hat{k}}, \\ & {}^{C_k}B_{x,\pm l} = (-1)^{x_1+\cdots+x_k}B^\dagger_{x+\hat{k},\pm l}, \quad {}^{C_k}\Phi_{x,\pm l,\pm l'} = \Phi_{x+\hat{k},\pm l',\pm l}. \end{aligned} \tag{9.23}$$

Note that the hopping term in the Hamiltonian (9.5) transforms to its Hermitian conjugate. On the first sight it might seem unnatural to transform the different gauge components of the fermions. However, this is what happens for fermions in the adjoint representation also in the continuum. Note further that the quantum link operators $O^{ab}_{x,y}$ and the

electric flux operators $L^a_{x,y}$ and $R^a_{x,y}$ actually undergo a unitary (orthogonal) transformation. In the fundamental representation with the basis $\{|\uparrow\uparrow\rangle_{x,y}, |\uparrow\downarrow\rangle_{x,y}, |\downarrow\uparrow\rangle_{x,y}, |\downarrow\downarrow\rangle_{x,y}\}$, we obtain

$$ {}^{C_k}O^{ab}_{x,y} = W_C O^{ab}_{x+\hat{k},y+\hat{k}} W_C^\dagger, \quad {}^{C_k}L^a_{x,y} = W_C L^a_{x+\hat{k},y+\hat{k}} W_C^\dagger, \quad {}^{C_k}R^a_{x,y} = W_C R^a_{x+\hat{k},y+\hat{k}} W_C^\dagger, \tag{9.24} $$

where

$$ W_C = (i\sigma^2) \otimes (i\sigma^2) = \begin{bmatrix} & & & 1 \\ & & -1 & \\ & -1 & & \\ 1 & & & \end{bmatrix}. \tag{9.25} $$

This means that the representation of the link operators did not change under the charge conjugation. This implies that the charge conjugation is a symmetry of the Hamiltonian in the fundamental representation. This is in contrast to $U(N)$ quantum link models, where for example among the rishon representations, only the one with $\mathcal{N}_{x,y} = N$ rishons per link was invariant.

One can check that the total number of baryons is transformed to

$$ {}^{C_k}B = -B. \tag{9.26} $$

This implies that the spectrum is the same for baryon number B and $-B$.

Parity Transformation The parity transformation inverts all coordinates of the operators and interchanges the operators on the left end of the link with the ones on the right end. Therefore the operators transform as

$$ \begin{aligned} P: \quad & {}^{P}O^{ab}_{x,y} = O^{ba}_{-y,-x}, \quad {}^{P}\psi^a_x = \psi^a_{-x}, \\ & {}^{P}L^a_{x,y} = R^a_{-y,-x}, \quad {}^{P}R^a_{x,y} = L^a_{-y,-x}, \quad {}^{P}\sigma^a_{x,\pm l} = \sigma^a_{-x,\mp l}, \\ & {}^{P}B_{x,\pm l} = B_{-x,\mp l}, \quad {}^{P}M_x = M_{-x}, \quad {}^{P}\Phi_{x,\pm l,\pm l'} = \Phi_{-x,\mp l,\mp l'}. \end{aligned} \tag{9.27} $$

This transformation is a symmetry of the Hamiltonian. Note that the hopping term transforms to its Hermitian conjugate.

Chiral Transformation As for $U(N)$ quantum link models (see section 7.6.4), the chiral transformation is a $\mathbb{Z}_2$ symmetry. The chiral transformation corresponds to a shift of the whole system by one lattice spacings in the k-direction. Consecutive shifts of one lattice spacing in an even number of directions corresponds to a flavor symmetry. The translation by one lattice spacing is defined as

$$ \begin{aligned} S_k: \quad & {}^{S_k}O^{ab}_{x,y} = O^{ab}_{x+\hat{k},y+\hat{k}}, \quad {}^{S_k}\psi^a_x = (-1)^{x_{k+1}+\cdots+x_d}\psi^a_{x+\hat{k}}, \\ & {}^{S_k}L^a_{x,y} = L^a_{x+\hat{k},y+\hat{k}}, \quad {}^{S_k}R^a_{x,y} = R^a_{x+\hat{k},y+\hat{k}}, \quad {}^{S_k}\sigma^a_{x,\pm l} = \sigma^a_{x+\hat{k},\pm l}, \\ & {}^{S_k}M_x = M_{x+\hat{k}}, \quad {}^{S_k}B_{x,\pm l} = (-1)^{x_{k+1}+\cdots x_x}B_{x+\hat{k},\pm l}, \quad {}^{S_k}\Phi_{x,\pm l,\pm l'} = \Phi_{x+\hat{k},\pm l,\pm l'}. \end{aligned} \tag{9.28} $$

For a non-zero mass m, the chiral symmetry is explicitly broken. The flavor symmetry is, however, always a symmetry of the Hamiltonian. For the massless case, $m = 0$, we associate a fake momentum with each energy eigenstate (see section 7.6.4).

9.4. $SO(3)$ Quantum Link Model in $(1+1)$ Dimensions

9.4.1. Hamiltonian

Let us write down the quantum link Hamilton in $(1+1)$ dimensions

$$\begin{aligned} H &= -t\sum_x \left(\psi_x^{a\dagger}\sigma_{x,+}^a\ \sigma_{x+1,-}^b\psi_{x+1}^b + \text{H.c.}\right) + m\sum_x (-1)^x \psi_x^{a\dagger}\psi_x^a \\ &= -t\sum_x \left(B_{x,+}^\dagger\ B_{x+1,-} + \text{H.c.}\right) + m\sum_x (-1)^x M_x. \end{aligned} \tag{9.29}$$

Because we are in $(1+1)$ dimensions, the plaquette term is absent. Let us quickly review all ingredients of this Hamiltonian: The term proportional to the hopping parameter t is responsible for the interaction between the fermionic (ψ^a) and the gauge degrees of freedom (represented by spin operators σ^a), which are associated with the left and right end of a link (see section 9.3.1). The operators $\psi^{a\dagger}$ and ψ^a are the creation and annihilation operators of staggered fermions in the adjoint representation with a color index a (see section 7.3.2) and mass m. In section 9.3.2 we have defined the gauge invariant operators $B_{x,\pm} = \psi_x^a \sigma_{a,\pm}^a$ and $M_x = \psi_x^{a\dagger}\psi_x^a$.

To investigate whether this model actually shows interesting physics, we now present some exact diagonalization results for a $(1+1)$-dimensional system with an $SO(3)$ gauge symmetry. It turns out, that in its original form, the Hamiltonian of equation (9.29) does not break chiral symmetry spontaneously. It is only possible to introduce an explicit breaking for non-zero masses $m \neq 0$. To obtain spontaneously broken chiral symmetry (for $m = 0$), we extend the Hamiltonian. This can be done by introducing additional terms, which favor a staggered pattern

$$\begin{aligned} H &= -t\sum_x \left(B_{x,+}^\dagger\ B_{x+1,-} + \text{H.c.}\right) + m\sum_x (-1)^x M_x \\ &\quad + G\sum_x \left(M_x - \tfrac{3}{2}\right)^2 + V\sum_x \left(M_x - \tfrac{3}{2}\right)\left(M_{x+1} - \tfrac{3}{2}\right). \end{aligned} \tag{9.30}$$

The two additional terms (the G-term and the V-term) are invariant under the various symmetries including the chiral symmetry (see section 9.3.3). This means that chiral symmetry is not broken explicitly. Nevertheless, the G-term with $G < 0$ disfavors the states $|2\rangle_x$ and $|3\rangle_x$. The V-term with $V > 0$, on the other hand, explicitly favors a staggered pattern. For example, the combinations of neighboring sites $|4\rangle_x|1\rangle_{x+1}$ or $|1\rangle_x|4\rangle_{x+1}$ are favored over states $|2\rangle_x|3\rangle_{x+1}$ or $|3\rangle_x|3\rangle_{x+1}$ and even more favored over states like $|4\rangle_x|4\rangle_{x+1}$.

Both of these terms eventually lead to a ground state, which can be qualitatively illustrated of as a "cartoon-state" $|414\ldots41\rangle = |4\rangle_0|1\rangle_1|4\rangle_2\cdots|4\rangle_{L-2}|1\rangle_{L-1}$ or a "cartoon-state" $|141\ldots14\rangle$. Both of these ground states break the chiral symmetry spontaneously.

In the following we will investigate the G-V phase diagram and search for phases with spontaneous broken chiral symmetry as well as for massless phases.

9.4.2. Gauss Law

The Hilbert space is a direct product space of a fermionic and a gauge part. The fermionic part can be characterized by the number of "baryons" b_x per site x. In this basis the operator M_x is diagonal and counts the number of "baryons" ($M_x|b_x\rangle_x = b_x|b_x\rangle_x$), while the operators $\psi_x^{a\dagger}$ and ψ_x^a raise and lower these numbers. When we work in the fundamental spinor-representation of the quantum link operators, the gauge part consists of two spins per site x, one on the left and one on the right side of x (denoted for example as $|\uparrow\downarrow\rangle_x$). The spin operators act on these states, for example, as

$$\sigma^3_{x,-}|\uparrow\downarrow\rangle_x = +|\uparrow\downarrow\rangle_x, \qquad \sigma^3_{x,+}|\uparrow\downarrow\rangle_x = -|\uparrow\downarrow\rangle_x. \tag{9.31}$$

The physical states $|\psi\rangle$ have to be invariant under $SO(3)$ gauge transformations, i.e. $G^a|\psi\rangle = 0$ (see section 9.2.3). It will turn out that (up to a phase) there are only four possible gauge invariant states at each site x. These states are characterized by the number of "baryons" at this site. For example, a state with zero baryons ($b_x = 0$) requires the two spins to form a singlet, which is possible only in one way: $\frac{1}{\sqrt{2}}(|\uparrow\downarrow\rangle - |\downarrow\uparrow\rangle)$. For a state with one baryon, we find that the two spins have to form a color triplet, which then couples with the triplet fermion to form a total color singlet, which is only possible in one way. Also the states with two and three fermions are built in a unique way, which are exactly:

$$\begin{aligned}
|b_x = 0\rangle_x &= \frac{1}{\sqrt{2}}\left(|\uparrow\downarrow\rangle - |\downarrow\uparrow\rangle\right)|0\rangle_x \\
|b_x = 1\rangle_x &= \frac{1}{\sqrt{6}}\Big[\left(|\downarrow\downarrow\rangle - |\uparrow\uparrow\rangle\right)\psi^{1\dagger} + i\left(|\downarrow\downarrow\rangle + |\uparrow\uparrow\rangle\right)\psi^{2\dagger} + \left(|\uparrow\downarrow\rangle + |\downarrow\uparrow\rangle\right)\psi^{3\dagger}\Big]|0\rangle_x \\
|b_x = 2\rangle_x &= \frac{i}{\sqrt{6}}\Big[\left(|\uparrow\downarrow\rangle + |\downarrow\uparrow\rangle\right)\psi^{1\dagger}\psi^{2\dagger} + \left(|\downarrow\downarrow\rangle - |\uparrow\uparrow\rangle\right)\psi^{2\dagger}\psi^{3\dagger} + i\left(|\downarrow\downarrow\rangle + |\uparrow\uparrow\rangle\right)\psi^{3\dagger}\psi^{1\dagger}\Big]|0\rangle_x \\
|b_x = 3\rangle_x &= \frac{i}{\sqrt{2}}\left(|\uparrow\downarrow\rangle - |\downarrow\uparrow\rangle\right)\psi^{1\dagger}\psi^{2\dagger}\psi^{3\dagger}|0\rangle_x
\end{aligned} \tag{9.32}$$

We use the states $\{|0\rangle_x, |1\rangle_x, |2\rangle_x, |3\rangle_x\}$ as a basis at each site x. By acting with the operators $B_{x,\pm}, M_x$ on the basis states one obtains

$$M_x = \begin{bmatrix} 0 & 0 & 0 & 0 \\ 0 & 1 & 0 & 0 \\ 0 & 0 & 2 & 0 \\ 0 & 0 & 0 & 3 \end{bmatrix}, \quad B_{x,+} = \begin{bmatrix} 0 & \sqrt{3} & 0 & 0 \\ 0 & 0 & 2 & 0 \\ 0 & 0 & 0 & \sqrt{3} \\ 0 & 0 & 0 & 0 \end{bmatrix}, \quad B_{x,-} = \begin{bmatrix} 0 & -\sqrt{3} & 0 & 0 \\ 0 & 0 & 2 & 0 \\ 0 & 0 & 0 & -\sqrt{3} \\ 0 & 0 & 0 & 0 \end{bmatrix}. \tag{9.33}$$

Because we have four possible states at each site x, we expect the dimension of the Hilbert space to scale as 4^L with the number L of lattice sites. However, we will use certain symmetries to prediagonalize the Hamiltonian, which reduces the dimension of the Hilbert space (see section 9.4.4). For example, we will fix the total number of baryons B and diagonalize each sector individually. This is possible because $[B, H] = 0$.

9.4.3. Boundary Conditions

It turns out that, in order to observe least perturbed physical spectra, it helps to choose adequate boundary conditions for the fermion operators in the spatial direction. We use periodic boundary conditions if $L/2+B =$ odd and antiperiodic boundary conditions if $L/2+B =$ even, where B is the baryon number as defined in equation (9.17) and L is the number of lattice sites in the spatial direction. Antiperiodic boundary conditions have consequences for the hopping terms and the symmetry transformations.

The hopping term in the Hamiltonian, which reads $-t\sum_x(B^\dagger_{x,+}\ B_{x+1,-} + B^\dagger_{x+1,-}\ B_{x,+})$ acquires some negative signs in the sum when using antiperiodic boundary conditions. The terms that reach over the boundary, will change sign as

$$-t\left(B^\dagger_{L-1,+}\ B_{L,-} + B^\dagger_{L,-}\ B_{L-1,+}\right) = +t\left(B^\dagger_{L-1,+}\ B_{0,-} + B^\dagger_{0,-}\ B_{L-1,+}\right). \tag{9.34}$$

In a similar way, after a symmetry transformation, which shifts the system by one or two lattice spacings, physical states acquire additional negative signs, when operators get shifted over the boundary.

9.4.4. Prediagonalizing the Hamiltonian

In order to reduce the dimension of the Hilbert space, we use certain symmetries to prediagonalize the system. One of these symmetries is the global $U(1)$ baryon number symmetry, which leads to the conservation of the total number of baryons

$$B = \sum_x \left(M_x - \frac{3}{2}\right), \tag{9.35}$$

with $[B, H] = 0$. This implies that we can choose a sub-basis of the Hilbert space including only states with a fixed total number of baryons and diagonalize the Hamiltonian only in this sector. The Hamiltonian can be diagonalized independently in each of these baryon number sectors. For example, if we choose the total baryon number to be $B = 0$ in an $L = 4$ system, we only have the basis states $|0033\rangle, |0132\rangle, |0123\rangle, |0231\rangle, |0222\rangle, |0213\rangle, |0330\rangle, \ldots$ On the other hand, if, for example, $B = 1$, we have $|0133\rangle, |0232\rangle, |0223\rangle, |0331\rangle, |0322\rangle, |0313\rangle, |1033\rangle, \ldots$

In the $(1+1)$-dimensional $U(2)$ quantum link model, we were able to diagonalize the Hamiltonian up to a system size of $L = 18$, thanks to the 2^L scaling of the dimension of the Hilbert space. In the $(1 + 1)$-dimensional $SO(3)$ quantum link model, the dimension of the Hilbert space scales as 4^L with the system size, which poses a great challenge. Even when prediagonalizing the Hamiltonian in the different baryon sectors, we only reach systems sizes up to $L = 12$.

In order to reach larger spatial volumes ($L = 14, 16$), we prediagonalized the Hamiltonian with respect to the true momentum p, which has been defined in section 7.6.1. In order to do so, we search for a basis, in which all states are eigenstates of the translation operations (by two lattice spacings) and all have the same true momentum p. This can be achieved by applying the following procedure: Some states are already a translation eigenstate with the

required momentum $T|\psi_0\rangle = \exp(ip)|\psi_0\rangle$. If a state is not an eigenstate of the translation operator, it is transformed back to the original state after $n \leq L/2$ consecutive translations

$$T|\psi_0\rangle = |\psi_1\rangle,\ T|\psi_1\rangle = |\psi_2\rangle,\ \ldots,\ T|\psi_{n-1}\rangle = |\psi_n\rangle = |\psi_0\rangle \quad \Longrightarrow \quad T^n|\psi_0\rangle = |\psi_0\rangle. \tag{9.36}$$

Based on this, we can construct an eigenstate of the translation operator with momentum p as

$$|\psi'_p\rangle = \frac{1}{\sqrt{n}} \sum_{l=0}^{n-1} \exp(-ipl) T^l |\psi_0\rangle \qquad \Longrightarrow \qquad T|\psi'_p\rangle = \exp(ip)|\psi'_p\rangle. \tag{9.37}$$

All the other states are not included in this basis. For our purpose, we only choose $p = 0$. This may seem as a severe restriction, but, in fact, it is not. We are only interested in large system sizes L, when investigating the spontaneous breaking of the chiral symmetry by studying whether there is an "almost degenerate" ground state. Both of these vacua are expected to have a zero true momentum $p = 0$.

9.4.5. Spontaneous Chiral Symmetry Breaking

In section 8.3.3, we have studied spontaneous chiral symmetry breaking in the $U(2)$ quantum link model. In this section we perform a similar study for the $SO(3)$ quantum link model by searching for spectra, where the ground state is almost degenerate. This means that the two lowest states in the spectrum are very close to each other and their energy difference scales as

$$\Delta E = E_1 - E_0 \sim \exp(-\alpha L), \tag{9.38}$$

with the system size L, and they both have momentum $p = 0$.

In figure 9.2 we show the spectrum of the quantum link Hamiltonian for $L = 12$. We plot the energy (in units of the hopping parameter t) of the lowest few eigenstates against the true momentum p (see section 7.6.1). In order to distinguish degenerate states, we slightly move the symbols in the plot to the left and to the right in a staggered fashion. The energy is normalized to be zero for the ground state in the zero baryon number sector ($B = 0$).

The upper two plots show spectra in the sector with baryon number $B = 0$. In the left plot (for a parameter $G/t = -4$) we find an almost degenerate spectrum. This suggests that we are in a phase, where the chiral symmetry is broken spontaneously. In the right plot we increased the parameter G to ($G/t = -3$) and we do not find an almost degenerate spectrum any more. We conclude that in this phase the chiral symmetry is no longer spontaneously broken. The state which was almost degenerate with the vacuum before, has now moved to higher energies. When we further increase the parameter G, this state goes even higher and we ultimately reach the spectrum, which corresponds to the one of a massless particle (see next section).

The two lower plots in figure 9.2 show the spectrum for a finite baryon density $\rho_B = B/L = 1/4$. Here, we have $B = 3$ baryons in a system of size $L = 12$. The energy difference ΔE is measured with respect to the ground state of the zero baryon number sector $B = 0$. The left plot again shows the spectrum at $G/t = -4$. We see that the spectrum is not degenerate any more, which implies that the chiral symmetry got restored at the finite baryon density.

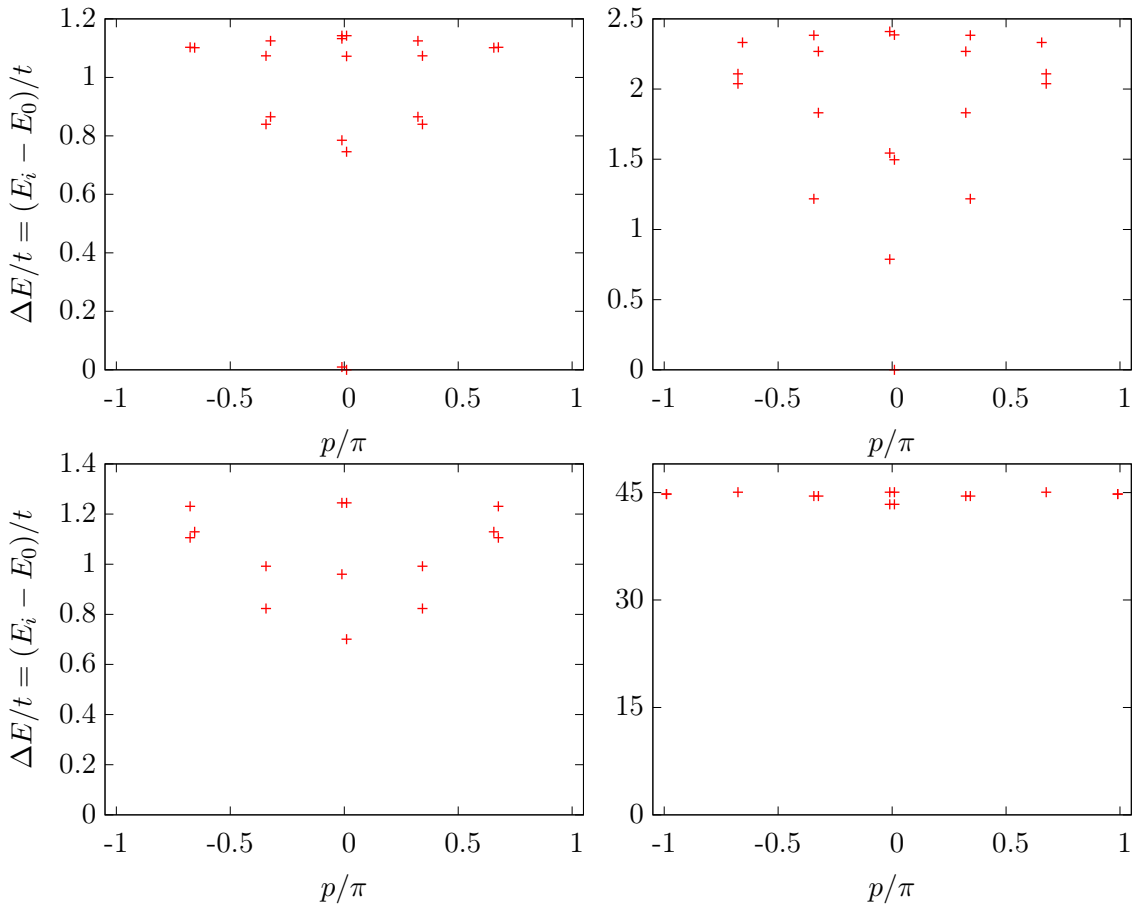

FIGURE 9.2.: Spectra of the $SO(3)$ quantum link Hamiltonian for system size $L = 12$. On the top, we find spectra for the baryon number zero sector $B = 0$. In the top left plot we find that chiral symmetry is spontaneously broken ($G/t = -4, V/t = 0$) and in the top right plot it is restored ($G/t = -3, V/t = 0$). The two lower plots show spectra in the sector with $B = 3$ baryons. In the left we do not find spontaneous breaking of chiral symmetry ($G/t = -4, V/t = 0$), but in the right plot we do ($G/t = 4, V/t = 8$).

On the other hand, there are also regions in the phase diagram, where chiral symmetry is spontaneously broken even at finite baryon density. This is shown in the plot on the right hand side, where we have incorporated the V term ($G/t = 4, V/t = 8$).

To verify spontaneous chiral symmetry breaking, we study the scaling behavior of the energy difference of the two lowest states $\Delta E = E_1 - E_0$ as a function of the volume. In case of spontaneous symmetry breaking, this energy difference vanishes exponentially with the volume L of the system. In figure 9.3 we show these energy differences for $G/t = 2, V/t = 6$. The exponential fall-off is obvious in the sector of zero baryons, which indeed confirms spontaneous chiral symmetry breaking. Also as we switch on a finite baryon density $\rho_B = 1/4$ the three points at $L = 8, 12, 16$ indicate an exponential fall-off. For $\rho_B = 1/2$ this scaling is lost and we conclude that chiral symmetry is restored at this finite baryon density.

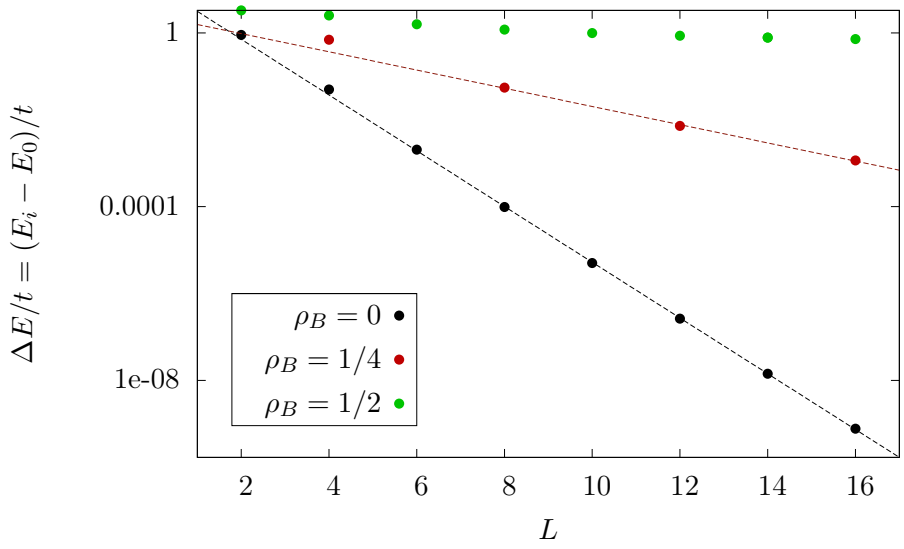

Figure 9.3.: The exponential scaling of the energy difference for $G/t = 2, V/t = 6$ of the almost degenerate vacua indicates the chiral symmetry breaking for zero baryon density $\rho_B = 0$. Chiral symmetry is restored for non-zero baryon densities.

We searched for spontaneous chiral symmetry breaking systematically in the whole G-V phase diagram and checked whether the symmetry gets restored at finite baryon density $\rho_B = B/L$. This is done by fitting the logarithm of the energy difference ΔE of the two lowest states (with $p = 0$) with a linear function

$$\log(\Delta E) = a \cdot L + b \tag{9.39}$$

for $L \geq 6$. The fit is done by minimizing the sum of the squares of the deviations to the measurements $\sum_L \delta_L^2$. We say that we find a broken chiral symmetry if this linear fit works fine. A fine fit requires the deviations to the measurements δ_L to be small compared to the whole range of values $R = \max_L(\log(\Delta E_L)) - \min_L(\log(\Delta E_L))$. It turned out that it is optimal to choose the fit limit to be

$$\max_L \delta_L / R < 0.035. \tag{9.40}$$

In addition we require the fit to be steep in order not to include a flat scaling with the volume

as we found it, for example, for $\rho_B = 1/2$ in figure 9.3. A minimal value of the slope of

$$|a| > 0.2 \tag{9.41}$$

turns out to be sufficient.

Figure 9.4 shows the phase diagram in the zero baryon number sector $B = 0$. In the green region, we find an exponential scaling of the energy difference ΔE with the volume L of the system. All spectra in this phase look qualitatively like the spectrum in figure 9.2 on the top left. We conclude that in the green region, chiral symmetry is broken spontaneously. This is just the region, where we expected the chiral symmetry to break spontaneously (for $G < 0$ and/or $V > 0$, see section 9.4.1). In the white region, we do not find an exponential scaling and thus conclude that in this region chiral symmetry is not spontaneously broken.

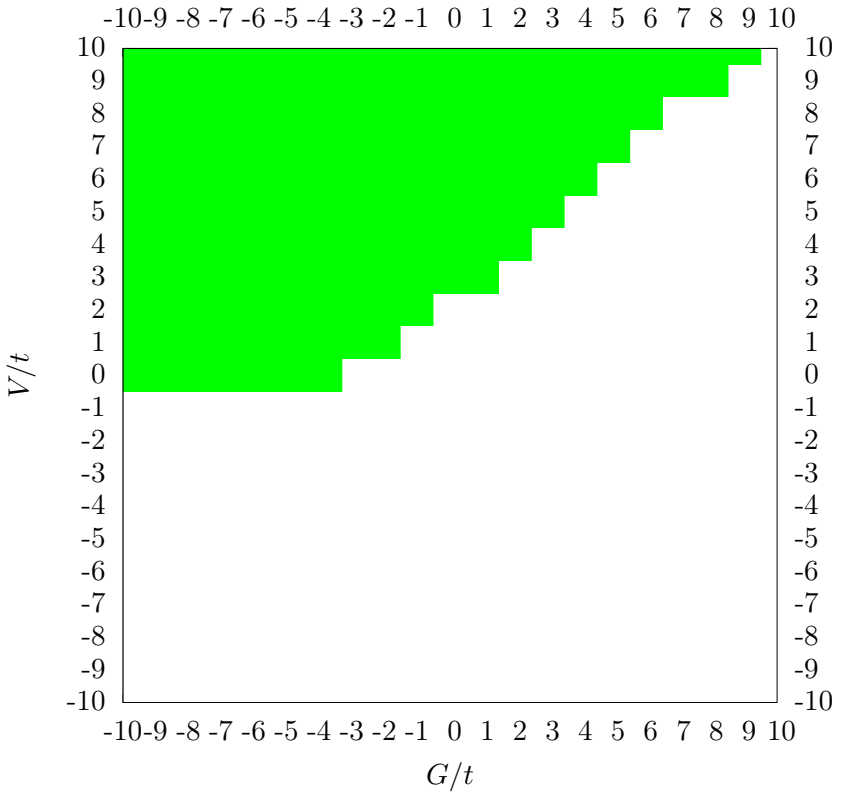

FIGURE 9.4.: G-V phase diagram of the quantum link Hamiltonian in the zero baryon number sector ($B = 0$) extracted from system sizes $L = 2$ to $L = 16$. In the green region we find a spontaneously broken chiral symmetry, while in the white region chiral symmetry is not broken.

In Figure 9.5 we present the same analysis at a finite baryon density $\rho_B = 1/4$ and $\rho_B = 1/2$. We see that only a small fraction of the chirally broken phase remains. This means that, in most regions of the phase diagram, chiral symmetry gets restored at finite baryon density ρ_B.

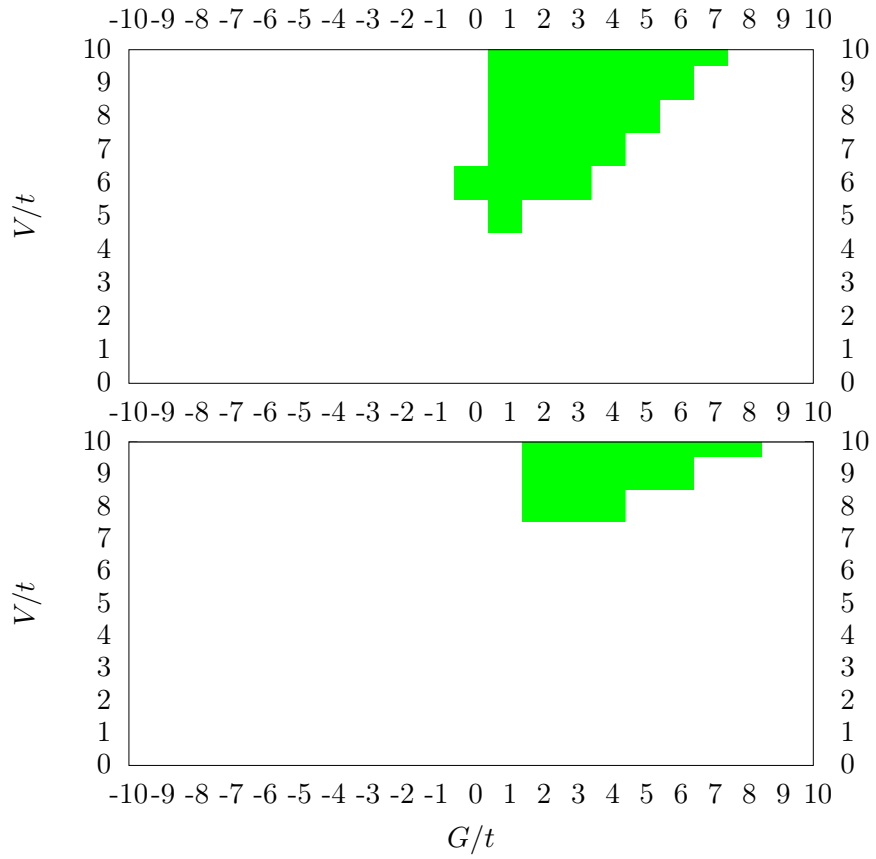

Figure 9.5.: G-V phase diagram of the quantum link Hamiltonian for finite baryon densities $\rho_B = 1/4$ (top) and $\rho_B = 1/2$ (bottom) extracted from system sizes $L = 2$ to $L = 16$. In the green region we find a spontaneously broken chiral symmetry, while in the white region chiral symmetry is not broken.

9.4.6. Massless Phase

The spectrum of a massless particle is characterized by a linear relation between the energy E and the momentum p

$$E(p) = cp, \tag{9.42}$$

where c is the "speed of light" (in appropriate units). In figure 9.6, we illustrate such a dispersion relation for the four-Fermi parameters $G/t = 2, V/t = -1$. It is remarkable that the linear behavior extends throughout the whole Brillouin zone and it does not flatten out for $p \approx \pi$.

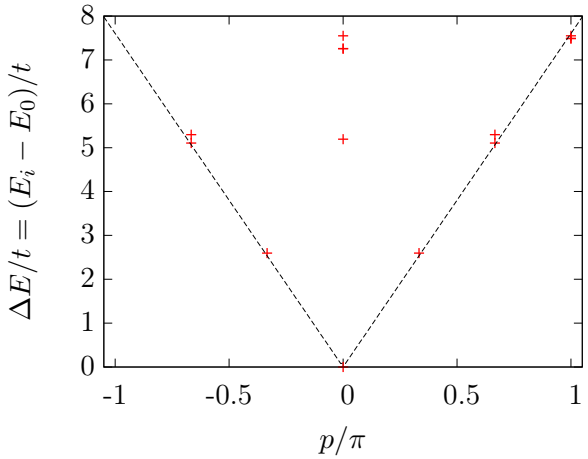

FIGURE 9.6.: Spectrum of the $SO(3)$ quantum link Hamiltonian for system size $L = 12$ in the baryon number zero sector $B = 0$. We find the spectrum of a massless particle for parameters $G/t = 2, V/t = -1$.

We search for massless phases in the G-V phase diagram by trying to fit linear functions to the dispersion relations. The result is shown in figure 9.7. In the yellow and the brown region we find spectra with a linear energy-momentum dispersion relation for all system sizes between $L = 6$ and $L = 12$. For each system size L we obtain the "speed of light" c as a fit parameter. This parameter should be more or less constant and not depend on the system size L. This is the case in the brown region, where the speed of light does not vary more than 5% for different system sizes L. This means that in the brown region we find a massless phase.

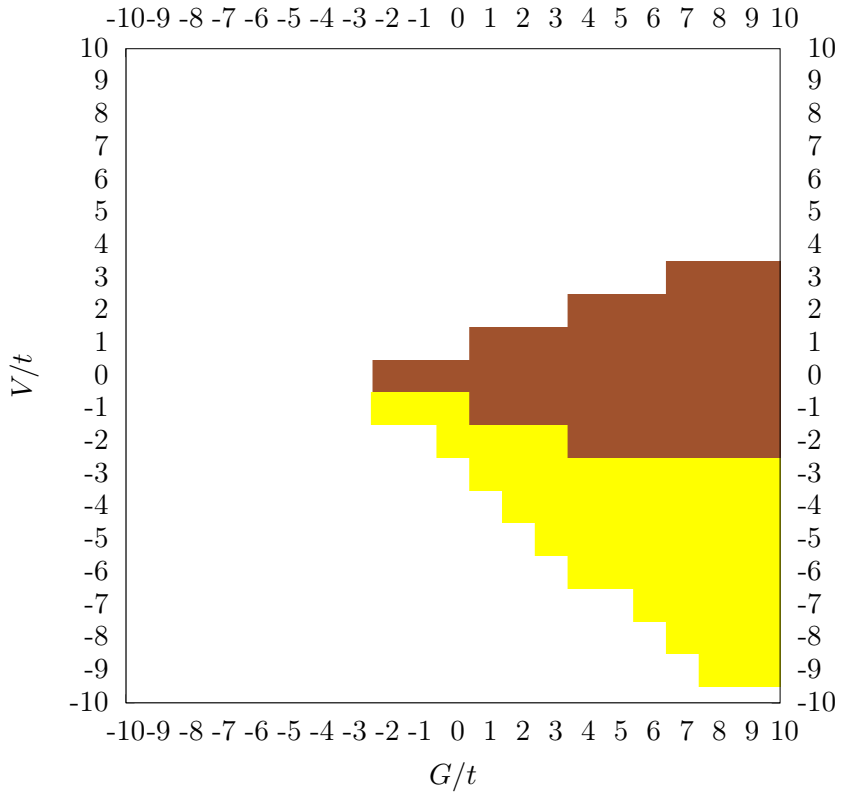

Figure 9.7.: G-V phase diagram of the quantum link Hamiltonian in the zero baryon number sector ($B = 0$) extracted from system sizes $L = 6$ to $L = 12$. In the yellow and the brown region we find a linear dispersion relation. In the brown region the estimated "speed of light" c is almost independent of system size L, indicating a massless phase. In the white region, there are no linear dispersion relations.

Chapter 10.

Conclusions and Outlook

In this thesis we investigated quantum link models in many details. These models are an extension of the Hamiltonian formulation of ordinary Wilson lattice gauge theory. The aim is to study non-perturbative effects, which also show up in QCD and can not be simulated on a classical computer. For example, we studied the spontaneous breaking of the chiral symmetry and its restoration at finite baryon density. The real-time evolution of a chirally restored hot-spot in a vacuum has also been calculated.

These studies are a preparatory work to motivate experiments in the field of quantum simulations. The quantum link formalism allowed us to suggest a possible implementation of lattice gauge theories in ultra-cold atomic gases in an optical lattice setup. Exact diagonalization results confirmed that these models indeed show interesting physics. The results also allow to validate a future experimental realization.

We have started with an introduction in lattice field theory and motivated Wilson's approach as a regulator of QCD. After rewriting and discussing this theory in the Hamiltonian formulation, we showed how to extend it to quantum link models. This was done by choosing a finite-dimensional Hilbert space, while giving up the commutativity of the elements of the link variables. We assigned a Hermitian operator to each matrix element of the link variables. These so-called quantum link operators act in an alternative Hilbert space.

We have presented an explicit construction of quantum simulators for $U(N)$ or $SU(N)$ gauge theories using an ultra-cold gas of alkaline-earth atoms in an optical lattice setup. This is realized by using quantum link operators coupled to staggered fermions. The rishon representation allowed us to rewrite the Hamiltonian in a Hubbard-like form, with only fermions hopping on the lattice. This is then used for the implementation in a quantum simulator. We presented exact diagonalization results for a $(1+1)$-d $U(2)$ quantum link model. Already in a simple model like this, we were able to demonstrate non-trivial physics including the real-time dynamics of a chirally restored hot-spot.

We further studied a quantum link model with an $SO(3)$ gauge symmetry. This model has a conserved baryon number and thus allows to simulate a system at finite baryon density. The spinor representation allowed to represent the Hilbert space in a pictorial form and will also help to implement this model in a quantum simulator. We investigated the phase diagram of this model by searching for a spontaneously broken chiral symmetry at different parameters. This was done at zero and non-zero baryon density. We observed that chiral symmetry got restored at finite baryon density in most parts of the phase diagram. We also found a massless phase.

In the future, we plan to further extend these models towards QCD, which requires to incorporate the $SU(3)$ gauge group, multi-component Dirac fermions, and higher dimensions, which needs to be done in several steps. It would also be interesting to simulate phenomena like baryon superfluidity, color superconductivity at high densities. A long-term goal is to quantum simulate full QCD in real-time and simulate systems at large baryon density or the real-time evolution of a heavy-ion collision for example. This requires a dimensional reduction of a $(4+1)$d quantum link model to $(3+1)$ dimensional QCD [65].

Of course it is a long way to reach this ultimate goal, so this work should be seen as a first step in this direction. Regarding the interesting results, we hope to encourage experimentalists to realize one of these models in a laboratory.

Acknowledgments

First, I would like to thank Uwe-Jens Wiese for giving me the opportunity to work with him on these very interesting projects. He gave me a lot of support to work out all these projects and gave me many useful advice for writing the thesis. In addition he made it possible for me to visit a summer school and several conferences from which I have profited a lot. I would also like to thank Ulli Wolff for accepting the responsibility of being the co-referee for this thesis.

Further thanks go to the colleagues of our group, Debasish Banerjee, Pascal Stebler, and Philippe Widmer for the interesting discussions and the support. They helped me in both, discussing problems in physics and by encouraging me to write up the thesis.

When working on the $O(3)$ model I profited a lot from the collaboration with Wolfgang Bietenholz, Michele Pepe, and Ferenc Niedermayer. We are all indebted to Janos Balog for providing exact values of the step scaling function at $\theta = \pi$ prior to publication.

I also thank all our collaborators from Innsbruck and Ulm for the interesting work we have done together. These are Marcello Dalmonte, Enrique Rico, and Peter Zoller, who worked with us on the quantum link projects.

Special thanks also go to Fu-Jiun Jiang for the collaboration and the discussions of interesting projects in condensed matter physics. I would also like to thank him for the invitation to Taipei, where I had the opportunity to work on two projects, to discuss certain problems with him, and also got to know the people and culture of his lovely home country.

I would also like to express my gratitude to the secretary of our institute, Ester Fiechter, for her help with all administrative issues. This work is supported by the Schweizerischer Nationalfonds.

I would also like to thank especially some friends at the institute including Kyle Steinhauer, Stefanie Marti, Lorena Rothen, and Peter Stoffer for their friendship and for their essential help with all the problems one encounters when writing a Ph.D. thesis. I would also like to thank my former office mate, David Baumgartner, my flat mates, Peter Feller and Kay Werndli, and many other friends for their support. Last, but not least, I thank my parents for their support and the encouragements especially during the time when I was writing up the thesis.

Bibliography

[1] A. D'Adda, P. Di Vecchia, and M. Lüscher, *Confinement and Chiral Symmetry Breaking in CP**n-1 Models with Quarks*, Nucl. Phys. B **152**, 125 (1979).

[2] D. Petcher and M. Lüscher, *Topology and Universality in the Lattice CP**2 Model*, Nucl. Phys. B **225**, 53 (1983).

[3] B. Berg and M. Lüscher, *Definition and Statistical Distributions of a Topological Number in the Lattice O(3) Sigma Model*, Nucl.Phys. B **190**, 412 (1981).

[4] A. Zamolodchikov and V. Fateev, *Disorder Fields in Two-Dimensional Conformal Quantum Field Theory and N=2 Extended Supersymmetry*, Sov. Phys. JETP **63**, 913 (1986).

[5] J. Balog and M. Niedermaier, *Off-shell dynamics of the O(3) NLS model beyond Monte Carlo and perturbation theory*, Nucl. Phys. B **500**, 421 (1997), `arXiv:hep-th/9612039`.

[6] A. B. Zamolodchikov and A. B. Zamolodchikov, *Factorized s Matrices in Two-Dimensions as the Exact Solutions of Certain Relativistic Quantum Field Models*, Annals Phys. **120**, 253 (1979).

[7] P. Hasenfratz, M. Maggiore, and F. Niedermayer, *The exact mass gap of the O(3) and O(4) nonlinear sigma models in d = 2*, Phys. Lett. B **245**, 522 (1990).

[8] J. Wess and B. Zumino, *Consequences of anomalous Ward identities*, Phys. Lett. B **37**, 95 (1971).

[9] S. Novikov, *The Hamiltonian formalism and a many valued analog of Morse theory*, Usp. Mat. Nauk **37N5**, 3 (1982).

[10] E. Witten, *Global Aspects of Current Algebra*, Nucl. Phys. B **223**, 422 (1983).

[11] F. D. M. Haldane, *Nonlinear Field Theory of Large-Spin Heisenberg Antiferromagnets: Semiclassically Quantized Solitons of the One-Dimensional Easy-Axis Néel State*, Phys. Rev. Lett. **50**, 1153 (1983).

[12] H. Bethe, *On the theory of metals. 1. Eigenvalues and eigenfunctions for the linear atomic chain*, Zeitschrift für Physik **71**, 205 (1931).

[13] J. Balog and Á. Hegedűs, *TBA Equations for excited states in the O(3) and O(4) nonlinear sigma model*, J. Phys. A **37**, 1881 (2004), `arXiv:hep-th/0309009`.

[14] M. Lüscher, P. Weisz, and U. Wolff, *A Numerical method to compute the running coupling in asymptotically free theories*, Nucl. Phys. B **359**, 221 (1991).

[15] R. Botet, R. Jullien, and M. Kolb, *Finite-size-scaling study of the spin-1 Heisenberg-Ising chain with uniaxial anisotropy*, Phys. Rev. B **28**, 3914 (1983).

[16] W. Bietenholz, A. Pochinsky, and U.-J. Wiese, *Meron-Cluster Simulation of the Theta Vacuum in the 2D O(3) Model*, Phys. Rev. Lett. **75**, 4524 (1995), arXiv:hep-lat/9505019.

[17] M. Lüscher, *Does the Topological Susceptibility in Lattice Sigma Models Scale According to the Perturbative Renormalization Group?*, Nucl. Phys. B **200**, 61 (1982).

[18] M. Blatter, R. Burkhalter, P. Hasenfratz, and F. Niedermayer, *Instantons and the fixed point topological charge in the two-dimensional O(3) sigma model*, Phys. Rev. D **53**, 923 (1996), arXiv:hep-lat/9508028.

[19] W. Bietenholz, U. Gerber, M. Pepe, and U.-J. Wiese, *Topological Lattice Actions*, JHEP **1012**, 020 (2010), arXiv:1009.2146.

[20] M. Bögli, F. Niedermayer, M. Pepe, and U.-J. Wiese, *Non-trivial θ-Vacuum Effects in the 2-d O(3) model*, JHEP **1204**, 117 (2012), arXiv:1112.1873.

[21] M. Bögli, F. Niedermayer, U.-J. Wiese, and M. Pepe, *Study of theta-Vacua in the 2-d O(3) Model*, PoS **LATTICE2012**, 228 (2012), arXiv:1211.2932.

[22] J. Balog, F. Niedermayer, M. Pepe, P. Weisz, and U.-J. Wiese, *Drastic Reduction of Cutoff Effects in 2-d Lattice O(N) Models*, JHEP **1211**, 140 (2012), arXiv:1208.6232.

[23] M. Hasenbusch, *An improved estimator for the correlation function of 2D nonlinear sigma models*, Nucl. Phys. B Proc. Suppl. **42**, 764 (1995), arXiv:hep-lat/9408019.

[24] J. Balog, F. Niedermayer, and P. Weisz, *The Puzzle of apparent linear lattice artifacts in the 2d non-linear sigma-model and Symanzik's solution*, Nucl. Phys. B **824**, 563 (2010), arXiv:0905.1730.

[25] J. Balog, private communication .

[26] P. de Forcrand, M. Pepe, and U.-J. Wiese, *Walking near a Conformal Fixed Point: the 2-d O(3) Model at theta near pi as a Test Case*, Phys. Rev. D **86**, 075006 (2012), arXiv:1204.4913.

[27] U. Wolff, *Collective Monte Carlo Updating for Spin Systems*, Phys. Rev. Lett. **62**, 361 (1989).

[28] R. Jackiw and C. Rebbi, *Vacuum Periodicity in a Yang-Mills Quantum Theory*, Phys. Rev. Lett. **37**, 172 (1976).

[29] C. G. J. Callan, R. Dashen, and D. J. Gross, *The Structure of the Gauge Theory Vacuum*, Phys. Lett. B **63**, 334 (1976).

[30] M. Bögli, *Worm algorithm in the O(N) model and related models*, Master's thesis (2010).

[31] U.-J. Wiese, *Numerical Simulation of Lattice θ Vacua: The 2-d U(1) Gauge Theory as a Test Case*, Nucl. Phys. B **318**, 153 (1989).

[32] J. Balog, F. Niedermayer, and P. Weisz, *Logarithmic corrections to O(a**2) lattice artifacts*, Phys. Lett. B **676**, 188 (2009), arXiv:0901.4033.

[33] K. Symanzik, *Continuum Limit and Improved Action in Lattice Theories. 1. Principles and phi**4 Theory*, Nucl. Phys. B **226**, 187 (1983).

[34] K. G. Wilson, *Confinement of Quarks*, Phys. Rev. D **10**, 2445 (1974).

[35] D. Horn, *Finite Matrix Models With Continuous Local Gauge Invariance*, Phys. Lett. B **100**, 149 (1981).

[36] P. Orland and D. Rohrlich, *Lattice gauge magnets: Local isospin from spin*, Nucl. Phys. B **338**, 647 (1990).

[37] S. Chandrasekharan and U.-J. Wiese, *Quantum link models: A discrete approach to gauge theories*, Nucl. Phys. B **492**, 455 (1997), arXiv:hep-lat/9609042.

[38] C. N. Yang and R. L. Mills, *Conservation of Isotopic Spin and Isotopic Gauge Invariance*, Phys. Rev. D **96**, 191 (1954).

[39] D. J. Gross and F. Wilczek, *Ultraviolet Behavior of Non-Abelian Gauge Theories*, Phys. Rev. Lett. **30**, 1343 (1973).

[40] H. D. Politzer, *Reliable Perturbative Results for Strong Interactions?*, Phys. Rev. Lett. **30**, 1346 (1973).

[41] Y. Aoki, G. Endrődi, Z. Fodor, S. Katz, and K. Szabo, *The Order of the quantum chromodynamics transition predicted by the standard model of particle physics*, Nature **443**, 675 (2006), arXiv:hep-lat/0611014.

[42] A. Bazavov, T. Bhattacharya, M. Cheng, N. Christ, C. DeTar, *et al.*, *Equation of state and QCD transition at finite temperature*, Phys. Rev. D **80**, 014504 (2009), arXiv:0903.4379.

[43] S. Dürr, Z. Fodor, J. Frison, C. Hoelbling, R. Hoffmann, S. D. Katz, S. Krieg, T. Kurth, L. Lellouch, T. Lippert, K. K. Szabo, and G. Vulvert, *Ab-Initio Determination of Light Hadron Masses*, Science **322**, 1224 (2008), arXiv:0906.3599.

[44] A. Bazavov, D. Toussaint, C. Bernard, J. Laiho, C. DeTar, *et al.*, *Nonperturbative QCD simulations with 2+1 flavors of improved staggered quarks*, Rev. Mod. Phys. **82**, 1349 (2010), arXiv:0903.3598.

[45] Y. Aoki *et al.*, *Continuum Limit Physics from 2+1 Flavor Domain Wall QCD*, Phys. Rev. D **83**, 074508 (2011), arXiv:1011.0892.

[46] M. Hermele, M. P. Fisher, and L. Balents, *Pyrochlore photons: The U(1) spin liquid in a S=1/2 three-dimensional frustrated magnet*, Phys. Rev. B **69**, 064404 (2004), arXiv:cond-mat/0305401.

[47] P. A. Lee, N. Nagaosa, and X.-G. Wen, *Doping a Mott insulator: Physics of high-temperature superconductivity*, Rev. Mod. Phys. **78**, 17 (2006).

[48] K. Rajagopal and F. Wilczek, *The Condensed matter physics of QCD*, At the frontier of particle physics **3***, 2061 (2000), `arXiv:hep-ph/0011333`.

[49] S. Chandrasekharan and U.-J. Wiese, *Meron-Cluster Solution of Fermion Sign Problems*, Phys. Rev. Lett. **83**, 3116 (1999), `arXiv:cond-mat/9902128`.

[50] S. Chandrasekharan, *Fermion bag approach to lattice field theories*, Phys. Rev. D **82**, 025007 (2010), `arXiv:0910.5736`.

[51] R. P. Feynman, *Simulating physics with computers*, Int. J. Theor. Phys. **21**, 467 (1982).

[52] J. Cirac and P. Zoller, *Quantum Computations with Cold Trapped Ions*, Phys. Rev. Lett. **74**, 4091 (1995).

[53] S. Lloyd, *Universal Quantum Simulators*, Science **273**, 1073 (1996).

[54] D. Jaksch, C. Bruder, J. I. Cirac, C. W. Gardiner, and P. Zoller, *Cold Bosonic Atoms in Optical Lattices*, Phys. Rev. Lett. **81**, 3108 (1998).

[55] M. H. Anderson, J. R. Ensher, M. R. Matthews, C. E. Wieman, and E. A. Cornell, *Observation of Bose-Einstein Condensation in a Dilute Atomic Vapor*, Science **269**, 198 (1995).

[56] K. B. Davis, M.-O. Mewes, M. R. Andrews, N. J. van Druten, D. S. Durfee, D. M. Kurn, and W. Ketterle, *Bose-Einstein Condensation in a Gas of Sodium Atoms*, Phys. Rev. Lett. **75**, 3969 (1995).

[57] I. Bloch, J. Dalibard, and S. Nascimbène, *Quantum simulations with ultracold quantum gases*, Nat. Phys. **8**, 267 (2012).

[58] M. Greiner, O. Mandel, T. Esslinger, T. W. Hänsch, and I. Bloch, *Quantum phase transition from a superfluid to a Mott insulator in a gas of ultracold atoms*, Nature **415**, 39 (2002).

[59] E. Kapit and E. J. Mueller, *Optical Lattice Hamiltonians for Relativistic Quantum Electrodynamics*, Phys. Rev. A **83**, 033625 (2011), `arXiv:1011.4021`.

[60] D. Banerjee, M. Dalmonte, M. Müller, E. Rico, P. Stebler, U.-J. Wiese, and P. Zoller, *Atomic Quantum Simulation of Dynamical Gauge Fields coupled to Fermionic Matter: From String Breaking to Evolution after a Quench*, Phys. Rev. Lett. **109**, 175302 (2012), `arXiv:1205.6366`.

[61] E. Zohar, J. I. Cirac, and B. Reznik, *Simulating (2 + 1)-Dimensional Lattice QED with Dynamical Matter Using Ultracold Atoms*, Phys. Rev. Lett. **110**, 055302 (2013), `arXiv:1208.4299`.

[62] H. P. Büchler, M. Hermele, S. D. Huber, M. P. A. Fisher, and P. Zoller, *Atomic Quantum Simulator for Lattice Gauge Theories and Ring Exchange Models*, Phys. Rev. Lett. **95**, 040402 (2005), arXiv:cond-mat/0503254.

[63] E. Zohar, J. I. Cirac, and B. Reznik, *Simulating Compact Quantum Electrodynamics with Ultracold Atoms: Probing Confinement and Nonperturbative Effects*, Phys. Rev. Lett. **109**, 125302 (2012), arXiv:1204.6574.

[64] L. Tagliacozzo, A. Celi, A. Zamora, and M. Lewenstein, *Optical Abelian Lattice Gauge Theories*, Annals Phys. **330**, 160 (2013), arXiv:1205.0496.

[65] R. Brower, S. Chandrasekharan, and U.-J. Wiese, *QCD as a quantum link model*, Phys. Rev. D **60**, 094502 (1999), arXiv:hep-th/9704106.

[66] R. Brower, S. Chandrasekharan, S. Riederer, and U.-J. Wiese, *D theory: Field quantization by dimensional reduction of discrete variables*, Nucl. Phys. B **693**, 149 (2004), arXiv:hep-lat/0309182.

[67] U.-J. Wiese, *Ultracold Quantum Gases and Lattice Systems: Quantum Simulation of Lattice Gauge Theories* (2013), arXiv:1305.1602.

[68] D. Banerjee, M. Bögli, M. Dalmonte, E. Rico, P. Stebler, U.-J. Wiese, and P. Zoller, *Atomic Quantum Simulation of U(N) and SU(N) Non-Abelian Lattice Gauge Theories*, Phys. Rev. Lett. **110**, 125303 (2013), arXiv:1211.2242.

[69] M. Dalmonte, E. Rico, P. Zoller, D. Banerjee, M. Bögli, P. Stebler, and U.-J. Wiese, to be published (2014).

[70] L. Tagliacozzo, A. Celi, P. Orland, and M. Lewenstein, *Simulations of non-Abelian gauge theories with optical lattices*, Nat. Commun. **4**, 2615 (2013), arXiv:1211.2704.

[71] E. Zohar, J. I. Cirac, and B. Reznik, *Cold-Atom Quantum Simulator for SU(2) Yang-Mills Lattice Gauge Theory*, Phys. Rev. Lett. **110**, 125304 (2013), arXiv:1211.2241.

[72] C. Gattringer and C. Lang, *Quantum Chromodynamics on the Lattice: An Introductory Presentation*, Lecture Notes in Physics (Springer, 2009), ISBN 9783642018497.

[73] K. Wilson, *Quarks: From Paradox to Myth*, Subnucl.Ser. **13**, 13 (1977).

[74] H. B. Nielsen and M. Ninomiya, *A No Go Theorem for Regularizing Chiral Fermions*, Phys. Lett. B **105**, 219 (1981).

[75] C. G. J. Callan and J. A. Harvey, *Anomalies and Fermion Zero Modes on Strings and Domain Walls*, Nucl. Phys. B **250**, 427 (1985).

[76] D. B. Kaplan, *A Method for simulating chiral fermions on the lattice*, Phys. Lett. B **288**, 342 (1992), arXiv:hep-lat/9206013.

[77] L. Susskind, *Lattice Fermions*, Phys. Rev. D **16**, 3031 (1977).

[78] J. B. Kogut and L. Susskind, *Hamiltonian Formulation of Wilson's Lattice Gauge Theories*, Phys. Rev. D **11**, 395 (1975).

[79] J. B. Kogut, *Lattice Gauge Theory Approach to Quantum Chromodynamics*, Rev. Mod. Phys. **55**, 775 (1983).

[80] D. Banerjee, F.-J. Jiang, P. Widmer, and U.-J. Wiese, *The (2 + 1)-d U(1) quantum link model masquerading as deconfined criticality*, J. Stat. Mech. **2013**, P12010 (2013), `arXiv:1303.6858`.

[81] D. Banerjee, P. Widmer, F.-J. Jiang, and U.-J. Wiese, *Crystalline Confinement* (2013), `arXiv:1311.2459`.

Appendix A.

Commutation Relations of the Embedding Algebra $su(2N)$

The algebra $su(2N)$ has $(2N)^2 - 1$ Hermitian generators, with $2(N^2-1)$ of them generating of the subalgebra $su(N) \oplus su(N)$. We identify these operators with $L^a_{x,y}$ and $R^a_{x,y}$, which generate the $su(N)_L \oplus su(N)_R$ subalgebra. In the fundamental representation of $su(2N)$, we express these operators explicitly as

$$L^a_{x,y} = \begin{bmatrix} 0 & 0 \\ 0 & \lambda^a \end{bmatrix}, \qquad R^a_{x,y} = \begin{bmatrix} \lambda^a & 0 \\ 0 & 0 \end{bmatrix}, \tag{A.1}$$

where λ^a are the $N \times N$ generators of $su(N)$. The remaining $2N^2 + 1$ generators are written as

$$M^{ij}_{x,y} = \begin{bmatrix} 0 & D^{(ij)} \\ D^{(ji)} & 0 \end{bmatrix}, \quad N^{ij}_{x,y} = \begin{bmatrix} 0 & -iD^{(ij)} \\ iD^{(ji)} & 0 \end{bmatrix}, \quad E_{x,y} = \frac{1}{2}\begin{bmatrix} \mathbb{1} & 0 \\ 0 & -\mathbb{1} \end{bmatrix}, \tag{A.2}$$

where $D^{(ij)}_{kl} = \delta_{il}\delta_{jk}$ are $N \times N$ matrices with all elements being zero, except the one in the column i, row j, which is equal to 1.

The commutation relations among the generators are

$$\begin{aligned}
[L^a, L^b] &= 2if^{abc}L^c, & [R^a, R^b] &= 2if^{abc}R^c, & [R^a, L^b] &= 0, \\
[L^a, E] &= 0, & [R^a, E] &= 0, & & \\
[M^{ij}, E] &= -iN^{ij}, & [N^{ij}, E] &= iM^{ij}, & & \\
[M^{ij}, M^{kl}] &= [N^{ij}, N^{kl}] = -i\left(\delta_{ik}\mathrm{Im}(\lambda^a_{jl})R^a + \delta_{jl}\mathrm{Im}(\lambda^a_{ik})L^a\right), & & & & \\
[M^{ij}, N^{kl}] &= i\left(\tfrac{4}{N}\delta_{ik}\delta_{jl}E + \delta_{ik}\mathrm{Re}(\lambda^a_{jl})R^a - \delta_{jl}\mathrm{Re}(\lambda^a_{ik})L^a\right), & & & & \\
[M^{ij}, L^a] &= i\sum_{k=1}^{N}\left(\mathrm{Re}(\lambda^a_{ik})N^{kj} + \mathrm{Im}(\lambda^a_{ik})M^{kj}\right), & & & & \\
[N^{ij}, L^a] &= -i\sum_{k=1}^{N}\left(\mathrm{Re}(\lambda^a_{ik})M^{kj} - \mathrm{Im}(\lambda^a_{ik})N^{kj}\right), & & & & \\
[M^{ij}, R^a] &= -i\sum_{k=1}^{N}\left(\mathrm{Re}(\lambda^a_{kj})N^{ik} + \mathrm{Im}(\lambda^a_{kj})M^{ik}\right), & & & & \\
[N^{ij}, R^a] &= i\sum_{k=1}^{N}\left(\mathrm{Re}(\lambda^a_{kj})M^{ik} - \mathrm{Im}(\lambda^a_{kj})N^{ik}\right). & & & &
\end{aligned} \tag{A.3}$$

Using the Hermitian generators of $su(2N)$, we represent the quantum link operators as [65]

$$U^{ij}_{x,y} = M^{ij}_{x,y} + iN^{ij}_{x,y}, \qquad U^{ij\dagger}_{x,y} = M^{ij}_{x,y} - iN^{ij}_{x,y}, \tag{A.4}$$

which are written in the fundamental representation of $su(2N)$ as

$$U^{ij}_{x,y} = \begin{bmatrix} 0 & 2D^{(ij)} \\ 0 & 0 \end{bmatrix}, \qquad U^{ij\dagger}_{x,y} = \begin{bmatrix} 0 & 0 \\ 2D^{(ji)} & 0 \end{bmatrix}.$$

Using equation (A.3), it is straightforward to show that this representation of the quantum link operators satisfies the commutation relations (7.68) and (7.69). Also the commutation relations among the quantum link operators can be derived as

$$[U^{ij}, U^{kl\dagger}] = 2(\tfrac{4}{N}\delta_{ik}\delta_{jl}E + \delta_{ik}\lambda^a_{lj}R^a - \delta_{jl}\lambda^a_{ik}L^a), \qquad [U^{\dagger ij}, U^{kl\dagger}] = [U^{ij}, U^{kl}] = 0. \tag{A.5}$$